

Collective behavior of colloids due to critical Casimir interactions

Anna Maciotek^{*}

*Institute of Physical Chemistry, Polish Academy of Sciences, Kasprzaka 44/52, PL-01-224 Warsaw, Poland,
Max-Planck-Institut für Intelligente Systeme, Heisenbergstraße 3, 70569 Stuttgart, Germany, and IV. Institut für Theoretische Physik, Universität Stuttgart, Pfaffenwaldring 57, 70569 Stuttgart, Germany*

Siegfried Dietrich[†]

Max-Planck-Institut für Intelligente Systeme, Heisenbergstraße 3, 70569 Stuttgart, Germany and IV. Institut für Theoretische Physik, Universität Stuttgart, Pfaffenwaldring 57, 70569 Stuttgart, Germany

 (published 5 October 2018)

If colloidal solute particles are suspended in a solvent close to its critical point, they act as cavities in a fluctuating medium and thereby restrict and modify the fluctuation spectrum in a way that depends on their relative configuration. As a result, effective, so-called critical Casimir forces (CCFs) emerge between the colloids. The range and the amplitude of CCFs depend sensitively on the temperature and the composition of the solvent as well as on the boundary conditions of the order parameter of the solvent at the particle surfaces. These remarkable, moreover universal features of the CCFs provide the possibility for an active control over the assembly of colloids. This has triggered a recent surge of experimental and theoretical interest in these phenomena. An overview is presented of current research activities in this area. Various experiments demonstrate the occurrence of thermally reversible self-assembly or aggregation or even equilibrium phase transitions of colloids in the mixed phase below the lower consolute points of binary solvents. The status is discussed of the theoretical description of these phenomena, in particular, the validity of a description in terms of effective, one-component colloidal systems and the necessity of a full treatment of a ternary solvent-colloid mixture. Perspectives are suggested on the directions toward which future research in this field might develop.

DOI: [10.1103/RevModPhys.90.045001](https://doi.org/10.1103/RevModPhys.90.045001)

CONTENTS

I. Introduction	1	A. General discussion	19
II. Effective One-component Approach	3	B. Monte Carlo studies	20
A. Effective interactions	4	C. Mean field theory	22
B. Critical Casimir pair potential	6	IV. Experiments	23
1. Mean field theory	8	A. Experimental studies of critical Casimir interactions	23
2. Beyond mean field theory	9	B. Phase transitions and aggregation in bulk	24
3. Computer simulations	10	C. Effective colloid-colloid pair potential	25
4. Derjaguin approximation	12	D. Applications of critical Casimir forces for self-assembly and aggregation of colloids	30
a. General discussion	12	E. Colloidal mixtures	33
b. Critical Casimir interactions for the film geometry	12	F. Effects of depletants on colloidal phase separations	34
5. Pair potential in the presence of depletants	14	G. Aggregation kinetics and structures of aggregates	34
6. The structure of the critical Casimir force between two identical colloids	15	V. Perspectives	37
C. Minimal model for a pair potential in a near-critical solvent	16	Acknowledgments	39
1. Stability	16	References	39
2. Phase behavior	17		
III. Multicomponent Mixture	19		

I. INTRODUCTION

Finite-size contributions to the free energy of a spatially confined fluid give rise to an effective force per area acting on the confining surfaces (Evans, 1990). Fisher and de Gennes (1978) made the crucial observation that this fluid-mediated interaction acquires a universal, long-ranged contribution f_C if the bulk critical point of the fluid is approached. This is due

^{*} amaciotek@ichf.edu.pl

[†] dietrich@is.mpg.de

to *critical fluctuations*, and hence the notion “critical Casimir force,” in analogy with quantum-mechanical Casimir forces which are due to quantum fluctuations of confined electromagnetic fields (Casimir, 1948; Kardar and Golestanian, 1999). In the case of colloidal suspensions with near-critical suspending fluids (referred to as solvents), the typically micrometer-sized colloidal particles act as cavities inside the critical solvent. At the colloid surfaces these cavities impose boundary conditions (BCs) for the fluctuating order parameter (OP) of the solvent and perturb the OP field on the length scale of the bulk correlation length ξ . Such modifications of the OP and the restrictions of its fluctuation spectrum depend on the spatial configuration of the colloids. Following the argument by Fisher and de Gennes (1978), this gives rise to the critical Casimir force (CCF) between the colloids, which is attractive for identical particles and has a range set by the bulk correlation length ξ of the solvent. Since $\xi[t = (T_c^{(s)} - T)/T_c^{(s)} \rightarrow 0] \sim |t|^{-\nu}$, where ν is a standard bulk critical exponent, this range diverges upon approaching the bulk critical temperature $T_c^{(s)}$ of the pure solvent.

The collective behavior of colloids dissolved in the near-critical solvent is determined by the interplay between the CCFs and other interactions acting between the constituents. In general, in colloidal suspensions the dissolved particles interact directly via van der Waals interactions; these are attractive and lead to irreversible aggregation (called coagulation) (Verwey and Overbeek, 1948). In charge-stabilized suspensions, the colloids acquire surface charges due to dissociation of the surface groups in water or due to chemical functionalization of the surface of the particles. This causes the formation of electric double layers around the colloids and results in electrostatic repulsion between them. In sterically stabilized suspensions, the short polymer chains grafted onto the surface of colloidal particles give rise to a repulsive interaction which is of entropic origin. Additionally, the presence of other smaller solute particles or macromolecular additives such as polymers, surfactants, or micelles (Likos, 2001) induces effective entropic interactions between the colloids, called depletion forces, which are predominantly attractive and short ranged (Asakura and Oosawa, 1954; Vrij, 1976). If the CCFs between colloidal particles are attractive and sufficiently strong to overcome the direct repulsive forces, one may expect the occurrence of a thermodynamically stable colloid-rich liquid or solid phase—even in the absence of any direct attractive interactions. If the resulting attractive potential is sufficiently strong, the condensation transition from a colloid-poor (“gas”) to a colloid-rich (“liquid”) phase may be preempted (on the characteristic time scales of the observations) by the formation of nonequilibrium aggregates in which the colloidal particles stick together. In general, such aggregates may grow or shrink and their structure varies from loose fractals through gels and glasses to crystals, depending on the packing fraction of the colloidal particles in the aggregates and on the strength of the attraction among the colloidal particles.

Beysens and Estève (1985) were the first to experimentally study aggregation phenomena for colloids suspended in binary solvents. They studied silica spheres immersed in a water-lutidine mixture by using light scattering. They found the formation of aggregates that sediment upon approaching

the bulk coexistence region of demixing from the one-phase region of the binary liquid mixture at constant composition of the solvent. Strikingly, the observed aggregation was thermally reversible; moving back the thermodynamic state deeply into the one-phase region the sediments dissolved again. In the decade following this pioneering work, quite a number of further experiments were performed leading to a similar behavior for various binary solvents and a variety of colloids. The structure of the aggregates and the kinetics of aggregation and the reverse process of fragmentation have been investigated. Silica, quartz powder, and polystyrene particles immersed in water-lutidine mixtures were studied by Gurfein, Beysens, and Perrot (1989), Gallagher, Kurnaz, and Maher (1992), Gallagher and Maher (1992), Broide, Garrabos, and Beysens (1993), Kurnaz and Maher (1995), Narayanan *et al.* (1995), and Kurnaz and Maher (1997), whereas Narayanan *et al.* (1993), Kline and Kaler (1994), Grill and Woermann (1997), Jayalakshmi and Kaler (1997), Koehler and Kaler (1997), and Rathke, Grill, and Woermann (1997) employed other solvents; for corresponding reviews, see Beysens *et al.* (1994), Beysens and Narayanan (1999), and Law (2001). These experiments, which were performed mostly in the one-phase region of a binary liquid mixture, revealed that reversible aggregation (termed flocculation) is accompanied by a strong adsorption phenomenon in the vicinity of the bulk two-phase coexistence curve. Generically, colloidal particles have a preference for one of the two components of the binary solvent. At the surface of the colloid this preference gives rise to an effective surface field conjugate to the OP at the surface and thus leads to an adsorption layer rich in this preferred component. The measurements demonstrated that the temperature-composition (T, c) region in which colloidal aggregation appears is not symmetric about the critical composition c_c of the binary solvent. Strong aggregation occurs on that side of the critical composition which is rich in the component not preferred by the colloids.

Various mechanisms were put forward for strong adsorption giving rise to attraction which in turn could explain the occurrence of (nonequilibrium) flocculation. For example, capillary condensation and/or wetting can occur when particles come close together via diffusion, even far off the critical composition of the solvent. In this case a liquid “bridge” can form which induces attractive solvation forces (Bauer, Bieker, and Dietrich, 2000) (see Sec. II.B.6). Another possibility is that the presence of an adsorption layer around the colloidal particles increases the strength of the direct attractive dispersion interactions. However, in the close vicinity of the bulk critical point of the solvent, in line with the predictions of Fisher and de Gennes, effective attraction induced by critical fluctuations is expected to be dominant. In their original paper, Beysens and Estève identified an “aggregation line” in the temperature-composition phase diagram of the solvent with a prewetting line. Yet, they observed that this aggregation line extends to temperatures below the lower demixing critical point of a solvent. However, in general such an extent of prewetting lines has not been found up to now, neither for planar nor for spherical substrates. Actually, positive curvature even shortens prewetting lines (Bieker and Dietrich, 1998a, 1998b). (Regrettably, the wetting behavior of

this system in planar geometry has never been investigated.) They did not comment on this difference nor did they admit the role of critical fluctuations and CCFs for aggregation in the critical region. They presumed that the aggregation process results from the attractive forces between the colloids due to the presence of the adsorption layer and referred to [de Gennes \(1981\)](#) as the one who proposed such fluctuation-induced interactions at and near the bulk critical point of the solvent, but they have not put their results into the proper context of de Gennes's predictions. According to another interpretation of the experimental findings previously mentioned, the observed phenomenon is regarded as a precursor of a bona fide phase transition in the ternary mixture rather than a nonequilibrium flocculation of colloidal particles ([Kline and Kaler, 1994](#); [Jayalakshmi and Kaler, 1997](#); [Koehler and Kaler, 1997](#)). A few theoretical ([Sluckin, 1990](#)) and simulation ([Löwen, 1995](#); [Netz, 1996](#)) attempts have been concerned with such an interpretation. The status of knowledge about reversible aggregation of colloids in binary solvents up to the late 1990s was reviewed by [Beysens and Narayanan \(1999\)](#). More recently, the scenario of “bridging” transitions has again been theoretically studied by [Archer *et al.* \(2005\)](#), [Okamoto and Onuki \(2011, 2013\)](#), and [Labbé-Laurent, Law, and Dietrich \(2017\)](#).

In spite of the relevance of aggregation phenomena for the stability of colloidal suspensions, the basic understanding of the collective behavior of colloids dissolved in a near-critical solvent has started to emerge only recently. This progress had to await the advances made during the last decade concerning the statistical mechanical theory and computer simulations of CCFs. The accumulated theoretical knowledge of two-body CCFs has also triggered an increase of experimental activities in this field. This renewed interest is driven by application perspectives, in particular, concerning the buildup of nanostructured materials of well-defined structure by using self-assembly of colloidal particles. In order to achieve a desirable morphology of aggregates, one has to be able to control colloidal self-assembly and to manipulate the particles. The remarkable features of CCFs offer such possibilities. The range and the strength of the CCFs, which depend sensitively on temperature via the bulk correlation length ξ , can be tuned reversibly and *continuously* by moving the thermodynamic state of the solvent around its critical point. The sign of f_C can be manipulated as well by suitable surface treatments of the colloids ([Hertlein *et al.*, 2008](#); [Gambassi *et al.*, 2009](#); [Nellen, Helden, and Bechinger, 2009](#)). Additional interest is sparked by the potential relevance of CCFs for lipid membranes. These are two-dimensional (2D) liquids consisting of two (or more) components, such as cholesterol and saturated and unsaturated lipids, which can undergo phase separation into two liquid phases, one being rich in the first two components and the other rich in the third ([Veatch and Keller, 2005](#)). Lipid membranes serve as model systems for cell plasma membranes ([Lingwood and Simons, 2010](#)). Recent experiments suggest that cell membranes are tuned to the miscibility critical point of the 2D Ising model ([Heinrich *et al.*, 2008](#); [Honerkamp-Smith *et al.*, 2008](#); [Gray *et al.*, 2013](#); [Kimchi and Machta, 2015](#)) so that CCFs may arise between macromolecules embedded in the membrane ([Machta *et al.*, 2011](#);

[Machta, Sethna, and Veatch, 2012](#); [Benet, Paillusson, and Kusumaatmaja, 2017](#)).

Other mechanisms, which—similar to the ones generating the critical Casimir effect—also induce solvent-mediated long-ranged interactions, occur *inter alia* in a chemical sol upon approaching its percolation transition ([Gnan, Zaccarelli, and Sciortino, 2014](#)), in a binary liquid mixture subjected to a steady temperature gradient due to the concomitant non-equilibrium concentration fluctuations ([Kirkpatrick, Ortiz de Zárate, and Sengers, 2015](#)), in driven noncohesive granular media due to hydrodynamic fluctuations ([Cattuto *et al.*, 2006](#)), or if the solvent comprises active matter such as bacteria or self-propelled colloidal particles ([Ray, Reichhardt, and Olson Reichhardt, 2014](#); [Ni, Stuart, and Bolhuis, 2015](#)). Related to the critical Casimir effect is also the behavior of a single polymer chain upon approaching the critical demixing point of its binary solvent ([Brochard and de Gennes, 1980](#); [Vilgis, Sans, and Jannink, 1993](#); [Venkatesu, 2006](#)). First, the polymer chain collapses as a result of the attractive CCFs between the monomers of the polymer chain. But when the correlation length of the solvent becomes larger than the globular size of the polymer, it reexpands.

Compared with other effective forces between colloid particles or macromolecules, CCFs have two advantages. First, due to the concept of universality for critical phenomena, to a large extent CCFs do not depend on microscopic details of the system. Second, whereas adding depletion agents or ions changes the resulting effective forces *de facto* irreversibly, the tuning of f_C via temperature is fully and easily reversible.

This review discusses current theoretical and numerical approaches toward the description of the static, equilibrium properties of colloidal suspensions with a near-critical binary solvent. The related experimental body of research is put into the corresponding context and a number of intriguing possible developments are highlighted. Recent developments concerning colloidal assembly due to CCFs with a focus on the experimental observations are reviewed by [Nguyen *et al.* \(2016\)](#).

II. EFFECTIVE ONE-COMPONENT APPROACH

A common approach to the statistical mechanical description of colloidal suspensions follows the ideas developed for multicomponent molecular liquids, such as ionic solutions, by considering the colloidal particles as “supramolecules” ([Vrij *et al.*, 1978](#); [Hansen, 1993](#); [Likos, 2001](#)). Within this approach, the degrees of freedom of the solvent and the ions, in the case of charged-stabilized suspensions, are traced out in order to construct an effective one-component system of colloidal particles interacting via state- and configuration-dependent forces. For most cases, carrying out the integration over microscopic degrees of freedom can be done only approximately, leading to additive pairwise interactions between the colloidal particles (see the corresponding discussion later). For any binary mixture with pair interactions for which the volume integral is finite, a formal expression for an effective Hamiltonian, describing particles of one species only but in the presence of the particles of the other species, was given by [Dijkstra, van Roij, and Evans \(1998, 1999\)](#). This effective Hamiltonian consists of zero-body, one-body, two-body, three-body, and higher-body interactions, which depend

on the density of the second species and have to be determined one by one. For additive hard-sphere mixtures with a large size asymmetry, a comparison with direct simulations of true binary mixtures has shown that the pairwise (depletion) potential approximation of the effective Hamiltonian between two large particles accounts remarkably well for the phase equilibria, even in limits for which one might expect that higher-body terms cannot be neglected. This success encourages one to use an effective one-component approach (with the approximation of an additive pairwise potential) to colloids suspended in a near-critical solvent, despite the fact that the CCFs are inherently nonadditive. The critical Casimir interaction between two colloidal particles depends on the instantaneous spatial configuration of all colloids (Mattos, Harnau, and Dietrich, 2013, 2015; Hobrecht and Hucht, 2015; Paladugu *et al.*, 2016; Vasilyev, Dietrich, and Kondrat, 2018). Only for dilute suspensions or for temperatures sufficiently far away from the bulk critical temperature $T_c^{(s)}$ of the pure solvent, such that the range of the critical Casimir interaction between the colloids is much smaller than the mean distance between them, the assumption of pairwise additive CCFs is expected to be reliable.

A. Effective interactions

In most of the experimentally studied systems, the solvent is a binary mixture of molecular liquids and the colloidal particles are microsized spheres of radius R . For such a sizewise highly asymmetric multicomponent system, one can ignore the discrete nature of the solvent and use a simplified pair potential model for the background interaction potential between the colloids, which is present also away from the critical temperature $T_c^{(s)}$ of the solvent. Such a model is supposed to capture only the essential features of a stable suspension on the relevant, i.e., mesoscopic, length scale. Besides the van der Waals contribution, discussed later, these features are the hard-core repulsion for center-to-center distances $r < 2R$ and a soft repulsive contribution, for which one can employ the Yukawa potential. This leads to the screened Coulomb model of suspensions which are charge stabilized against flocculation (Russel, Saville, and Schowalter, 1989; Hansen and Löwen, 2000; Barrat and Hansen, 2003):

$$\frac{V_{\text{rep}}(D)}{k_B T} = U_{\text{rep}}(D) = \frac{U_0}{\kappa(D + 2R)} e^{-\kappa D}, \quad D = r - 2R > 0, \quad (1)$$

where D is the surface-to-surface distance and k_B is the Boltzmann constant. The range κ^{-1} of the repulsion is the Debye screening length $\kappa^{-1} = \sqrt{\epsilon \epsilon_0 k_B T / e^2 \sum_i \rho_i}$ [see, e.g., Parsegian (2006)], where e is the elementary charge, ϵ the permittivity of the solvent relative to the vacuum, $\epsilon_0 = 8.854 \times 10^{-12} \text{ C}^2/\text{Jm}$ is the vacuum permittivity, and $\{\rho_i\}$ the number densities of all ions (regardless of the sign of their charges). The potential given by Eq. (1) is in fact a repulsive contribution to the classical Derjaguin, Landau, Verwey, and Overbeek (DLVO) theory, which invokes the Debye-Hückel approximation to linearize the Poisson-Boltzmann equation for two charged

spheres immersed in a dielectric medium containing counterions. The DLVO potential also contains the van der Waals contribution (Verwey and Overbeek, 1948). A simplified, purely exponential form of the repulsive pair potential,

$$U_{\text{rep}}(D) = A e^{-\kappa D}, \quad (2)$$

is often used for distances $D \ll R$ at which all curvature effects associated with the spherical shape of the colloidal particles effectively drop out (Israelachvili, 1998; Levin, 2002), provided $D \gtrsim \kappa^{-1}$. These conditions imply $\kappa^{-1} \ll R$, which in practice is satisfied for experimentally relevant systems for which the Debye length is of the order of 10 nm and the colloidal size of the order of 1 μm . For the effective Coulomb interaction screened by counterions the amplitude A is given by (Russel, Saville, and Schowalter, 1989)

$$A = 2\pi(\epsilon \epsilon_0)^{-1} \Upsilon^2 \kappa^{-2} R / k_B T, \quad (3)$$

where Υ is the surface charge density of the colloid. For small, highly charged colloidal particles, for which the linearized Debye-Hückel theory breaks down, the pair potential can still be given by Eq. (1) or (2), but the bare colloidal charge is replaced by an effective renormalized charge (Levin, 2002; Frydel, Dietrich, and Oettel, 2007). The literature concerning the electrostatic forces between two charged colloids in a suspension is very extensive; thus for more details the interested reader is referred to reviews such as Alexander *et al.* (1984), Belloni (1998), or Levin (2002). The purely exponential form of repulsion [Eq. (2)] can also describe sterically stabilized suspensions beyond the hard-sphere model (Israelachvili, 1998). In that case the range κ^{-1} of the repulsion is associated with the length of the grafted polymers and the strength A of the repulsion depends on the surface coverage of grafted polymers.

In order to describe certain experimental systems, one has to also consider the interaction which accounts for effectively attractive van der Waals forces. Among them are the so-called London or dispersion forces, which are quantum mechanical in nature and caused by induced charge fluctuations in neutral atoms or molecules with no permanent dipoles. The quantum fluctuations of the electrons in neighboring (even neutral) atoms lead to the formation of an instantaneous dipole. The fluctuation-induced dipole in one atom induces an instantaneous dipole in the other; these two dipoles are parallel which gives rise to attraction. The induced dipole-dipole interaction decays as $1/D^6$ (in contrast to the decay $\propto 1/D^3$ for the permanent dipole-dipole interaction). This algebraic decay is due to the scale invariance of the Coulomb interaction. As discussed in detail in Sec. II.B, the CCF decays algebraically only at the critical point but exponentially off criticality. However, its range can be changed continuously by varying the temperature. Such a tuning of the range of the van der Waals forces is not possible. Even though the London interactions of two molecules are rather weak, at short distances the overall interactions between two macroscopic bodies can become significant compared with $k_B T$. Indeed, for two spheres, the nonretarded van der Waals forces contribute to the total potential through a term (Hamaker, 1937; Parsegian, 2006)

$$\begin{aligned}
 V_{\text{vdW}}(\Delta)/k_B T & \\
 &= U_{\text{vdW}}(\Delta) \\
 &= -\frac{A_H}{6k_B T} \left[\frac{2}{\Delta(\Delta+4)} + \frac{2}{(2+\Delta)^2} + \ln\left(\frac{1+4/\Delta}{(1+2/\Delta)^2}\right) \right], \quad (4)
 \end{aligned}$$

where A_H is the Hamaker coefficient, which has a typical value of $\simeq 10^{-20}$ J. As $\Delta = D/R$ increases, this term crosses over from the behavior $U_{\text{vdW}}(D \ll R) \simeq -(A_H/12)(R/D)$ to $U_{\text{vdW}}(D \gg R) \simeq -(16A_H/9)(R/D)^6$. For larger distances, however, the retardation effect due to the finite velocity of light sets in and the London forces cross over to the classical Casimir interaction. The leading decay of the potentials of these interactions [not captured by Eq. (4)] is $\propto -1/D^2$. Here we refer to a recent review (Klimchitskaya, Mohideen, and Mostepanenko, 2009) on classical Casimir forces and on the closely related van der Waals forces. We note that the complete continuum theory for dielectric macroscopic bodies immersed in a dielectric medium was developed by Lifshitz, Dzyaloshinskii, and Pitaevskii (Lifshitz, 1955; Dzyaloshinskii, Lifshitz, and Pitaevskii, 1961). This theory is derived in terms of the frequency-dependent dielectric permittivities $\varepsilon_j(\omega)$, $j = 1, 2$, of the two bodies and of $\varepsilon_0(\omega)$ for the medium. It is valid for any distance, large on molecular scales, between the surfaces of the macroscopic bodies. Moreover, it does not assume pairwise additivity of the interactions and includes in a consistent way two limits: the van der Waals limit at small separations, for which the retardation effects can be neglected, and the opposite limit at large distances, where the classical Casimir force dominates. However, for intermediate distances and geometries other than planar, the implementation of the Lifshitz theory is rather cumbersome. In particular, the expression for the interaction energy does, in general, not factorize into a material-dependent (via the Hamaker coefficient) and a geometrical contribution as in Eq. (4). However, one can estimate the significance of the van der Waals interactions between two spheres by considering a planar geometry. For the latter the interaction energy for two parallel walls across a film of thickness D can be expressed in terms of $A_H(D)$ as (Parsegian, 2006)

$$V(D, T)/k_B T = -\frac{1}{12\pi k_B T} \frac{A_H(D)}{D^2}. \quad (5)$$

Within a first approximation (Parsegian, 2006) one has

$$\begin{aligned}
 A_H(D) &\simeq \frac{3}{2} k_B T \sum_{n=0}^{\infty} \left. \frac{\varepsilon_1 - \varepsilon_0}{\varepsilon_1 + \varepsilon_0} \frac{\varepsilon_2 - \varepsilon_0}{\varepsilon_2 + \varepsilon_0} \right|_{i\omega_n} R_n(D) \\
 &\equiv A_{n=0} + A_{n>0}(D), \quad (6)
 \end{aligned}$$

where the permittivities $\varepsilon_j(\omega)$ of the various materials are evaluated at the imaginary frequencies $i\omega_n$, with $\omega_n = 2\pi k_B T n / \hbar$, $n \in \mathbb{N}_0$. The factor $R_n(D)$ accounts for retardation which, however, does not affect the zero-frequency term $A_{n=0}$. The prime in Eq. (6) indicates that the contribution of the static permittivities, i.e., $n = 0$, is to be multiplied by $1/2$. By using index-of-refraction-matched colloidal suspensions (Israelachvili, 1998) the value of A_H can be strongly reduced. This way dispersion forces can be effectively switched off. For

polar solvents such as water, the static dielectric constant $\varepsilon(\omega = 0)$ is large, which makes the contribution of the zero-frequency mode $A_{n=0}$ to A_H dominant. In this case, it is not possible to reduce the strength of the dispersion forces uniformly at all frequencies. On the other hand, $A_{n=0}$ can be screened by adding salt to the solvent. Therefore, in colloidal suspensions with aqueous solvents, even though the van der Waals interactions are still present, their relevance can be restricted to very short distances. Often, these distances are below the range which can be resolved experimentally such as, e.g., the measurements of CCFs between a colloid, immersed in a mixture of water and 2,6-lutidine, and a planar wall (Hertlein *et al.*, 2008; Gambassi *et al.*, 2009). [A detailed discussion of the Hamaker constant for a polystyrene colloid near a silica glass substrate immersed in a mixture of water and 2,6-lutidine can be found in Gambassi *et al.* (2009).]

Additionally, in the presence of small co-solutes such as free polymer coils or smaller colloids in a sterically stabilized colloidal suspension, one has to consider depletion interactions which arise between large colloidal particles due to entropic effects caused by the small solutes. This so-called depletion interaction is mainly attractive and has a range proportional to the size of the depletant (Asakura and Oosawa, 1954; Vrij, 1976). There are several theories and approximations for the depletion potential, which are summarized by Götzelmann, Evans, and Dietrich (1998) and Roth, Evans, and Dietrich (2000). For example, for a fluid of large hard spheres of radius R and a small spherical depletant of diameter σ , which on its own behaves as an ideal gas, the depletion potential is (Vrij, 1976)

$$\frac{V_d(D)}{k_B T} = U_d(D) = \begin{cases} -n_b V_{\text{ov}}(D), & 0 \leq D \leq \sigma, \\ 0, & D \geq \sigma, \end{cases} \quad (7)$$

where $V_{\text{ov}}(D) = (\pi/6)(\sigma - D)^2(3R + \sigma + D/2)$. In Eq. (7) n_b is the bulk number density of the small spheres. Note that $|V_d(D)|$ in Eq. (7) is equal to the pressure ($p = n_b k_B T$) times the overlap volume V_{ov} between the excluded volumes denied to the centers of the small spheres around each big sphere. Taking into account hard-core repulsion among the depletants produces a repulsive contribution to the depletion interaction as well as an oscillatory decay at large distances (Götzelmann, Evans, and Dietrich, 1998; Roth, Evans, and Dietrich, 2000). For many actual colloidal suspensions the depletion attraction is strong enough to induce colloidal aggregation and, despite its rather short range, a gas-liquid-like phase separation, because even a small degree of polydispersity or nonsphericity of the particles causes the fluid phase to not be preempted by crystallization.

If the depletant is only a co-solute in the suspension in which the solvent becomes critical, the resulting depletion potential simply adds to the background potential. It may, however, occur that due to an effective depletant-depletant interaction the depletant itself exhibits a phase transition with a critical point. This means that the solvent, which is common to both the big spheres and the depletant, does not display a critical point of its own as the one discussed previously. A system that realizes this interesting scenario was studied experimentally by Buzzaccaro *et al.* (2010) and Piazza *et al.* (2011) and via Monte Carlo (MC) simulations (Gnan *et al.*, 2012) (see Secs. II.B.5 and IV.F where we review the results of these studies). In such a case one

expects that the depletant produces one unique effective pair potential between the big particles. Far away from the critical point of the depletant, this unique pair potential has the character of a depletion interaction, whereas close to the critical region of the depletant it should display the features of the CCFs pair potential. As has been shown by [Buzzaccaro *et al.* \(2010\)](#) and [Piazza *et al.* \(2011\)](#), the framework of density functional theory (DFT) ([Evans, 1979](#)), which is commonly adopted in colloidal science, can provide both forms for the effective pair potential in the corresponding limits (see Sec. II.B for details). [Gnan *et al.* \(2012\)](#) numerically determined the effective pair potential $V_{\text{eff}}(r)$ between two big hard-sphere colloids for two models of the depletant particles within a wide range of state points, including the critical region. In the first model, the spherical depletant particles interact via a pairwise square-well (SW) potential:

$$V^{\text{SW}}(r) = \begin{cases} \infty, & r < \sigma, \\ -d_w, & \sigma \leq r \leq 1 + r_w \sigma, \\ 0, & r \geq (1 + r_w) \sigma, \end{cases} \quad (8)$$

where r is the center-to-center distance between two depletant particles, r_w is a dimensionless well width, and d_w is the well depth. The second depletant model is an anisotropic three-patches (3P) Kern-Frenkel system which consists of hard-sphere particles decorated with three attractive sites ([Kern and Frenkel, 2003](#)). The critical packing fraction of these patchy particles is very small—as in the experimental system studied by [Buzzaccaro *et al.* \(2010\)](#) and [Piazza *et al.* \(2011\)](#). For this kind of depletant, the numerically determined effective pair potential $V_{\text{eff}}(r)$ between two big spheres has subsequently been used in a grand canonical off-lattice MC simulation in order to analyze the stability of the colloidal suspension for a system of colloidal particles interacting via the pairwise additive interaction $V_{\text{HS}}(r) + V_{\text{eff}}(r)$, where $V_{\text{HS}}(r)$ is a hard-sphere potential. The results of this study are discussed in Sec. II.B.5.

Upon approaching the bulk critical point $(T_c^{(s)}, c_c)$ of the solvent, CCFs between the particles emerge and the corresponding pair potential $V_C/k_B T = U_C$ appears in addition to the background contribution. In the next section we discuss the details of the pair potential of critical Casimir interactions (CCP).

B. Critical Casimir pair potential

The solvent-mediated force between two spherical particles, a surface-to-surface distance D apart, is defined as the negative derivative of the excess free energy $\mathcal{F}^{\text{ex}} = \mathcal{F} - V f_b$,

$$f_s = -\frac{\partial \mathcal{F}^{\text{ex}}}{\partial D} = -\frac{\partial (\mathcal{F} - V f_b)}{\partial D}, \quad (9)$$

where f_b is the bulk free energy density of the solvent and \mathcal{F} is the free energy of the solvent in the macroscopically large volume V excluding the volume of two suspended colloids. The derivative in Eq. (9) is carried out at constant T and at a constant number of solvent molecules. If the solvent is in contact with a reservoir, one has to consider the excess grand potential Ω^{ex} and the derivative has to be taken at constant T and at constant chemical potential μ . It follows from the

definition in Eq. (9) that, in an open system, f_s per surface area is excess pressure over the bulk value (fixed by the reservoir). As already discussed in the Introduction, the CCF f_C is the long-ranged universal contribution to f_s which emerges upon approaching the bulk critical point of the solvent. The CCF arises due to the modifications of the structure of the solvent and due to the restrictions of the thermal fluctuations of the corresponding OP which are caused by the surfaces of the colloids at a fixed distance. These surface induced modifications extend spatially to distances set by the bulk correlation length ξ . If the separation between the two colloids is smaller than ξ , i.e., $D \lesssim \xi$, the second colloid interacts with a solvent which is significantly modified by the first one and therefore an effective interaction between the two objects emerges with a spatial range set by ξ . Since at criticality ξ diverges, upon approaching the critical point this effective force becomes long ranged and acquires a universal character. Universality means that material properties and microscopic details of the interaction between the colloid and the solvent are largely irrelevant for the behavior of the CCF at mesoscopic scales D , $\xi \gg \xi^{(0)}$, where $\xi^{(0)}$ is a molecular size of the solvent. If many colloidal particles are suspended in the near-critical solvent, the modifications of the solvent generated by each particle are experienced by all the others. Therefore, an effective many-body critical Casimir interaction emerges. Because of its many-body nature, this interaction does not simply follow from the linear superposition of the separate effects caused by the various bodies, but it is expected to show genuine and interesting n -body interactions which cannot be accounted for by pairwise summation of two-body interactions only.

The pair CCP associated with the CCF is

$$V_C(D, R, T, h_b) \equiv \int_D^\infty dz f_C(z, R, T, h_b) \quad (10)$$

so that the CCF is given by

$$f_C(D, R, T, h_b) = -\frac{\partial}{\partial D} V_C(D, R, T, h_b).$$

According to finite-size scaling theory ([Barber, 1983](#); [Privman, 1990](#)), near criticality the singularities of thermodynamic functions are rounded and shifted when the bulk correlation length ξ becomes comparable to the characteristic linear size D of the finite system. This phenomenological argument implies that the finite-size contribution to the free energy, and hence also the CCP, is expected to be a scaling function of the scaling variable D/ξ . One can argue more formally by using the fact that due to the self-similarity of the critical fluctuations the singular part of the free energy is a generalized homogeneous function of the relevant scaling fields, including the separation D and, in the case of two identical spheres, their radius R . Further support can be gained by invoking systematic field-theoretical renormalization group theory [see [Krech and Dietrich \(1992\)](#)] and see, e.g., [Diehl \(1986\)](#) and [Esser, Dohm, and Chen \(1995\)](#)]. It follows that in the well-defined scaling limit $T \rightarrow T_c$ and all length scales of the system being large on molecular scales, U_C attains a scaling form ([Barber, 1983](#); [Privman, 1990](#)) in terms of suitable dimensionless scaling variables describing the

distance between the colloids, the dependence on the thermodynamic state of the solvent, and the shape of the colloidal particles. For example, for the spherical particles one has

$$\begin{aligned} \frac{V_C(D)}{k_B T} &= U_C(D) \\ &\simeq \frac{R}{D} \Theta \left(\mathcal{Y} = \text{sgn}(t) \frac{D}{\xi_t}, \Delta = \frac{D}{R}, \Lambda = \text{sgn}(h_b) \frac{D}{\xi_h} \right), \\ D &= r - 2R > 0. \end{aligned} \quad (11)$$

Θ is a universal scaling function determined solely by the so-called universality class of the continuous phase transition occurring in the bulk, the geometry of the setup, and the surface universality classes of the confining surfaces (Diehl, 1986; Krech, 1994; Brankov, Dantchev, and Tonchev, 2000; Gambassi, 2009). The relevant bulk universality class for colloidal suspensions is the Ising universality class in spatial dimension $d = 3$ or 2 . For the CCF one has

$$\begin{aligned} \frac{f_C}{k_B T} &\simeq \frac{R}{D^2} \vartheta(\mathcal{Y}, \Delta, \Lambda) \\ &= \frac{R}{D^2} \left[\Theta - \mathcal{Y} \frac{\partial}{\partial \mathcal{Y}} \Theta - \Delta \frac{\partial}{\partial \Delta} \Theta - \Lambda \frac{\partial}{\partial \Lambda} \Theta \right]. \end{aligned} \quad (12)$$

In Eq. (11), $\xi_t(t \geq 0) = \xi_{t,\pm}^{(0)} |t|^{-\nu}$, with $t = \pm(T - T_c^{(s)})/T_c^{(s)}$ for an upper (+) and a lower (−) critical point, respectively, is the true correlation length governing the exponential decay of the solvent bulk two-point OP correlation function for $t \rightarrow 0^\pm$ and $h_b = 0$, where h_b is the bulk ordering field conjugate to the OP. The amplitudes $\xi_{t,\pm}^{(0)}$ (with \pm referring to the sign of t) are nonuniversal but their ratio $\xi_{t,+}^{(0)}/\xi_{t,-}^{(0)}$ is universal. The correlation length $\xi_h = \xi_h^{(0)} |h_b|^{-\nu/\beta\delta}$ governs the exponential decay of the solvent bulk two-point OP correlation function for $t = 0$ and $h_b \rightarrow 0$, where $\xi_h^{(0)}$ is a nonuniversal amplitude related to $\xi_{t,\pm}^{(0)}$ via universal amplitude ratios; ν , β , and δ are standard bulk critical exponents (Pelissetto and Vicari, 2002). For the demixing phase transition of a binary liquid mixture, the OP ϕ is proportional to the deviation of the concentration of species, say a ,

$$c_a = \frac{Q_a}{Q_a + Q_b} \quad (13)$$

from its value $c_{a,c}$ at the critical point, i.e., $\phi \sim c_a - c_{a,c}$; here Q_α , $\alpha \in \{a, b\}$ are the number densities of the particles of species a and b , respectively. The bulk ordering field, conjugate to this OP, is proportional to the deviation of the difference $\Delta\mu = \mu_a - \mu_b$ of the chemical potentials μ_α , $\alpha \in \{a, b\}$ of the two species from its critical value, i.e., $h_b \sim \Delta\mu - \Delta\mu_c$. We note that the actual scaling fields of fluids are linear combinations of h_b and of the reduced temperature t .

A crucial ingredient for an effective one-component approach is to have an accurate CCP between two colloidal particles. This is not only relevant for the investigation of aggregation or the bulk phase behavior of colloids, but it is also of intrinsic scientific interest. In recent years the experimental technique of total internal reflection microscopy (TIRM) (Walz, 1997; Prieve, 1999; Hertlein, 2008) has been

developed which allows one to directly measure and with femto-Newton resolution the effective potential of the CCF between a colloidal particle, suspended in a near-critical binary mixture, and a fixed object such as a planar wall (Hertlein *et al.*, 2008; Gambassi *et al.*, 2009; Nellen, Helden, and Bechinger, 2009). Video microscopy has also been used in order to determine the CCP between two spherical colloids (Dang *et al.*, 2013; Nguyen *et al.*, 2013; Shelke *et al.*, 2013; Paladugu *et al.*, 2016; Stuij *et al.*, 2017). For discussions of experimental studies of CCFs see Sec. IV.A. Although the resolution and the sophistication of such experiments keep increasing, it is difficult to interpret the raw data of these measurements mainly due to the inevitable, simultaneous presence of various contributions to the effective pair potential (see the corresponding discussion in Sec. IV.C). Therefore, reliable theoretical results are required in order to improve the interpretations of the experimental data.

The main difficulty in theoretically determining the scaling function of CCFs and their potential lies in the character of the critical fluctuations; an adequate treatment has to include non-Gaussian fluctuations. Usually colloidal particles exert a potential on the surrounding fluid which is infinitely repulsive at short distances and attractive at large distances. Such potentials give rise to pronounced peaks in the density profile of the fluid near the surface of the particle, i.e., there is strong adsorption. In terms of a field-theoretical description this corresponds to the presence of a strong (dimensionless) surface field $h_s \gg 1$. For binary liquid mixtures one has $h_s \sim \delta\Delta\mu_s/k_B T$ so that there is a local increment at the surface of the chemical potential difference between the two species. It determines which species of the solvent is preferentially adsorbed at the surface of the colloid. The preference for one component of a binary liquid mixture may be so strong as to saturate the surface of the colloids with the preferred component, which corresponds to $h_s = +\infty$ ($-\infty$). For two colloids this gives rise to symmetry-breaking BCs [denoted by (++) or (−−)] for the solvent OP. The resulting spatial variation of the order parameter poses a significant complication for obtaining analytic results. Moreover, nonplanar geometries lower the symmetry of the problem. Apart from a few exceptions and limiting cases, the presently available analytical results for CCFs are of approximate character.

At first, for two spherical colloidal particles, the corresponding CCP has been studied theoretically right at the bulk critical point. Early on, de Gennes (1981) proposed the singular effective interaction potential between two widely separated spheres by using a free energy functional, which goes beyond mean field in the sense that it incorporates the nonclassical bulk critical exponents, but neglects the critical exponent η ; η is the standard bulk critical exponent for the two-point correlation function at criticality with $\eta \sim 0.04$ in $d = 3$ and $\eta = 1/4$ in $d = 2$ (Pelissetto and Vicari, 2002). Within this approach he found that for $d = 3$ the energy of interaction in the limit $D \gg R$ is $-4\pi \times 1.69(4) \times k_B T_c^{(s)} R/D$. For that interaction potential, the so-called protein limit, which corresponds to $D/R, \xi/D \gg 1$ and which is based on exact arguments using conformal invariance, renders within a small-sphere expansion (Burkhardt and Eisenriegler, 1995; Eisenriegler and Ritschel, 1995)

$$U_C(D; T = T_c^{(s)}, h_b = 0, R) \sim (R/D)^{d-2+\eta} \stackrel{d=3}{=} (R/D)^{1+\eta} \stackrel{d=2}{=} (R/D)^\eta, \quad (14)$$

which implies for the scaling function in Eq. (11)

$$\Theta(\mathcal{Y} = 0, \Delta = D/R \rightarrow \infty, \Lambda = 0) \propto \Delta^{-(d-3+\eta)} \stackrel{d=3}{=} \Delta^{-\eta}.$$

Burkhardt and Eisenriegler (1995) estimated the amplitude of U_C in $d = 3$ to be slightly larger than $\sqrt{2} \simeq 1.41(4)$,

$$U_C(D; T = T_c^{(s)}, h_b = 0, R) \sim (R/D)^{(d-1)/2} \stackrel{d=3}{=} (R/D) = \Delta^{-1} \stackrel{d=2}{=} (R/D)^{1/2} = \Delta^{-1/2}. \quad (15)$$

This in turn implies for the scaling function in Eq. (11)

$$\Theta\left(\mathcal{Y} = 0, \Delta = \frac{D}{R} \rightarrow 0, \Lambda = 0\right) \stackrel{d=3}{=} \text{const.}$$

These results confirm that the CCFs can indeed successfully compete with direct dispersion (Dantchev, Schlesener, and Dietrich, 2007; Valchev and Dantchev, 2017) or electrostatic forces in determining the stability and phase behavior of colloidal systems. In Sec. II.C we discussed the minimal model for the effective pair potential describing the effects of a critical solvent on dissolved colloids due to CCFs. Since the shape of the total pair potential depends sensitively on details of the CCP, there is a need to elaborate on it. This is done in the following sections where we also survey various approaches used to determine the CCP and its universal scaling function.

Before proceeding we comment on the terminology used in the context of CCFs. The notion “critical Casimir effect,” which has been adopted for the phenomenon described in this section, stems from a certain analogy with the “classical” Casimir effect which is due to the confinement of the quantum fluctuations of the electromagnetic field (either in vacuum or in a medium, at nonzero or zero temperature). Indeed, at large separations both the classical Casimir force and the CCF right at the critical point are long ranged and universal. One often alludes to the common origin of the two effects in the sense that both of them involve a confinement of the region in space within which a relevant field (electromagnetic or the order parameter of the continuous phase transition) fluctuates. Beyond these analogies there are important differences between these effective forces. For example, the fluctuations of the electromagnetic field in vacuum are Gaussian, whereas the fluctuations of the order parameter near the critical point are non-Gaussian. The analogy with the fluctuation-induced classical Casimir interactions gives rise to some confusion concerning the rightfulness of using the notion of CCFs when the confining surfaces impose one or more symmetry-breaking BCs on the OP, i.e., if the surface fields are present. In such a case, the mean field OP is spatially inhomogeneous and depends on the separation between the confining surfaces D . This way, the corresponding mean field free energy density also depends on D and is commonly referred to as the critical

which by and large checks with the prediction given by de Gennes (1981)—up to the factor of 4π , which is the surface area of the three-dimensional unit sphere. In the opposite, the so-called Derjaguin limit $D \ll R$, the CCP for two parallel plates has been employed after conformally mapping two spheres at separation D into two concentric spheres and using conformal invariance in order to obtain (Burkhardt and Eisenriegler, 1995; Eisenriegler and Ritschel, 1995)

Casimir energy. Using the notion CCF in this context is sometimes questioned because, in view of the analogy with the classical Casimir effect, only fluctuation-induced interactions are considered to be Casimir like. However, in fact, the OP profiles include some contributions from fluctuations. Moreover, in practice it is impossible to determine separately and uniquely the contributions which the CCF receives either from the mean field profiles of the OP field or from fluctuations around the latter. In addition, even within mean field theory of continuous phase transitions the correlation length diverges at the critical point. This divergence is the very reason for the emergence of universality which in turn characterizes, *inter alia*, the critical Casimir effect.

The universal nature of CCFs distinguishes them from the depletion forces discussed in the previous section. The latter ones are due to short-ranged fluctuations and thus are very sensitive to microscopic details (on the scale of the size of the depletion agents or shorter). In contrast, CCFs are due to long-ranged fluctuations. The long-ranged fluctuations can give rise to algebraically decaying forces whereas depletion forces always decay at least exponentially and they exhibit oscillations, which signal the presence of microscopic length scales. Instead, CCFs decay monotonically, because they do not depend on microscopic length scales.

1. Mean field theory

Concerning the full range of parameters, theoretical predictions for the universal scaling function of the CCP between spheres are available only within mean field theory (Hanke *et al.*, 1998; Schlesener, Hanke, and Dietrich, 2003).

Within the Landau-Ginzburg-Wilson approach, the CCF is conveniently calculated using the stress tensor $\mathcal{T}(\phi(\mathbf{r}))$ in terms of the mean field profile $\phi(\mathbf{r})$ (Cardy, 1987):

$$\mathbf{f}_C = k_B T \int_{\mathcal{A}} d^{d-1} r \mathcal{T}(\phi(\mathbf{r})) \cdot \mathbf{n}, \quad (16)$$

where \mathcal{A} is an arbitrary $(d-1)$ -dimensional surface enclosing a colloid, \mathbf{n} is the outward normal of this surface, and $\mathbf{f}_C = f_C \mathbf{e}$ is the force between two colloids, where \mathbf{e} is a unit vector along the line connecting their centers. The orientation of \mathbf{e} is such that $f_C < 0$ (> 0) corresponds to attraction (repulsion). In most cases the mean field profile $\phi(\mathbf{r})$ is determined by

numerical minimization of the Landau-Ginzburg-Wilson Hamiltonian encompassing suitable surface contributions from the colloid surfaces in order to account for symmetry-breaking BCs there. In $d = 3$ spatial dimensions such a theory is approximate. In the spirit of a systematic expansion in terms of $\epsilon = 4 - d$, it is exact in $d = 4$ for four-dimensional spheres. Within the Landau-Ginzburg-Wilson mean field approach, the universal scaling function can be determined only up to an unknown prefactor. An appropriate way to cope with this uncertainty and in order to facilitate the comparison with experimental or other theoretical results is to express the scaling function in units of the well-known critical Casimir amplitude for the film geometry so that in this ratio the unknown prefactor drops out (see Sec. II.B.4).

Recently, the same approach was employed in order to calculate the scaling function of the CCFs for three-dimensional spheres posing as hypercylinders ($H_{d=4,d^*=3}$) in spatial dimension $d = 4$,¹ where $H_{d,d^*} = \{\mathbf{r} = (\mathbf{r}_\perp, \mathbf{r}_\parallel) \in \mathbb{R}^{d^*} \times \mathbb{R}^{d-d^*} \mid |\mathbf{r}_\perp| \leq R\}$ (Mohry *et al.*, 2014). The results obtained differ from the ones for four-dimensional spherical particles $H_{d=4,d^*=4}$ in $d = 4$. This raises the question whether $H_{d=4,d^*=3}$ or $H_{d=4,d^*=4}$ renders the better mean field approximation for the physically relevant case of three-dimensional spheres $H_{d=3,d^*=3}$ in $d = 3$. Because of this uncertainty more accurate theoretical approaches are highly desirable. Recent MC simulations of a sphere near a wall constitute the first step in this direction (Hasenbusch, 2013).

The mean field Landau-Ginzburg-Wilson theory is a versatile approach for calculating CCFs. In the case of the simple film geometry, this approximate approach correctly reproduces the qualitative behavior of CCFs (i.e., their sign, functional form, and structure) for various combinations of surface universality classes. Therefore it has been used to calculate CCFs for various shapes of colloidal particles and for other geometries. Nonspherical, i.e., highly ellipsoidal or spherocylindrical colloids, or elongated particles such as cylindrical micelles (Gilroy *et al.*, 2010), block copolymers (Walther *et al.*, 2009), the mosaic tobacco virus (Namba and Stubbs, 1986), and carbon nanotubes (Pérez-Juste *et al.*, 2005; Zhao and Fang, 2006) are experimentally available and widely used in the corresponding current research efforts, with application perspectives toward new materials in mind. The orientation-dependent CCP for ellipsoidal particles near a planar wall at vanishing bulk field $h_b = 0$ was studied by Kondrat, Harnau, and Dietrich (2009). In this case, due to the anisotropy of the particles, there is not only a force but also a torque acting on the particle. This may lead to additional interesting effects such as the orientational ordering of nonspherical colloids in a critical solvent. The behavior of hypercylinders $H_{d=4,d^*=3}$ and $H_{d=4,d^*=2}$ near planar, chemically structured substrates was studied by Tröndle *et al.* (2009, 2010). Mattos, Harnau, and Dietrich (2013) calculated the scaling function associated with CCFs for a system consisting of two spherical particles facing a planar, homogeneous substrate. This allows one to determine the change of the lateral CCF between two colloids upon approaching a wall

which acts like a large third body. Within the applied mean field theory, this many-body contribution can reach up to 25% of the pure pair interaction. As one would expect, the many-body effects were found to be more pronounced for small distances as well as for temperatures close to criticality. This trend has been confirmed by studying three parallel hypercylinders within mean field theory (Mattos, Harnau, and Dietrich, 2015) and three disks in $d = 2$ within MC simulations (Hobrecht and Hucht, 2015). Three-body interactions in $d = 3$ for spherical colloids have been determined experimentally (Paladugu *et al.*, 2016). However, at the present stage these data cannot yet be compared quantitatively with theoretical results. Labbé-Laurent *et al.* (2014) determined the CCP for the ensuing alignment of cylindrical colloids near chemically patterned substrates within mean field theory. The case in which the particles exhibit spatially inhomogeneous surface properties, forming so-called Janus particles carrying two opposing BCs, was also considered (Labbé-Laurent and Dietrich, 2016). The experimental fabrication of such particles is of research interest in itself (Prasad *et al.*, 2009; Walther *et al.*, 2009; Yi, Pine, and Sacanna, 2013; Labbé-Laurent and Dietrich, 2016) as is the theoretical understanding of the interactions between spherical (Hong *et al.*, 2006; Sciortino, Giacometti, and Pastore, 2009; Labbé-Laurent and Dietrich, 2016) or nonspherical Janus particles (Li *et al.*, 2012; Liu *et al.*, 2012; Labbé-Laurent and Dietrich, 2016), because they are considered to be promising building blocks for self-assembling materials (Viry *et al.*, 2010; Jiang *et al.*, 2011; Iwashita and Kimura, 2013, 2014).

2. Beyond mean field theory

Beyond mean field theory, theoretical predictions for the CCP for two spheres immersed in a critical fluid are available from conformal field methods which, however, are restricted to the bulk critical point of the solvent and to $d = 2$. As mentioned in passing, the exact analytical results for the limiting behavior of spheres which nearly touch [Eq. (15)] and spheres which are widely separated [Eq. (14)] have been obtained by using conformal invariance of the free energy and taking the Derjaguin limit in the first case and applying the small-sphere expansion in the second case, respectively (Burkhardt and Eisenriegler, 1995). For the 2D Ising universality class, the CCP has been calculated numerically (Burkhardt and Eisenriegler, 1995) within the full range of distances D between two spheres. More recently, this was also achieved analytically (Machta, Sethna, and Veatch, 2012) via the partition function of the critical Ising model on a cylinder, using a conformal mapping onto an annulus. For nonspherical colloidal particles with their dumbbell or lens shapes being small compared to the correlation length and to the interparticle distances, exact results for the orientation-dependent CCFs have been obtained by using a small-particle operator expansion and by exploiting conformal invariance for $d \lesssim 4$ and $d = 2$ (Eisenriegler, 2004). In fact, in $d = 2$ conformal field theory provides a general scheme for critical Casimir interactions between two (or more) objects of arbitrary shape (Bimonte, Emig, and Kardar, 2013). This can be achieved by using the local conformal mappings of the exterior region of two such objects onto a circular annulus for which the stress

¹In the present notation d and d^* correspond to D and d used by Mohry *et al.* (2014), respectively.

tensor is known. Assuming the availability of a simple transformation law for the stress tensor under any such local conformal mappings, the CCFs are obtained from the contour integral of the transformed stress tensor along a contour surrounding either one of the two objects (Bimonte, Emig, and Kardar, 2013).

Another nonperturbative approach, which allows one to calculate CCFs directly at a fixed specific spatial dimension potentially an advantage over field-theoretic approaches based on a systematic expansion in terms of $\epsilon = 4 - d$, is the use of semiempirical free energy functionals for critical inhomogeneous fluids and Ising-like systems. They were developed by Fisher and Upton (1990) in order to extend the original de Gennes–Fisher critical-point ansatz (Fisher and de Gennes, 1978; Fisher and Au-Yang, 1980). Upon construction, these functionals fulfill the necessary analytic properties as a function of T and a proper scaling behavior for arbitrary d . The only input needed is the bulk Helmholtz free energy and the values of the critical exponents. (However, the available functional is valid only for symmetry-breaking BCs.) The predictions of this functional for films with $(+, +)$ boundary conditions are in very good agreement with previous results obtained by ϵ expansion and conformal invariance for the scaling function of the OP and for the critical Casimir amplitudes (Borjan and Upton, 1998). Also the predictions for the full scaling functions of the CCFs at $h_b = 0$ (Borjan and Upton, 2008) are in good agreement with results from MC simulations. These predictions have been obtained from a linear parametric model, which in the neighborhood of a critical point provides a simple scaled representation of the Helmholtz free energy in terms of “polar” coordinates (r, θ) centered at the critical point $(t, h_b, \phi) = (0, 0, 0)$, where r is a measure of the distance from the critical point and which assumes a linear relationship between the OP ϕ and θ . A similar local-functional approach proposed by Okamoto and Onuki (2012) used a form of the bulk Helmholtz free energy which differs from the one employed by Borjan and Upton (2008), in that it is a field-theoretic expression for the free energy with (in the sense of renormalization group theory) renormalized coefficients. Such a version does not seem to produce more accurate results for the Casimir amplitudes (Okamoto and Onuki, 2012). Within this renormalized local-functional approach, the CCFs between two spherical particles immersed in a near-critical binary solvent (consisting of a and b particles) have been calculated as a function of both scaling fields T and h_b (Okamoto and Onuki, 2013). The focus of the study is the situation that the b -rich phase forms on the colloid surfaces in thermal equilibrium with the subcritical a -rich bulk solvent ($T < T_c^{(s)}$ and $h_b < 0$). This gives rise to a bridging transition between two spherical particles and the resulting effective forces are of different nature than the CCFs (see Sec. II.B.6). We note that the validity of the extended de Gennes–Fisher or renormalized local-functional approach in the presence of bulk ordering fields has not yet been tested, not even for the simple film geometry.

3. Computer simulations

In cases in which one cannot obtain analytical results, MC simulations offer a highly welcome tool in order to overcome

the shortcomings of approximate theoretical approaches and to study CCPs within the whole temperature range and also in the presence of the bulk ordering field h_b . In the case that the solvent is a simple fluid and in the spirit of the universality concept of critical phenomena, one can study the simplest representative of the corresponding universality class of the critical solvent, e.g., spin models such as the Ising lattice gas model. In the case of a lattice, the derivative in Eq. (9) is replaced by a finite difference $\Delta \mathcal{F}^{\text{ex}}$ associated with a single lattice spacing. This also requires one to introduce a lattice version of a spherical particle. In general, MC methods are not efficient to determine quantities such as the free energy, which cannot be expressed in terms of ensemble averages. Nevertheless, free energy differences can be cast into such a form via the so-called “coupling parameter approach” (Mon, 1989; Mon and Binder, 1990). This approach can be applied for systems characterized by two distinct Hamiltonians \mathcal{H}_0 and \mathcal{H}_1 but the same configurational space. In such a case, one can introduce the crossover Hamiltonian $\mathcal{H}_{cr}(\lambda) = (1 - \lambda)\mathcal{H}_0 + \lambda\mathcal{H}_1$, which interpolates between \mathcal{H}_0 and \mathcal{H}_1 as the crossover parameter $\lambda \in [0, 1]$ increases from 0 to 1. The difference between the free energies of two systems characterized by these different Hamiltonians can be conveniently expressed as an integral with respect to λ over canonical ensemble averages of $\mathcal{H}_1 - \mathcal{H}_0$ (with the averages taken by using the corresponding crossover Hamiltonian for a given value of the coupling parameter). Alternatively, the free energy difference can be determined by integrating the corresponding difference of internal energies over the inverse temperature. The drawback of both methods is that they usually require knowledge of the corresponding bulk free energy density (as in the case of CCFs for a slab geometry). The accurate computation of the bulk free energy density poses a numerical challenge by itself and extracting it from finite-size data requires an accurate analysis. Moreover, the internal energy differences, when determined by using standard MC algorithms, are affected by large variances, especially for nonplanar geometries such as the sphere-planar wall or the sphere-sphere geometry. In such geometries, the differences between local energies of the two systems with different (by one lattice spacing) sphere-wall or sphere-sphere distances are large only close to the sphere or the wall. This implies that the variance is dominated by the remaining part of the system, for which the local energy difference is very small. Recently a more sophisticated algorithm (Hasenbusch, 2013) and new approaches (Hobrecht and Hucht, 2014) were developed in order to overcome these problems. The numerical method proposed by Hobrecht and Hucht (2014) is analogous to the experimental one used by Hertlein *et al.* (2008) according to which the CCP is inferred directly from the Boltzmann distribution function of the positions of the two interacting objects. (In this experiment a sphere performs Brownian motion near a planar substrate.) So far, the improved algorithm of Hasenbusch (2013) and the dynamic method of Hobrecht and Hucht (2014) have been applied only to the slab geometry and to the geometry of a single sphere (or disk) near a planar wall. The only available simulation data for two quasisphears in the $d = 3$ Ising model have been obtained by using a method based on the integration of the local magnetization over the applied local magnetic field (Vasilyev,

2014). In that study, the CCP has been calculated at fixed distances between the two spheres as a function of the temperature scaling variable [related to $\text{sgn}(t)(D/\xi_t)$] for a few values of h_b , or as a function of the bulk field scaling variable [related to $\text{sgn}(h_b)(D/\xi_h)$] for several temperatures. Results of this calculation have been obtained only for small separations $D \leq 2R$, where $R = 3.5$ (in units of the lattice spacing a) is the radius of the particle, because the strength of the potential decreases rapidly upon increasing D . The accuracy of these data deteriorates at low temperatures.

Alternative ways of computing the sphere-sphere CCP via MC simulations have been used for two-dimensional lattice models. One of them (Machta, Sethna, and Veatch, 2012) uses Bennett's method (Bennett, 1976), according to which one can efficiently estimate the free energy difference between two canonical ensembles, characterized by two different energies E_0 and E_1 with the same configuration space, provided that these two ensembles exhibit a significant overlap of common configurations. This method was employed for the 2D Ising model, with frozen spins forming two quasisphears with an effective radius R ; in the reference ensemble (with energy E_0) the quasisphears are separated by a distance D whereas in the second ensemble (with energy E_1), they are separated by a distance $D + a$ (Machta, Sethna, and Veatch, 2012). In order to estimate the corresponding free energy difference, within this approach one considers a trial move which keeps the configuration space the same but switches the energy from E_0 to E_1 , e.g., by mimicking the move of one of the particles from a distance D to a distance $D + a$ by suitably changing and exchanging spins. The estimate of the free energy difference is given by $F_1 - F_0 = -k_B T \ln \langle \exp[(E_0 - E_1)/k_B T] \rangle_0$, where the canonical ensemble average $\langle \cdot \rangle_0$ is taken with respect to the "reference" ensemble with the energy E_0 . Integrating this free energy difference up to infinity, one obtains the CCP. Machta, Sethna, and Veatch (2012) provided the results for the CCP as a function of distance $D/R \gtrsim 25$ for four values of the temperature in the disordered phase of the solvent, i.e., $T \geq T_c^{(s)}$ and $h_b = 0$. At the critical temperature, these MC simulation results agree well with the analytical ones obtained from conformal field theory. Still another route toward determining the CCP from MC simulations was followed by Edison, Tasios *et al.* (2015) and Tasios *et al.* (2016) for two quasidisks immersed in a 2D lattice model of a binary liquid mixture (Rabani *et al.*, 2003). Here the pair potential $V_C(x, y)$ was obtained from the numerically determined probability $P(x, y)$ of finding one colloid at position (x, y) provided that another one is fixed at the origin: $V_C(x, y) = -k_B T \ln[P(x, y)/P(\infty, \infty)]$. In order to determine $P(x, y)$ accurately at fixed values of $h_b \sim \Delta\mu - \Delta\mu_c$ and T , the so-called transition matrix MC technique (Errington, 2003) was employed. This technique relies on monitoring the attempted transitions between macrostates, as defined, for example, by specific positions of the two quasidisks, and on using this knowledge in order to infer their relative probability $P(Y)/P(Y')$, where Y and Y' are two distinct states of the system; once sufficient transition data are collected, the entire probability distribution $P(Y)$ can be constructed. The studies of Edison, Tasios *et al.* (2015) and Tasios *et al.* (2016) focused on the case that the b -rich phase adsorbs on the colloid

surfaces in thermal equilibrium with a supercritical a -rich bulk solvent ($T \geq T_c^{(s)}$ and $h_b \leq 0$). It was found that data for $U_C = V_C/k_B T$ obtained for $h_b = 0$ and $D \ll R$ collapse on a common master curve if multiplied by $(D/R)^{1/2}$ and plotted as a function of D/ξ_t , i.e.,

$$\begin{aligned} (D/R)^{1/2} U_C &= \Theta(\mathcal{Y} = \text{sgn}(t)D/\xi_t, \Delta = D/R = 0, \Lambda \\ &= \text{sgn}(h_b)D/\xi_h = 0). \end{aligned}$$

The scaling exponent $1/2$ for the prefactor agrees with the prediction in Eq. (15) for $d = 2$, which is obtained based on the conformal invariance in the Derjaguin limit $D \ll R$, and which implies $\Theta(y \rightarrow 0, \Delta \rightarrow 0, \Lambda \rightarrow 0) = \text{const.}$

The standard algorithms used for the MC simulation studies described are based on trial moves generating a trial configuration, which are local (Metropolis-type flips of spins) and hence become very slow near the critical point. This critical slowing down effect can be weakened by using so-called cluster algorithms such as the Swendsen and Wang (1987) or the Wolff (1989) algorithm in which instead of a single spin a whole cluster of spins is flipped simultaneously. The Wolff algorithm constructs clusters which consist of spins that are aligned and connected by bonds. The proof that the Wolff algorithm obeys detailed balance, and hence generates the Boltzmann distribution, hinges on the spin inversion symmetry of the Hamiltonian. [The Wolff algorithm can be generalized to systems that contain bulk or surface fields (Landau and Binder, 2009).] One can also exploit other symmetries in order to develop a cluster method, for example, by using geometric operations on the spin positions such as point reflection or rotation with respect to a randomly chosen "pivot." Hobrecht and Hucht (2015) extended the geometric cluster algorithm (GCA) introduced by Heringa and Blöte (1998) for bulk Ising models in the absence of external fields to the case of Ising systems containing areas of spins with a fixed orientation, facilitated by infinitely strong bonds, which mimic a colloidal suspension. The GCA makes use of the invariance of the Hamiltonian with respect to a point inflection in order to construct two symmetric clusters of spins which are then exchanged. Contrary to the Wolff cluster algorithm, the GCA conserves the OP. The modification due to Hobrecht and Hucht consists of including into the clusters not only spins but also the bond configuration between them. This way, the particles, encoded into the bond configuration, can be moved and the configuration of a solvent represented by the Ising spins can be updated within one cluster step. In the cluster exchange the neighboring lattice sites i and j as well as the connecting bond $\langle ij \rangle$ are mapped via point reflection with respect to a pivot onto the sites i' and j' and the bond $\langle i'j' \rangle$, respectively. Using this apparently efficient MC cluster algorithm, Hobrecht and Hucht (2015) studied two-dimensional systems with a fixed number of identical, disklike particles defined as regions of fixed positive spins, which thus effectively impose symmetry-breaking (+) BC onto the surrounding free spins. Within this scheme, they calculated the two- and three-body CCP at the bulk critical point of the Ising model. They reported strong finite-size effects: for periodic simulation boxes with a fluctuating total magnetization, the presence of a nonzero number density of colloidal

particles with a non-neutral surface preference for up and down spins shifts the system away from the critical point. As a result, their MC results for the CCP do not exhibit the form expected to hold at the critical point for a single pair of particles in solution [Eqs. (14) and (15)]. In order to suppress this effect, [Hobrecht and Hucht \(2015\)](#) proposed to use a fixed total magnetization $M = 0$ or to insert in addition the same number of particles but with the opposite surface preference.

4. Derjaguin approximation

a. General discussion

Within the so-called Derjaguin approximation curved, smooth surfaces are approximated by surfaces which are a steplike sequence of parallel planar pieces ([Hobrecht and Hucht, 2015](#)). Between two *vis à vis*, flat pieces of the opposing surfaces partitioned this way, locally a force acts as in the slab geometry and the total force is taken to be the sum of the forces between each individual pair with the appropriate areal weight. For two spheres with the same radius R , this yields for the radial force F at surface-to-surface separation $D \ll R$:

$$F(D) = \pi R V_{\parallel}(D), \quad (17)$$

where $V_{\parallel}(D)$ is the interaction energy per unit area of two parallel walls separated by D . The Derjaguin approximation is widely used to estimate the effective interactions between colloidal particles, because the forces between parallel surfaces are much easier to calculate. Indeed, for the slab geometry the CCFs are known even beyond mean field theory (see later). Therefore, by using this approximation one can account even for non-Gaussian critical fluctuations, albeit at the expense of not fully considering the shape of the particles. The Derjaguin approximation is valid for temperatures which correspond to $\xi_t \lesssim R$, because under this condition the CCFs between the colloids act only at surface-to-surface distances D which are small compared with R . In many cases this approximation is surprisingly reliable even for $D \lesssim R$ ([Gambassi et al., 2009](#); [Tröndle et al., 2009, 2010](#)).

Knowing the universal scaling function $\tilde{\vartheta}_{\parallel}^{(d=3)}(\mathcal{Y}, \Lambda) = f_C^{\parallel}(D, T, h_b) D^3 / k_B T S$ of the CCF for the film geometry (\parallel) with macroscopically large surface area S of each wall, one can calculate the scaling function of CCF between two spheres ($\circ\circ$). Summing up the contributions stemming from all parallel planar pieces one obtains, in $d=3$, $f_C^{\circ\circ} / k_B T \simeq \int dS f_C^{\parallel} = 2\pi \int_0^R d\rho \rho f_C^{\parallel}(D(\rho))$, where $D(\rho) = D + 2R[1 - \sqrt{1 - (\rho/R)^2}]$. This leads to the scaling function

$$\vartheta_{(\circ\circ)}^{(d=3, \text{Derj})}(\mathcal{Y}, \Delta, \Lambda) = \pi \int_1^{1+2\Delta^{-1}} dx x^{-d} \left[1 - \frac{\Delta}{2}(x-1) \right] \tilde{\vartheta}_{\parallel}^{(d)}(x\mathcal{Y}, x\Lambda). \quad (18)$$

In many instances it is sufficient to set Δ to zero in Eq. (18). Thus, in this limit and within the Derjaguin approximation, the scaling function $\vartheta_{(\circ\circ)}^{(d=3, \text{Derj})}$ does not depend on Δ .

Based on exact results in $d=2$ ([Evans and Stecki, 1994](#); [Abraham and Maciolek, 2010, 2013](#)) and in $d=4$ ([Krech,](#)

[1997](#)), and based on the predictions from the local-functional approach in $d=3$ ([Borjan and Upton, 2008](#)), it is expected that the CCF $f_C(D)$ between two planar walls with symmetry-breaking ($++$) BCs at separation D varies as $\exp(-D/\xi_t)$ for $D \gg \xi_t$ and $t > 0$, i.e., in the one-phase region of the solvent. This implies that the asymptotic behavior of the scaling function is given by

$$\begin{aligned} \tilde{\vartheta}_{\parallel}^{(d=3)}(\mathcal{Y} = \text{sgn}(t)D/\xi_t \gg 1, \Lambda = \text{sgn}(h_b)D/\xi_h = 0) \\ = \mathcal{A}_+ \mathcal{Y}^d \exp(-\mathcal{Y}), \end{aligned}$$

where $\mathcal{A}_+ = 1.2\text{--}1.5$ is a universal number valid for ($++$) BCs ([Gambassi et al., 2009](#)). By applying the Derjaguin approximation to this functional form of the CCFs, one obtains the following asymptotic behavior of the scaling function $\Theta_{\oplus\oplus}^{(d=3, \text{Derj})}(\mathcal{Y}, \Lambda = \text{sgn}(h_b)D/\xi_h = 0)$ for the sphere-sphere CCP:

$$\begin{aligned} \Theta_{\oplus\oplus}^{(d=3, \text{Derj})}(\mathcal{Y} \rightarrow \infty, \Lambda = \text{sgn}(h_b)D/\xi_h = 0) = \pi \mathcal{A}_+ \mathcal{Y} e^{-\mathcal{Y}}, \\ D \gg \xi_t, \quad t > 0, \end{aligned} \quad (19)$$

so that in this limit

$$U_C^{(d=3, \text{Derj})} = \pi \mathcal{A}_+ \frac{R}{\xi_t} e^{-D/\xi_t} \quad (20)$$

[Eq. (11)]. Because the Derjaguin approximation is extensively used in the context of critical Casimir interactions, in the next section we summarize the present knowledge of CCFs for the film geometry.

b. Critical Casimir interactions for the film geometry

In the absence of a bulk ordering field, i.e., for $h_b = 0$ and strongly adsorbing ($++$) confining surfaces, the results for the critical Casimir interactions in the film geometry have been provided by field-theoretical studies ([Krech, 1997](#)), the extended de Gennes–Fisher local-functional method ([Borjan and Upton, 2008](#); [Okamoto and Onuki, 2012](#); [Mohry et al., 2014](#)), and MC simulations of the Ising model ([Vasilyev et al., 2007, 2009](#); [Hasenbusch, 2012](#)) or improved models which offer the benefit that the amplitude of the leading bulk correction to scaling vanishes ([Hasenbusch, 2010, 2012, 2015](#); [Toldin and Dietrich, 2010](#); [Parisen Toldin, Tröndle, and Dietrich, 2013](#)). Within MC simulations the case of weakly adsorbing surfaces was also considered ([Hasenbusch, 2011](#); [Vasilyev, Maciolek, and Dietrich, 2011](#)). In this latter case the corresponding surface field h_s might be so small that upon approaching the critical point one effectively observes a crossover of boundary condition imposed on the OP from symmetry-preserving to symmetry-breaking BCs. In this case there appears to be no effective enhancement of the OP upon approaching the confining wall. The CCP reflects such crossover behaviors; depending on the film thickness, the CCP can even change sign ([Mohry, Maciolek, and Dietrich, 2010](#); [Hasenbusch, 2011](#); [Vasilyev, Maciolek, and Dietrich, 2011](#)). On the basis of scaling arguments one expects that for moderate adsorption

preferences the scaling function of the CCP in film geometry additionally depends on the dimensionless scaling variables $y_s^{(i)} = a_i h_s^{(i)} L^{\Delta_1/\nu}$, $i = 1, 2$, where $h_s^{(1)}$ and $h_s^{(2)}$ are the effective surface fields at the two confining surfaces, a_1 and a_2 are nonuniversal amplitudes, and $\Delta_1 = 0.45672(5)$ (Hasenbusch, 2011) is the surface crossover exponent at the so-called ordinary surface phase transition (see Sec. IV.C for an experimental example).

Knowledge of the dependence of CCP on the bulk ordering field h_b is rather limited, although it is crucial for understanding the aggregation of colloids near the bulk critical point of their solvent. The presently available MC simulations for Ising films provide such results only along the critical isotherm $T = T_c^{(s)}$ (Vasilyev and Dietrich, 2013). In Schlesener, Hanke, and Dietrich (2003), Mohry, Maciolek, and Dietrich (2012a, 2012b), and Mohry *et al.* (2014) the variation of CCFs with h_b has been approximated by adopting the functional form obtained within mean field theory ($d = 4$) by using a field-theoretical approach within the framework of the Landau-Ginzburg-Wilson theory, but by keeping the actual critical exponents in $d = 3$ for the scaling variables. Within this “dimensional” approximation, the scaling function of the CCF for the film geometry is taken to be

$$\begin{aligned} \vartheta_{\parallel}^{(d=3)}(\mathcal{Y} = \text{sgn}(t)D/\xi_t, \Sigma = \Lambda/\mathcal{Y} = \text{sgn}(th_b)\xi_t/\xi_h) \\ \simeq \vartheta_{\parallel}^{(d=3)}(\mathcal{Y}, \Sigma = 0) \vartheta_{\parallel}^{(d=4)}(\mathcal{Y}, \Sigma) / \vartheta_{\parallel}^{(d=4)}(\mathcal{Y}, \Sigma = 0), \end{aligned}$$

where $\vartheta_{\parallel}^{(d=3)}(\mathcal{Y}, \Sigma = 0)$ has been adopted from MC simulation data (Vasilyev *et al.*, 2007, 2009). [The normalization by $\vartheta_{\parallel}^{(d=4)}(\mathcal{Y}, \Sigma = 0)$ eliminates a nonuniversal prefactor carried by the Landau-Ginzburg-Wilson expression for the scaling function of the CCF.] Mohry *et al.* (2014) compared the scaling functions $\vartheta_{\parallel}^{(d=3)}$ resulting from the dimensional approximation with those obtained within the extended de Gennes–Fisher local functional. This allows us to compare in Fig. 1 (unpublished) results for the scaling function $\Theta_{\oplus\oplus}^{(d=3, \text{Derj})}(\mathcal{Y}, \Sigma)$ of the sphere-sphere CCP [see Eq. (11)] within the Derjaguin approximation, i.e.,

$$\begin{aligned} \Theta_{\oplus\oplus}^{(d=3, \text{Derj})}(\mathcal{Y}, \Sigma) &\simeq (D/R)U_c \\ &= \pi \int_1^{\infty} dx (x^{-2} - x^{-3}) \vartheta_{\parallel}^{(d=3)}(x\mathcal{Y}, \Sigma) \end{aligned}$$

(Mohry *et al.*, 2014), where $\vartheta_{\parallel}^{(d=3)}$ is obtained by using these two aforementioned approaches. Only for weak bulk fields the curves in Fig. 1 for both approaches compare well. Otherwise there are clear quantitative discrepancies, the origin of which is not clear. The dimensional approximation might deteriorate upon increasing h_b . On the other hand, as mentioned, the reliability of the local-functional approach for $h_b \neq 0$ has not yet been tested systematically. For example, the result of the local-functional approach for the scaling function of the CCFs along the critical isotherm differs substantially from the MC simulations (Mohry *et al.*, 2014). Buzzaccaro *et al.* (2010) and Piazza *et al.* (2011) reported results of a long wavelength

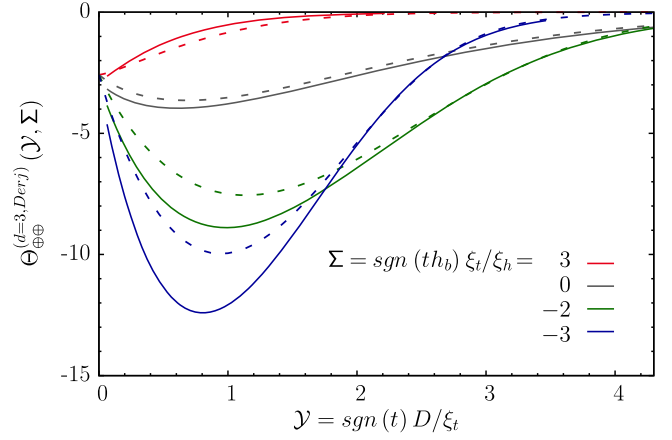


FIG. 1. Scaling function $\Theta_{\oplus\oplus}^{(d=3, \text{Derj})}(\mathcal{Y}, \Sigma) \simeq (D/R)U_c(D; t, h_b, R)$ [see Eq. (11) and the main text] of the sphere-sphere CCP, as obtained within the Derjaguin approximation by using the extended de Gennes–Fisher functional (solid lines) and the “dimensional” approximation (dashed lines) as a function of the surface-to-surface distance D (in units of ξ_t) for several values of the scaling variable $\Sigma = \Lambda/\mathcal{Y} = \text{sgn}(th_b)\xi_t/\xi_h$ related to the bulk ordering field h_b . At fixed temperature in the one-phase region of the solvent ($t > 0$), the CCP is shorter ranged and much weaker for $h_b > 0$ (i.e., $\Sigma > 0$), which favors the same (+) phase of the solvent as the one preferred by the colloid surfaces, than for $h_b < 0$ (i.e., $\Sigma < 0$), which favors the other phase.

analysis of density functional theory for the scaling function of the CCF (see also Sec. II.B.5); they are in qualitative agreement with the results obtained using the extended de Gennes–Fisher local functional (Mohry *et al.*, 2014). The first microscopic off-lattice results for the scaling function of the CCF, both along the critical isochore and in the off-critical regime, have been worked out by Anzini and Parola (2016). Anzini and Parola (2016) studied a hard-core Yukawa model of a fluid by using DFT within a specific weighted density approximation (Leidl and Wagner, 1993), coupled with hierarchical reference theory (Parola and Reatto, 1995). This kind of DFT weighted density approximation, related to the one proposed early on by Tarazona (1985) and independently by Curtin and Ashcroft (1985), captures the short-ranged correlations of the underlying hard-sphere fluid rather accurately, whereas the hierarchical reference theory is also able to account for the critical properties of a homogeneous fluid. Anzini and Parola (2016) applied this technique in order to determine the effective interaction between two hard walls immersed in that fluid. This approach facilitates investigating the crossover between depletionlike roots of such effective forces at high temperatures and the critical Casimir effect upon approaching the critical point of the fluid. It appears that for hard-core Yukawa fluids the universal features of CCF emerge only in close neighborhood of the critical point. The predictions obtained by Anzini and Parola (2016) for the scaling function of the CCF for various temperatures along the critical isochore ($h_b = 0$) differ significantly from the Ising model MC simulation results by Vasilyev *et al.* (2009). Moreover, the data along various isotherms do not collapse as expected from scaling theory. Anzini and Parola (2016) interpreted these deviations as an

indication of strong corrections to scaling occurring in the hard-core Yukawa fluid.

Recently, in the slab geometry the first direct computation of the CCF from off-lattice simulations of a binary liquid mixture was reported (Puosi *et al.*, 2016). A binary liquid mixture of species a and b which interact via smoothly truncated Lennard-Jones potentials was simulated in the semigrand canonical ensemble, by using hybrid molecular dynamics and Metropolis MC simulations. The differential of the semigrand canonical (SGC) potential $\Omega_{\text{SGC}}(T, N, V, \Delta\mu)$ is given by

$$d\Omega_{\text{SGC}} = -SdT - (p - \mu n)dV - \Delta N d(\Delta\mu), \quad (21)$$

where $n = N/V$ is the overall number density, which is kept constant, $N = N_a + N_b$ is the fixed total number of molecules, $\Delta N = N_a - N_b$, $\Delta\mu = \mu_a - \mu_b$ is the difference of the chemical potentials μ_α , $\alpha \in \{a, b\}$, of the two species, and $\mu = (\mu_a + \mu_b)/2$. This implies that within the semigrand canonical ensemble the CCF emerges from the system size dependence of the generalized pressure $\tilde{p} = p - \mu n$, which is conjugate to volume changes at fixed n rather than from the pressure itself. Within molecular dynamics simulations the pressure can be computed from the virial formula (Hansen and McDonald, 1986). However, the determination of the excess generalized pressure, which is the difference between two strongly fluctuating quantities, proved to be at the limit of available computing resources. Accordingly, the numerical data are very noisy and thus carry large error bars. However, the results obtained by Puosi *et al.* (2016), although being interesting as such, in particular, concerning the occurrence of the pressure anisotropy associated with the confinement, are not relevant for colloidal systems because the simulation data pertain to periodic BCs.

As far as experimental data for the film geometry are concerned, they are available only indirectly from measurements of the thickness of wetting films; they correspond to opposing (+ −) BCs (Fukuto, Yano, and Pershan, 2005; Rafai *et al.*, 2007). The scaling function of the CCF determined by Fukuto, Yano, and Pershan (2005) compared well with the theoretical predictions. The measurements performed by Rafai *et al.* (2007) provided data which show stronger deviations from the theoretical curves, in particular, around the maximum of the CCF. The scaling function of the CCF for wetting films corresponding to (+ +) BCs could not be determined due to the collapse of the incomplete wetting film in the course of the measurements (Rafai *et al.*, 2007). For a discussion of experimental studies of CCFs see Sec. IV.A.

5. Pair potential in the presence of depletants

In order to interpret their experimental data (see Sec. IV.E for details), Buzzaccaro *et al.* (2010) and Piazza *et al.* (2011) determined the effective pair potential between two large hard spheres immersed in a fluid of depletants close to their gas-liquid critical point. They used DFT, which is a powerful tool for describing equilibrium properties of colloidal suspensions (see Sec. II.A). The hard spheres have been analyzed within the Derjaguin approximation, which is inherent in recent approaches to depletion forces acting in hard-sphere mixtures.

In this context, the Derjaguin approximation relates the force between the two big objects to the integral of the solvation force $f_{\text{solv}}(D) = -(1/S)((\partial\Omega/\partial D)_{\mu,T,S} - p)$ of the small particles (i.e., the depletant agents) confined between two parallel planar walls with cross-sectional area S . (The film solvation force f_{solv} per surface area S is an excess pressure over the bulk value p of the confined fluid described by the grand potential Ω .) In the limiting case of hard walls exposed to an ideal gas of depletants, this relation reproduces the well-known Asakura-Oosawa result for depletion forces (Asakura and Oosawa, 1954). This scheme can also be applied to interacting systems. In fact, such a relation is equivalent to the general formula obtained by Derjaguin (1934) relating the force between two convex bodies to the free energy, in excess of its bulk value, of a fluid confined between planar walls. Within an actual DFT approach this formula holds even for approximations of the excess part of an intrinsic Helmholtz free energy functional of a fluid. Within nonlocal DFT, the solvation force between two hard walls can be determined via the exact statistical mechanical relation (Henderson, 1986)

$$f_{\text{solv}}(D) = k_B T [\rho_D(0^+) - \rho_\infty(0^+)], \quad (22)$$

where $\rho_D(0^+)$ is the fluid density at contact with the wall in a confined system, whereas $\rho_\infty(0^+)$ is the corresponding quantity for the separation $D = \infty$. Buzzaccaro *et al.* (2010) and Piazza *et al.* (2011) have not used the contact theorem given by Eq. (22)—rather they employed the square gradient approximation (for which the contact theorem does not hold). The square gradient local-density approximation for the intrinsic Helmholtz free energy functional, which enters into DFT, is valid only for spatially slowly varying depletant number densities ρ such that $\nabla\rho/\rho \ll 1/\xi_t$. In order to incorporate the non-Gaussian behavior near the gas-liquid critical point of the depletant, in the spirit of the Fisk-Widom or local-functional approach (Fisk and Widom, 1969; Fisher and Upton, 1990; Okamoto and Onuki, 2012), Buzzaccaro *et al.* (2010) and Piazza *et al.* (2011) adopted the scaling form for the singular part of the bulk free energy density of the fluid $[f(\rho) - f(\rho_c)]/k_B T = a_{11}t^{2-\alpha}\Psi(x)$ with the scaling variable $x = b_1\phi t^{-\beta}$, where $\phi = \rho - \rho_c$ is the bulk OP, a_{11} and b_1 are nonuniversal, dimensional constants, and β and α are standard bulk critical exponents (Pelissetto and Vicari, 2002). By using a parametric expression for Ψ (Pelissetto and Vicari, 2002) and the critical exponents of the 3D Ising universality class, they obtained good agreement between this analytic approach and the scaling function of the CCF obtained from MC simulations (Vasilyev *et al.*, 2009) at $h_b = 0$. This is not surprising because, within the square gradient local-density approximation, DFT reduces to the local-functional approach which turned out to correctly capture critical fluctuations (Fisher and Upton, 1990; Borjan and Upton, 1998, 2008), at least for $h_b = 0$.

This theoretical approach has been followed up by MC simulation studies (Gnan *et al.*, 2012) aiming at the computation of the CCP between two hard-sphere colloids suspended in an implicit solvent in the presence of interacting depletant particles. In these off-lattice MC simulations of fluctuation-induced forces, the effective potential between two hard spheres has been determined upon approaching the

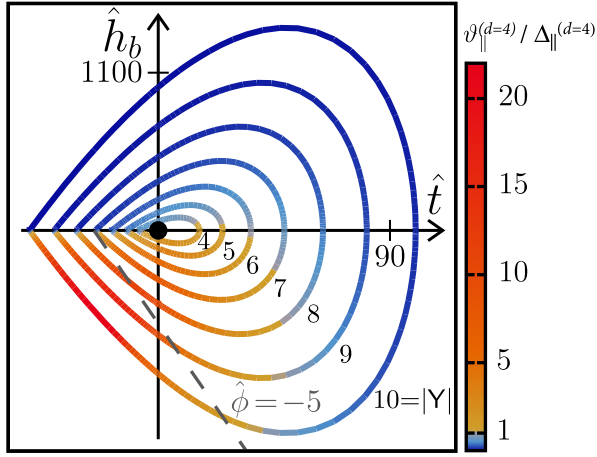


FIG. 2. Normalized mean field CCF scaling function $\vartheta_{\parallel}^{(d=4)}(\mathbf{Y}, \mathbf{\Sigma}) = D^4 f_{\parallel}^{\parallel} / k_B T S$, where $\mathbf{Y} = \text{sgn}(t)D/\xi(t, h_b)$ and $\mathbf{\Sigma} = \text{sgn}(th_b)\xi_t/\xi_h$ for films (of thickness D and macroscopically large cross-sectional area S) along isolines of constant scaling variable $Y = 4, 5, \dots, 10$ (from the inner to the outermost ring) in the thermodynamic state space of the solvent spanned by $\hat{t} = (D/\xi_{t,+})^{1/\nu}t$ and $\hat{h}_b = (D/\xi_h^{(0)})^{\beta\delta/\nu}h_b$; $\xi(t, h_b)$ is the bulk correlation length of the solvent with $\xi_t = \xi(t, h_b = 0)$ and $\xi_h = \xi(t = 0, h_b)$. Note that depending on the particular thermodynamic path under consideration, representations of the scaling function of the critical Casimir force can be more convenient in terms of other scaling variables, such as in Fig. 1 where $\mathcal{Y} = \text{sgn}(t)D/\xi_t$ is chosen. The color along the lines of constant Y indicates the absolute value $|\vartheta_{\parallel}^{(d=4)} / \Delta_{\parallel}^{(d=4)}|$. The bulk critical point of the solvent $(\hat{t}, \hat{h}_b) = (0, 0)$ is indicated by \bullet . The region shown here lies above the capillary transition critical point, where the film coexistence line ends. For $(++)$ BCs, the capillary condensation transition occurs for $\hat{t} < 0$ and $\hat{h}_b < 0$. The dashed line indicates the path of constant OP $\hat{\phi}$ of the solvent $\hat{\phi} = (D/\xi_{t,+})^{1/\nu}\phi/B = -5$, where B is the nonuniversal amplitude of the bulk OP $\phi = B|t|^\beta$. Within mean field theory $\nu = \beta = 1/2$, $\nu/\beta\delta = 1/3$, and $\Delta_{\parallel}^{(d=4)} = \vartheta_{\parallel}^{(d=4)}(Y = 0, \mathbf{\Sigma} = 0)$. From Mohry *et al.*, 2014.

gas-liquid critical point of the depletant for two different depletant models, one for SW and one for 3P particles [see Eq. (8) and thereafter]. Given the computational limitations, they have considered the size ratio q between the hard-sphere depletant and the hard-sphere colloid within the range $0.05 < q < 0.2$. The resulting effective colloid-colloid force has been evaluated by using canonical MC simulations for various fixed values of the depletant concentration in the reservoir. The method consists of performing virtual displacements of each colloid from its fixed position and computing the probability of encountering at least one collision with a depletant particle. The effective colloid-colloid potential follows from integrating the corresponding force. These MC results show that upon cooling the effective potential between two colloidal particles gradually loses its high-temperature, pure hard-sphere depletion character of exhibiting oscillations and transforms into a completely attractive potential with a progressive and significant increase of its range, signaling the onset of critical Casimir forces. For large distances between the

surfaces of the two colloids, the MC data for the CCP fit well to the asymptotic form given by Eq. (20). This numerical study has been extended to the case in which colloids interact with SW depletant particles; this interaction has been continuously modified from hard-core repulsion to strong attraction, thus changing from $(--)$ BCs (i.e., preference for the gas phase) to $(++)$ boundary conditions (i.e., preference for the liquid phase) (Gnan, Zaccarelli, and Sciortino, 2012). For strong colloid-depletant attraction, the effective colloid-colloid potential exhibits oscillations as they occur for the high-temperature depletion potential, modulating its exponentially decaying attractive tail. The variation of the colloid-colloid effective potential upon crossing over from $(--)$ to $(+-)$ and from $(++)$ to $(+-)$ BCs has been determined too. In the asymptotic spatial range these two crossovers are the same. However, in the numerical study by Gnan, Zaccarelli, and Sciortino (2012) only the behavior at short distances has been probed, where the effective potential is dominated by nonuniversal aspects of the solvent-colloid interaction so that the aforementioned pairs of BCs are no longer equivalent.

6. The structure of the critical Casimir force between two identical colloids

We close this section by discussing the structure of critical Casimir interactions between two colloidal particles in very dilute suspensions. This is crucial for interpreting the experimental data concerning the onset of aggregation around the consolute point of the binary solvent in such suspensions, which will be reviewed in Sec. IV.B.

The results for spheres in $d = 3$, obtained from the variety of methods described, tell that they share the same qualitative features of the CCFs with “spheres” in $d = 2$ and 4 as well as with planar walls. This refers to the property that for like BCs CCFs are attractive and it refers to the position of a force maximum along various thermodynamic paths. Around the consolute point of a binary solvent the main features of the CCFs between two planar walls are summarized in Fig. 2 in terms of the force scaling function $\vartheta_{\parallel}^{(d=4)}(\mathbf{Y}, \mathbf{\Sigma})$ obtained from Landau theory [see Fig. 1 of Mohry *et al.* (2014)]. The main message conveyed by Fig. 2 is the asymmetry of the CCFs around the critical point of the solvent with the maximum strength occurring at $h_b \sim \Delta\mu - \Delta\mu_c < 0$, where $\Delta\mu = \mu_a - \mu_b$ is the chemical potential difference of the two species. This asymmetry is a result of the strong influence of capillary condensation, i.e., the shift of the bulk phase diagram due to the presence of surface fields $h_s \sim \delta\Delta\mu_s/k_B T$, where $\delta\Delta\mu_s$ is a local increment at the surface of the chemical potential difference between the two species. In films with identical surfaces, for surface fields $h_s > 0$ two-phase coexistence occurs along the line $h_{cx}(T) < 0$ ending in a (capillary) critical point $(T_{\text{cap}}, h_{\text{cap}})$, where $T_{\text{cap}}(h_s) < T_c$ (for solvents with an upper critical point) and $h_{\text{cap}}(h_s) < 0$ (Evans, 1990).

The analog of capillary condensation for geometries in which one or both surfaces are nonplanar is a bridging transition (Bauer, Bieker, and Dietrich, 2000; Archer *et al.*, 2005; Okamoto and Onuki, 2013). However, there is a conceptual difference. Contrary to capillary condensation, bridging transitions are interfacial phase transitions which leave the bulk phase diagram unchanged. Bridging occurs at

temperatures for which two phases may coexist, i.e., for $T > T_c$ in the case of a binary liquid mixture with a lower consolute point, and it depends on the adsorption properties of the surfaces. If, say, both surfaces favor the α phase rich in species a over the β phase rich in species b , one expects the α phase to form a bridge between the surfaces for a certain chemical potential μ_a of species a such that $\mu_a < \mu_a^{cx}$, where μ_a^{cx} is the value corresponding to bulk coexistence. In an alternative description, this occurs at a concentration $c_a < c_a^{cx}$ slightly smaller than its value c_a^{cx} at bulk coexistence. If the surfaces favor the β phase, the β phase fills the gap between the surfaces forming a bridge for $\mu_a > \mu_a^{cx}$, i.e., the phase separation line for this morphological transition occurs on the other side of the bulk phase diagram, i.e., for $c_a > c_a^{cx}$. Bridging may occur in the presence of thin wetting layers on both surfaces, i.e., in the partial wetting regimes of the two individual surfaces or if one or both surfaces are covered by a thick wetting film (Bauer, Bieker, and Dietrich, 2000). As discussed in the Introduction, such kind of bridge formation around the particles was first invoked as a possible explanation for the flocculation of colloidal particles (Beysens and Estève, 1985; Beysens and Narayanan, 1999). This explanation is plausible if the concentration of the binary liquid mixture differs significantly from the critical one. However, the colloidal aggregation occurring in regions of the solvent

phase diagram which extend far from the two-phase coexistence line and from the wetting transition (into the homogeneous phase) cannot be related to prewetting phenomena.

Near capillary condensation or bridging phase transitions, the effective force acting between the confining surfaces, i.e., the solvation force, is attractive, exhibits a jump, and is very strong: the depth of the corresponding potential can reach a few hundred $k_B T$. Upon changing temperature toward the critical temperature of the solvent, due to the critical fluctuations of the intervening fluid, the solvation force acquires a universal contribution, which turns into the CCF. The concomitant strong increase of the absolute value of the CCF occurring for noncritical compositions results from the residual capillary condensation or bridging. This is reflected by the corresponding universal scaling function and extends to the thermodynamic region beyond the capillary condensation or bridging critical point, even to temperatures $T > T_c^{(s)}$ ($T < T_c^{(s)}$ for solvents with the lower critical point).

C. Minimal model for a pair potential in a near-critical solvent

The minimal model for a pair potential, describing the effects of a critical solvent on dissolved colloids due to CCFs, corresponds to the sum of Eqs. (2) and (11) with $\Sigma = \Lambda/\mathcal{Y}$:

$$U(r) = \begin{cases} \infty, & D < 0, \\ U_{\text{rep}} + U_C^{(d=3)} = A \exp(-\kappa D) + (1/\Delta)\Theta^{(d=3)}(\mathcal{Y}, \Delta, \Sigma), & D > 0. \end{cases} \quad (23)$$

The effective pair potential given by Eq. (23) is applicable only for sufficiently large distances $D \gtrsim \kappa^{-1}$, because it takes into account only the electrostatic repulsive interactions and neglects possible short-ranged contributions to the effective van der Waals interactions. Furthermore, the CCP attains its universal form as given by the scaling function $\Theta^{(d=3)}$ only in the scaling limit, i.e., for distances D which are sufficiently large compared with the correlation length amplitude $\xi_{t,+}^{(0)} \approx 0.25$ nm. Analogously, ξ_t and ξ_h must also be sufficiently large compared with microscopic scales. From the behavior of the scaling function $\Theta^{(d=3)}$ [discussed by Mohry, Maciolek, and Dietrich (2012b) within the Derjaguin approximation] it follows that along the typical thermodynamic paths realized experimentally, the range of attraction due to the CCF grows steadily upon increasing the bulk correlation length ξ_t , but the amplitude of the CCF is a nonmonotonic function of ξ_t with its maximal strength attained for an intermediate value of ξ_t . Depending on the values of A in Eq. (23) and of ξ_t , the CCFs compensate the repulsion for all values of D or only within certain ranges of D , i.e., a secondary attractive minimum of $U(r)$ can occur at a certain distance D_{min} (in addition to the primary, global minimum at $D \rightarrow 0^+$) while for small distances $D < D_{\text{min}}$ and for $D < 0$ the potential maintains a repulsive part. The presence of the repulsive barrier and the attractive secondary minimum in the effective potential, and thus the occurrence of flocculation, depends on temperature. But also in the case in which for all values of ξ_t a

repulsive barrier remains, coagulation can appear, due to a deep secondary minimum. However, this mechanism differs from the one for aggregation due to the primary minimum. While in the latter case the colloids will stick together with their surfaces in contact, in the former case they are close but not in contact. The shape of the total potential exhibiting the secondary minimum has not yet been probed experimentally (see Sec. IV.C).

The model given in Eq. (23) was used by Bonn *et al.* (2009), Gambassi and Dietrich (2010), Mohry, Maciolek, and Dietrich (2012a, 2012b), Dang *et al.* (2013), Nguyen *et al.* (2013), and Mohry *et al.* (2014). Zvyagolskaya, Archer, and Bechinger (2011) modeled the electrostatic repulsion via a hard-disk repulsion with an effective diameter, instead of a soft repulsive potential of the form as in Eqs. (2) and (3). In some of the studies cited, a simplified functional form of the universal scaling function Θ was employed (Bonn *et al.*, 2009; Gambassi and Dietrich, 2010; Dang *et al.*, 2013; Nguyen *et al.*, 2013), such as using a form similar to the one given in Eq. (20), which is valid only asymptotically for large values of the temperature scaling variable neglecting the dependence on the other, also relevant scaling variables.

1. Stability

Knowing the effective pair potential for colloids one can investigate the kinetic stability of the colloidal suspensions and the aggregation of colloids. These phenomena are related to kinetic processes (Russel, Saville, and Schowalter, 1989),

which are based on the diffusion of single particles in the presence of other particles of the same kind, interacting with them via interaction potentials which contain both attractive and repulsive contributions. Aggregation occurs if the attractive interactions of the particles dominate over their thermal kinetic energy, which is responsible for the Brownian motion of the particles. Hydrodynamic interactions may also play a role, e.g., by slowing down the aggregation process for solvents with high viscosity.

In the initial phase of aggregation the individual particles form dimers. In order to quantify the behavior of interacting particles, which irreversibly stick together once their surfaces touch each other, Fuchs (1934) introduced the concept of a stability ratio. It is defined as the ratio $W = J_0/J$ between the Brownian motion induced pair formation rate J_0 in the absence of other than excluded volume interactions between the particles and the corresponding formation rate J of particle pairs in the presence of such interactions. The stability ratio is accessible experimentally through the measurements of the rates J and J_0 by using various experimental techniques such as turbidimetry, light scattering, or fluorescent correlation spectroscopy. W can be calculated by extending Smoluchowski's diffusion equation for the radially symmetric relative motion of two coagulating spherical particles of radius R in order to account for their interaction potential (Fuchs, 1934):

$$W = 2R \int_{2R}^{\infty} \frac{\exp\{U(r)\}}{r^2} dr. \quad (24)$$

The analysis, which leads to this expression, is valid only in the early stages of coagulation before triplets, etc., are formed. However, it does not deal with the very beginning of the coagulation process but considers only the steady-state situation, which is established quickly. In the analysis based on Smoluchowski's equation hydrodynamic interactions are neglected. From the definition of W it follows that for hard spheres $W = 1$, while for $W > 1$ ($W < 1$) the repulsive (attractive) part of the pair potential ($k_B T$) U dominates. In the case of a potential barrier, i.e., if $U(r) \gg 1$ for a certain range of distances $r > 2R$, which leads to $W > 1$, one can expect that on intermediate time scales the suspension will be in a (meta) stable homogeneous state. The cluster formation will set in only on a very large time scale.

For the mixed phase of the solvent and for a diversity of possible shapes of the effective pair potential given in Eq. (23), the ratio W was calculated by Mohry, Maciolek, and Dietrich (2012b). The results of this calculation are useful for predicting the onset of nonequilibrium aggregation as a function of experimentally relevant parameters. However, this possibility has not yet been explored experimentally. Mohry, Maciolek, and Dietrich (2012b) complemented the investigations of the stability ratio by the analysis of the bulk structure of colloidal suspension. To this end, the radial distribution function $g(r)$ was calculated within the integral equation approach by using the hypernetted chain and the Percus-Yevick closure (Hansen and McDonald, 1986). The results for both types of closure are almost the same. [The applicability and reliability of this integral equation approach was discussed in detail by Caccamo (1996).] For temperatures far from the critical temperature of the solvent, the colloids

behave effectively as hard spheres with an effective diameter $\sigma > 2R$ due to the soft repulsive background contribution U_{rep} . Accordingly, for such values of ξ_t , $g(r)$ has the corresponding characteristics of a fluid of hard spheres, such as the rather broad first peak for small values of D . Because of the emerging attractive CCFs, for increasing ξ_t the radial distribution function $g(r)$ is enhanced close to the surfaces of the colloids. This implies an enhanced short-ranged order and that the formation of colloidal dimers is favored. The way in which the shape of the radial distribution function $g(r)$ changes upon increasing the temperature reveals whether the effective potential exhibits a repulsive barrier at small values of D and is attractive throughout large distances or whether an attractive minimum develops at intermediate values of D upon increasing temperature while repulsion remains at small and large values of D .

Since, through W as given by Eq. (24), the rate of association of two colloids depends on the strength of the interparticle potential, it allows one to address the issue whether a relationship can be established between the onset of aggregation and the behavior of the second virial coefficient B_2 , which is accessible both theoretically and experimentally. For dilute suspensions, the second virial coefficient (Hansen and McDonald, 1986) provides information about the strength of the radially symmetric attraction between spherical particles:

$$\begin{aligned} B_2 &= \frac{1}{2} \int d^3r (1 - e^{-U(r)}) \\ &= 2\pi \int_0^{\infty} dr r^2 (1 - e^{-U(r)}) = 2\pi \int_0^{\infty} dr r^2 [1 - g(r)], \end{aligned} \quad (25)$$

where $g(r)$ is taken in the dilute limit. Beyond the ideal gas contribution it determines the leading nontrivial term in the expansion of the pressure $p(\rho)/k_B T \rho = 1 + B_2 \rho + \dots$ in terms of powers of the number density ρ . Mohry, Maciolek, and Dietrich (2012b) calculated B_2 for the potential given by Eq. (23) at the state points for which, according to the experiments reported by Gallagher, Kurnaz, and Maher (1992) and Gallagher and Maher (1992), aggregation sets in. These experiments have been performed for very small ($10^{-7} - 10^{-3}$) packing fractions of the colloids. It turns out that at these states of aggregation onset, the values of B_2 are close to each other and that to a certain extent those B_2 isolines, which emerge by belonging to these experimental data points, agree with each other and with the possible shape of the aggregation onset line (see Fig. 3). However, this analysis was based on many fitting parameters and hence it is not compelling. Further efforts in this direction, as undertaken by Stuij *et al.* (2017), have combined theory and experiment in order to provide more accurate values of the relevant parameters (for details see Sec. IV.C). The outcome has demonstrated that B_2 serves well as a quantitative indicator for the onset of aggregation, at which the system separates into a colloid-rich and a colloid-poor phase (see the next section).

2. Phase behavior

In suspensions with sufficiently large packing fractions of colloids, the attraction among them due to CCFs can induce a

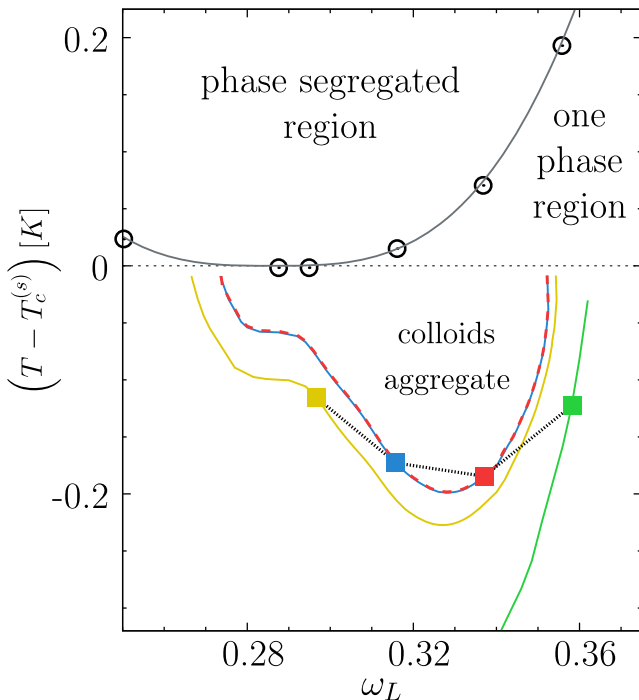


FIG. 3. The experimentally determined coexistence points (\odot) of the water-2,6-lutidine mixture (Gallagher, Kumaz, and Maher, 1992; Gallagher and Maher, 1992) which exhibits a lower, continuous demixing phase transition. $T_c^{(s)}$ is the critical temperature of this demixing transition and ω_L is the mass fraction of lutidine. These coexistence points on the binodal of phase segregation agree well with $|\omega_L - \omega_{c,L}| = B_\omega |t|^\beta$, where $\beta = 0.3265$ and $B_\omega = 0.765$ (dark gray line). Squares denote the experimental state points of the onset of aggregation (the straight black dotted lines in between are a guide to the eye) from the middle panel of Fig. 1 in Gallagher, Kumaz, and Maher (1992). Each isoline of constant B_2 (solid, colored lines; for visibility of the blue line the red one is dashed, both lines nearly coincide) corresponding to one of the state points (squares), is calculated by using the effective potential given by Eq. (23); their values are $B_2/(4\pi/3)R^3 = -67$ (red square), -65 (blue square), -23 (yellow square), and 5.4 (green square). Each B_2 isoline can capture some qualitative trends of the possible shape of the line of onset of aggregation. The blue and the red lines reveal large agreement, but the yellow and the green one do not. From Mohry, Maciolek, and Dietrich, 2012b.

so-called “liquid-gas” phase separation of the colloids, i.e., the separation of two phases which differ with respect to their colloidal number density. Adopting the effective one-component approach allows one to use standard liquid state theory in order to determine the onset of phase separation. Within this effective approach, feedback mechanisms of the colloids, acting on the solvent and changing its critical behavior, are neglected. Therefore, this approximation does not allow one to reliably describe all details of the full many-component system. However, one can identify certain regions of the thermodynamic phase space for which this approach is applicable. One expects the effective one-component model to work well for temperatures corresponding to the one-phase region of the pure solvent and for an intermediate range of values of the colloid number density ρ . The latter should be large enough so that the competition between the

configurational entropy and the potential energy due to the effective forces can induce a phase separation, but small enough so that the approximation of using an effective pair potential between the colloids is valid and the influence of the colloids on the phase behavior of the solvent is secondary. This is in fact true for most of the experimental conditions discussed in Sec. IV.

In Mohry, Maciolek, and Dietrich (2012a), for particles interacting via the effective pair potential given in Eq. (23), the phase coexistence curve $T_{cx}^{(eff)}$ ($\eta = (4/3)\pi R^3 \rho |c_a$) with the critical-point temperature $T_c^{(eff)}$ and the spinodal (i.e., the loci where, within mean field theory, the isothermal compressibility χ_T diverges) have been calculated using DFT within the so-called random-phase approximation (RPA) (Evans, 1979) and the integral equation approach (Hansen and McDonald, 1986). The results obtained from these two approaches, presented in Fig. 4 [Fig. 2 of Mohry, Maciolek, and Dietrich (2012a)], differ only slightly. The loci of the phase separation depends sensitively on the strength A of the repulsive part of the effective pair potential [Eq. (3)] and the solvent compositions. For solvent compositions, which are somewhat poor in the component preferred by the colloids, even short correlation lengths suffice to bring about phase separation. The critical value η_c of the colloidal packing fraction $\eta = (4\pi/3)R^3 \rho$ (in terms of number density ρ) is rather small, i.e., $\eta_c \approx 0.07$, because the effective hard-sphere diameter σ , which results from the soft repulsion U_{rep} , is larger than $2R$. Furthermore, the binodals shown in Fig. 4 are rather flat compared with the ones for hard spheres interacting via a short-ranged, attractive, and temperature independent potential. In the present system, the deviation of T from the critical temperature $T_c^{(s)}$, which corresponds to a range of η for the coexisting phases as large as the one shown in Fig. 4, is about 1%, whereas for a system of hard spheres with an additional attractive interaction the corresponding temperature deviation is a few percent. The critical temperature $T_c^{(eff)}$ obtained within DFT agrees with the simple prediction $B_2^* = B_{2,c}^*$, acting as an implicit equation for T_c , as suggested by Vliegthart and Lekkerkerker (2000) and Noro and Frenkel (2000) (VLNF), where $B_2^*(T) \equiv B_2(T)/B_2^{(HS)}$ is the reduced second virial coefficient and $B_{2,c}^*$ is the critical value of B_2^* for Baxter’s model of adhesive hard spheres (Baxter, 1968).

$B_2^{(HS)} = (2\pi/3)\sigma^3$ is the second virial coefficient of a suitable reference system of hard spheres with diameter σ . The effective hard-sphere diameter can be taken as $\sigma = \int_0^{r_0} (1 - \exp[-U(r)]) dr$, with $U(r=r_0) = 0$. One can also adopt other definitions of σ (Andersen, Weeks, and Chandler, 1971). According to VLNF, B_2^* is a useful indicator of the occurrence of a phase separation into a colloidal-rich (liquid) and a colloidal-poor (gas) phase. An extended law of corresponding states proposed by VLNF predicts that the value of the reduced second virial coefficient B_2^* at the critical point is the same for all systems composed of particles with short-ranged attractive interactions, regardless of the details of these interactions. This approximate empirical rule is supported by experimental data (Vliegthart and Lekkerkerker, 2000) and theoretical results (Largo and Wilding, 2006; Foffi and Sciortino, 2007; Orea and Duda, 2008; Gazzillo, 2011).

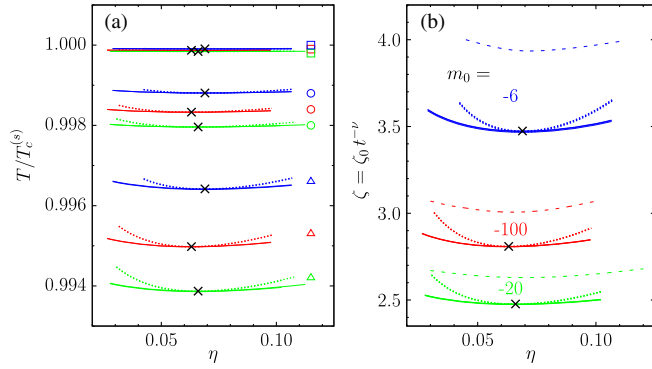


FIG. 4. In the plane spanned by temperature and colloidal packing fraction η : (a) colloidal gas-liquid phase coexistence curves $T_{cx}^{(\text{eff})}(\eta = (4/3)\pi R^3 \rho |c_a|)$ (solid lines, cf., Fig. 5), spinodals (i.e., loci of mean field divergence of the isothermal compressibility χ_T , dotted lines), and the critical points $T_c^{(\text{eff})}$ (crosses) of an effective, one-component system of large colloidal particles as obtained by density functional theory. These particles of radius R interact via an effective potential given by Eq. (23) with parameters $\kappa R = 10$ and $A = 1000$ (Mohry, Maciołek, and Dietrich, 2012a) at $T_c^{(s)}$. The curves correspond to a solvent with a lower critical temperature $T_c^{(s)}$ and with various fixed solvent compositions c_a [Eq. (13)] represented by the variable $m_0 = \text{sgn}(\phi)(\zeta_0)^{1/\nu}|\mathcal{B}/\phi|^{1/\beta} = -100$ (red), -20 (green), and -6 (blue). \mathcal{B} is defined via the shape of the solvent binodal $\phi = \mathcal{B}|t|^\beta$ and $\zeta_0 = \kappa \xi_{r,+}^{(0)}$ (see later). The bulk critical exponents used here are $\nu = 1/2$ and $\beta = 1/2$. Close to the phase separation of the solvent the dominant temperature dependence within the effective approach described by Eq. (25) is that of the CCFs, encoded in $\zeta(t = 1 - T/T_c^{(s)}) = \text{sgn}(t)\kappa \xi_r(t) = \text{sgn}(t)\zeta_0|t|^{-\nu}$. Therefore, if the temperature (a) is expressed in terms of ζ (b) the members of each set of curves with equal color in (a), corresponding to various values of ζ_0 [$\zeta_0 = 0.01$ (\square), 0.05 (\circ), and 0.1 (Δ)] fall *de facto* on top of each other and are characterized by m_0 . The dashed lines in (b) correspond to the spinodals determined within the integral equation approach. [Because of $m_0 \sim (c_a - c_{a,c}^{(s)})^{-1}$, the quantities $m_0 = \pm\infty$ correspond to the critical composition $c_{a,c}^{(s)}$.] For solvent compositions which are somewhat poor in the component preferred by the colloids, i.e., for intermediate negative values such as $m_0 \simeq -20$, the CCFs are strongly attractive. Therefore, short correlation lengths suffice to bring about phase separation; accordingly, the binodals occur at small values of ζ . Here only thermodynamic states of the solvent which are in the one-phase region, i.e., for $t > 0$, are considered. From Mohry, Maciołek, and Dietrich, 2012a.

III. MULTICOMPONENT MIXTURE

A. General discussion

For the kind of systems considered here, the determination of phase equilibria is rather subtle because, due to the concomitant adsorption phenomena, which are state dependent, the effective potential between the colloids depends on the thermodynamic state itself. Experiments have revealed (Gallagher, Kurnaz, and Maher, 1992; Gallagher and Maher, 1992; Grill and Woermann, 1997; Rathke, Grill, and Woermann, 1997) that for suspensions very dilute in colloids and with a phase-separated solvent, basically all colloidal

particles are populating the phase rich in the component, say a , preferred by the colloids (this phase has concentration $c_a^{(1)}$). This implies that in coexisting distinct phases the effective potential acting between the particles is different. This is not captured by the effective potential approach discussed previously. Besides the colloid-solvent the solvent-solvent interactions can also influence the effective potential and, accordingly, the phase behavior of the effective colloidal system. This has been demonstrated by recent MC studies in which various kinds of model solvents have been used (Gnan *et al.*, 2012). On the other hand, the presence of colloidal particles may alter the phase behavior of the solvent. In the case of molecular fluids, it is well established that the phase diagrams of ternary mixtures, as they emerge from those of binary mixtures by adding a third component, are distorted and become more complex relative to the underlying original binary ones (Andon and Cox, 1952; Cox, 1952; Prafulla, Narayanan, and Kumar, 1992). Similar distortions and complex features of phase diagrams are observed experimentally (Kline and Kaler, 1994; Jayalakshmi and Kaler, 1997; Koehler and Kaler, 1997) upon adding colloidal particles to binary solvents. In particular, one finds a decrease of the lower critical temperature. Such a shift of the critical point of a binary liquid mixture can also occur due to impurities which are considerably more soluble in one of its two components. The effects of impurities on the phase diagram of a simple mixture have been studied theoretically, e.g., by Rice (1976), and more recently also experimentally (for a polymer impurity) (Venkatesu, 2006). If the number density of the colloids is very low, they can be regarded as impurities. However, for reliably determining phase diagrams of colloidal suspensions with binary solvents, especially for smaller particles at higher concentrations, the full many-component mixture has to be considered. The importance of considering the colloidal suspension with a binary solvent as a truly ternary mixture was already pointed out by Sluckin (1990). If a microscopic model of the colloidal suspension with a binary solvent could be solved exactly, the emerging nonadditive, configuration-dependent CCFs would be included automatically in the free energy from which the phase behavior of such ternary mixtures follows. Nonetheless, taking into account those characteristic features of the CCP, which neglect the many-body interactions, one can try to predict the expected topology of the phase diagrams for ternary solvent-solvent-colloid mixtures (Mohry, Maciołek, and Dietrich, 2012a). Upon adding colloids, the two-phase region of the demixed phases of the pure solvent extends into the three-dimensional thermodynamic space of the actual colloidal suspension. At fixed pressure this space is spanned by T , the concentration c_a of the component a of the binary solvent, and by the colloidal number density ρ . The actual shape of the two-phase region forming a tubelike manifold is expected to depend sensitively on all interactions present in the ternary mixture (see Fig. 5). The foremost difficulty in describing such mixtures theoretically or in dealing with them via computer simulations consists of the fact that the sizes of their constituents differ by a few orders of magnitude. This property distinguishes them significantly from mixtures of hard spheres, needles, and polymers (Schmidt and Denton, 2002; Schmidt, 2011), for

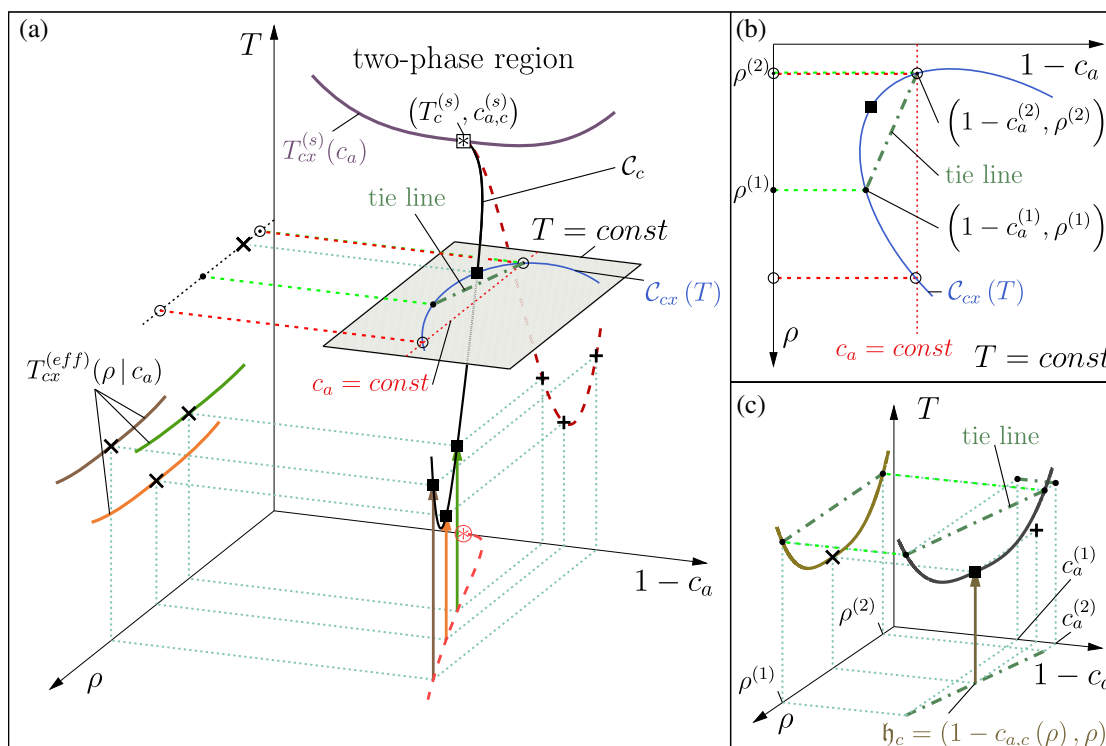


FIG. 5. Sketch of the phase diagram for colloids immersed in a binary liquid mixture at fixed pressure corresponding to a liquid state of the system. Upon adding colloids the phase separation curve $T_{cx}^{(s)}(c_a)$ of a pure solvent in the $(T, c_a, \rho = 0)$ plane extends to a tubelike two-phase region $T_{cx}(c_a, \rho)$ in the 3D thermodynamic (td) space spanned by the temperature T , the concentration c_a , and the colloidal number density ρ . The lower critical point \boxtimes ($T_c^{(s)}, c_{a,c}^{(s)}, \rho = 0$) of a pure solvent extends to a line \mathcal{C}_c (black curve) of critical points (some of which are shown as black squares). Its shape reflects the fact that the 2D manifold $T_{cx}(c_a, \rho)$ of coexisting states is not straight but bent and twisted due to the specific properties of the CCP. The red dashed curves denote the projections of \mathcal{C}_c onto the planes (ρ, c_a) and (T, c_a) . Within the effective one-component approach the coexistence curves are explicit functions of ρ only and depend parametrically on the overall concentration c_a . All three panels show that in general for $T = \text{const}$ the coexisting phases (i.e., the points connected by a tie line) differ with respect to both ρ and c_a . Thus the effective one-component approach has a limited applicability for determining the phase diagram. Experimentally or within suitable, sufficiently rich models, upon increasing temperature (along thermodynamic paths indicated by vertical arrows) one is able to determine a coexistence curve [black line in (c)] in the 3D td space. From Mohry, Maciolek, and Dietrich, 2012a.

which the constituents are of comparable size, i.e., none of them is larger by a factor of 10 or more than the others. In contrast to molecular ternary mixtures as modeled in terms of a lattice gas (Mukamel and Blume, 1974; Sivardière and Lajzerowicz, 1975), in colloidal suspensions the colloidal particles influence the other two components not only by direct interactions but also via strong entropic effects. These occur because their surfaces act as confinements to fluctuations of the concentration of the solvent and they also generate a sizable excluded volume for the solvent particles.

B. Monte Carlo studies

MC simulations for a lattice model of ternary mixtures, suitably mimicking colloidal particles suspended in a near-critical binary solvent, offer the advantage over other available approaches that they account for both fluctuations and non-additivity of the emerging CCFs. Because of the large size difference between the colloid and solvent particles and due to the critical slowing down of the ternary mixture upon approaching its critical point, studying the corresponding three-dimensional systems by MC simulations is computationally challenging. As a computationally cheaper substitute,

two-dimensional lattice models have been treated by this method in Edison, Tasios *et al.* (2015), Hobrecht and Hucht (2015), and Tasios *et al.* (2016). In the first of such a MC simulation study (Edison, Tasios *et al.*, 2015), the colloids have been modeled as discretized hard disks of radius R (in units of the lattice spacing) occupying a fraction η of sites on the square lattice. The remaining lattice sites have been taken to be occupied by a solvent molecule of either species a or b with no empty sites left. A similar model of solvent-solvent-colloid mixtures was considered earlier by Rabani *et al.* (2003) in order to study drying-mediated self-assembly of nanoparticles. Edison, Tasios *et al.* (2015) and Tasios *et al.* (2016) considered only the nearest-neighbor repulsive interactions between the components of a binary solvent. This drives phase segregation, which in the absence of colloids has a critical point belonging to the 2D Ising universality class. In order to mimic the preference of the colloids for component b of the binary solvent, a nearest-neighbor attractive interaction between the colloid and component b was taken into account. It was assumed that there is only a nearest-neighbor repulsion between the colloid and component a . In the limit $\Delta\mu_s = \mu_a - \mu_b \rightarrow \infty$ of the chemical potential difference between the components a and b , the

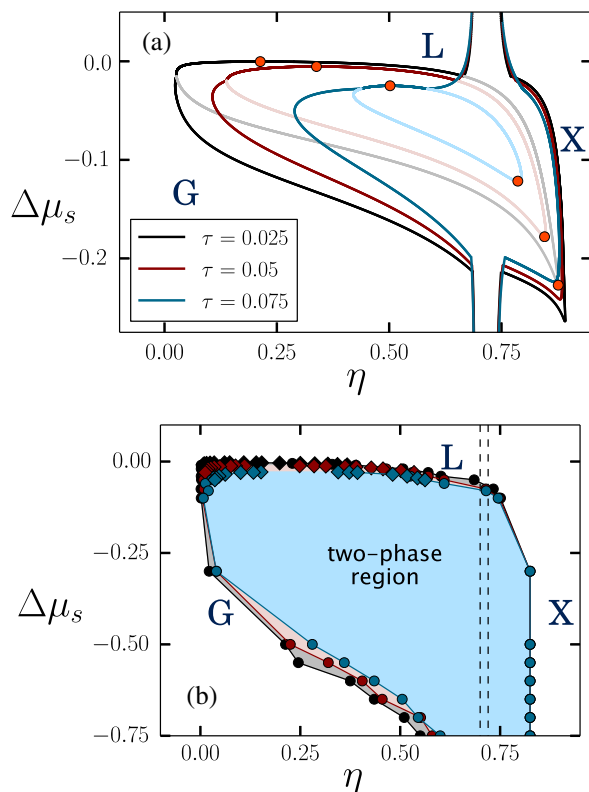


FIG. 6. Phase diagrams of the full ternary colloid-solvent a -solvent b 2D lattice model for three values of $t = 1 - T/T_c^{(s)}$ [in Edison, Tasios *et al.* (2015) denoted by τ]: 0.025 (black), 0.05 (dark red), and 0.075 (blue) in the $(\Delta\mu_s, \eta)$ plane of the solvent chemical potential difference and the colloidal packing fraction. The quantity $\Delta\mu_s = \mu_a - \mu_b$ is the chemical potential difference between species a and b (in units of the solvent a -solvent b interaction strength). (a) Results obtained within mean field theory. The gray, pale red, and pale blue curves correspond to metastable colloidal gas-liquid (G-L) coexistence, which also terminates at the critical point. For each τ the upper (stable) and lower (metastable) gas-liquid critical points are indicated by red dots. X denotes the solid phase. (The various phases are inferred from monitoring their free energies.) (b) The corresponding phase diagrams as determined by MC simulations. The diamonds and dots denote the phase boundaries as obtained from grand canonical staged insertion MC simulations and $(\Delta\mu_s/k_B T, \eta, \tau)$ ensemble MC simulations, respectively. Their color corresponds to the value of τ given in the upper panel. The blue area corresponds to the two-phase region for $\tau = 0.075$; for $\tau = 0.05$ and 0.025 the two-phase regions encompass the previous regions and have added (colored) slices. The vertical dashed lines denote fluid-solid coexistence for pure colloidal hard disks. $T_c^{(s)} = T_c^{\text{MFT}}$ and $T_c^{(s)} = T_c^{\text{MC}}$ is the critical temperature of the binary (ab) solvent within mean field theory and MC simulations, respectively. From Edison, Tasios *et al.*, 2015.

ternary mixture reduces to a binary mixture of 2D hard disks and solvent component a , which exhibits coexistence between a fluid and a solid phase. In the study by Edison, Tasios *et al.* (2015), the preclusion of solvent-mediated colloidal aggregation, arising from complete wetting and capillary condensation, was implemented by focusing on colloids, which are immersed in a supercritical mixed phase of components a and

b , such that b -rich critical adsorption layers [for critical adsorption profiles at spheres and cylinders see Flöter and Dietrich (1995), Hanke and Dietrich (1999), and Yabunaka and Onuki (2017) and references therein] form on the colloid surfaces in equilibrium with a supercritical a -rich solvent in the bulk. The simulation study by Tasios *et al.* (2016), in which the solvent has been treated grand canonically at constant pressure, revealed the existence of gas-liquid and fluid-solid transitions, occurring in a region of the thermodynamic variables $[\eta, t = (T - T_c^{(s)})/T_c^{(s)}, \Delta\mu_s = \mu_a - \mu_b]$ of ternary mixtures which extends well away from the critical point of the solvent reservoir (especially concerning the fluid-solid transitions). It has been found that in all phases the local solvent composition is strongly correlated with the local colloid density. The coexisting colloidal liquid and solid phases are poor in component a , whereas in the gas phases coexisting with the liquid or the solid phases the solvent composition is very close to the composition of the solvent reservoir, which, however, is far from its critical composition. These features agree with experimental observations (Gallagher, Kurnaz, and Maher, 1992; Gallagher and Maher, 1992; Grüll and Woermann, 1997; Rathke, Grüll, and Woermann, 1997) and cannot be captured by an effective one-component approach as discussed in the previous section. As expected (Evans *et al.*, 1994), all pair correlation functions decay exponentially on the scale of the same correlation length. Strikingly, the correlation length found in the homogeneous supercritical state of the ternary mixture was much larger than the colloid radius ($R = 6$), which in turn exceeded the correlation length of the solvent reservoir. Upon adding a small volume fraction of colloids, the gas-liquid critical point of a ternary mixture shifts continuously from that of the colloid-free solvent to the negative values of $\Delta\mu_s$, which decrease upon increasing t . In addition, the MC simulation data indicate the existence of a second, lower metastable gas-liquid critical point located at larger values of η . The gas-liquid-solid triple point is also expected to occur near the fluid-solid coexistence of pure hard disks shown as the vertical dashed lines in Fig. 6. Tasios *et al.* (2016) checked to what extent a description in terms of an effective pair potential can account for the phase behavior observed in their MC simulations as shown in Fig. 4(d) of Edison, Tasios *et al.* (2015). They concluded that those approaches, which exclusively employ effective pair potentials, as obtained from planar slit studies combined with the Derjaguin approximation, overestimate the extent of gas-liquid coexistence and underestimate how much the critical point of the ternary mixture is shifted relative to that of the solvent reservoir.

Hobrecht and Hucht (2015) treated the two-dimensional Ising model with embedded colloids represented as disklike clusters of spins with fixed orientation, by the geometric cluster algorithm (see Sec. II.B.3). However, the focus of this study has not been the phase behavior of a ternary mixture but rather the two- and three-body CCPs. Employing the geometric cluster algorithm facilitated the study of the same lattice model as in Edison, Tasios *et al.* (2015) and Tasios *et al.* (2016) but in $d = 3$ (Tasios and Dijkstra, 2017). As anticipated by Edison, Tasios *et al.* (2015) and Tasios *et al.* (2016), the phase diagram displays the same qualitative features as in the two-dimensional case. Examples of colloidal gas-liquid

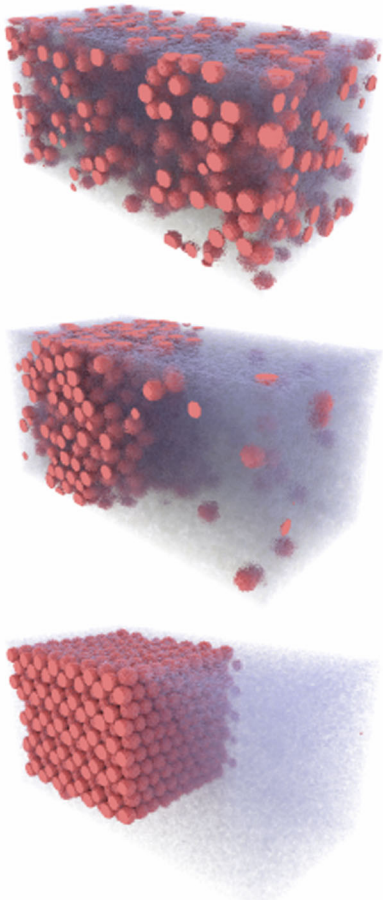


FIG. 7. Representative configurations of the full three-component (colloid–solvent a –solvent b) three-dimensional lattice model at the reduced temperature $t = 1 - T/T_c^{(s)} = 0.05$ [in Tasios and Dijkstra (2017) denoted as τ], colloid radius $R = 6$ (in units of the lattice constant), and for three chemical potentials $\Delta\mu_s$; top: $\Delta\mu_s = 0.002$ (supercritical phase); middle: $\Delta\mu_s = 0.008$ (colloidal gas-liquid coexistence); and bottom: $\Delta\mu_s = 0.3$ (colloidal gas-solid coexistence). The pink-colored particles represent the colloids, while the blue-colored ones represent the species b of the solvent; solvent a is not represented. The quantity $\Delta\mu_s = \mu_a - \mu_b$ is the chemical potential difference between species a and b (in units of the solvent a –solvent b interaction strength). The strong fractionation of the solvent species b , which is favored by the colloids, is particularly visible in the middle panel. The colloidal gas phase is poor in solvent species b so the right side of the simulation box has a light blue color. On the other hand, the colloidal liquid is rich in solvent species b so that the space between the colloids on the left side of the simulation box has a dark blue color. The phase diagram of the two-dimensional version of this model is shown in Fig. 6. From Tasios and Dijkstra, 2017.

and colloidal gas-solid coexistence as well as a supercritical configuration are shown in Fig. 7 [Fig. 3 of Tasios and Dijkstra (2017)]. The significant fractionation of the solvent species favored by the colloids is visually evident.

C. Mean field theory

The mean field approximation of the model considered by Tasios *et al.* (2016) was studied in more detail by Edison, Belli

et al. (2015). It is based on free-volume arguments, according to which the Helmholtz free energy is taken as the sum of three contributions, describing the direct interactions among the pure colloids, the pure binary mixture of solvent a and solvent b , and the colloid, solvent b mixture. For the pure-colloid contribution the hard-disk free energy has been employed, with its distinct expressions for the fluid (Santos, López de Haro, and Bravo Yuste, 1995) and the solid (Young and Alder, 1979) phases. In the free space between the colloids, the mean field free energy for the a - b mixture has been taken; the solvent is excluded from the volume of the colloids. Concerning the colloid–solvent b contribution, the mean adsorption energy of component b at the colloid surface has been taken. As inferred from Fig. 6, the topology of the resulting phase diagram and its temperature dependence agree qualitatively with the simulations [see Fig. S2 in the Supplemental Material of Tasios *et al.* (2016)] and Fig. 1 of Edison, Belli *et al.* (2015). In particular, a lower critical point has been found. However, as expected on the basis of the different spatial dimensions, there is no quantitative agreement; the parameter values used in order to obtain phase diagrams, which are similar to those from simulations, were chosen empirically. It seems that in these studies the underlying mean field approximation severely underestimates the effect of the hard-core repulsion of the colloids. In addition to the colloidal gas and colloidal liquid, this theory predicts the occurrence of two crystal phases which have the same (hexagonal) structure but with different lattice spacings. In the 3D thermodynamic state space of a ternary mixture spanned by $\Delta\mu_s$, η , and t one finds also upper and metastable lower colloidal gas-liquid critical lines and a colloidal solid-solid critical line. [The critical points in Fig. 6(a) lie in the planes cutting the full phase diagram at three constant temperatures.] The fluid-solid transition corresponds to a first-order freezing transition. The critical point of the colloid-free solvent ($t = 0$, $\Delta\mu_s = 0$, $\eta = 0$) is shifted considerably upon adding a small amount of colloids [see the red dots in Fig. 6(a)]. Edison, Belli *et al.* (2015) pointed out that experiments on colloidal aggregation are typically performed by suspending a fixed number of colloids in a solvent at a fixed (pure) solvent composition, which we denote by $c_a^{(s)}$, and then by adjusting the temperature of the system to reversibly induce aggregation. They identified the so-called aggregation line, i.e., the loci of the points $(t, c_a^{(s)})$ at fixed η and $c_a^{(s)}$ at which aggregation is observed first, as the line which demarcates the one-phase region of the ternary mixture, which lies at the outside of the line, and the region at its inside where colloidal phase separation can be found. Such a line (see Fig. 8) ends at an η -dependent critical point of the ternary mixture, which is shifted from the critical point of the pure solvent toward a higher (η -dependent) temperature. In the vicinity of their end points these lines are slightly bent, which indicates reentrant dissolution. Such lines qualitatively resemble the experimental results for strong aggregation reported by Beysens and Estève (1985) (see the solid line in Fig. 3). This tends to support the view on the aggregation lines as the line of onset of colloidal phase separation in the full ternary mixture. The mean field calculation was performed in $d = 2$ (Edison, Tasios *et al.*, 2015) and then

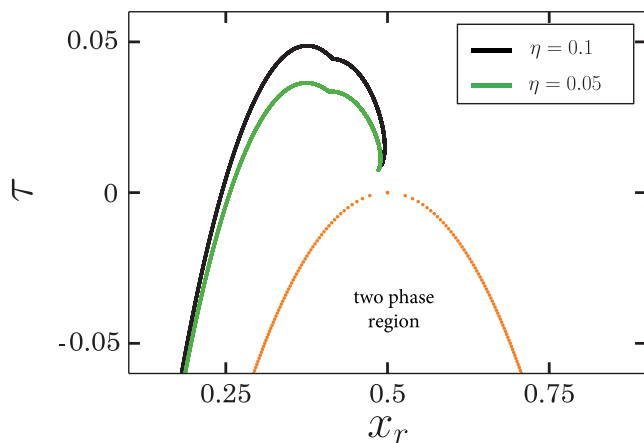


FIG. 8. Aggregation lines (black and green) for a ternary colloid–solvent a –solvent b mixture (interpreted as a colloidal condensation transition), as determined within mean field theory for the lattice model considered by Edison, Tasios *et al.* (2015) plotted in the reduced temperature composition of the pure solvent in the reservoir ($t = 1 - T/T_c^{(s)}, c_a$) representation [in Edison, Belli *et al.* (2015) denoted by $(\tau = (T - T_c^{\text{MFT}})/T_c^{\text{MFT}}, x_r)$]. A point on the aggregation line at x_r gives the temperature at which phase separation of colloids is observed first, upon cooling the suspension at a fixed packing fraction η of colloids and for fixed solvent composition x_r . The 2D calculations have been performed for a parameter v_c (approximately equal to the area of the colloidal disk) chosen to be equal to $1000a^2$ [in order to reproduce most closely the MC simulations results of Edison, Tasios *et al.* (2015)], where a is the lattice spacing for the coupling strength between colloid and solvent species b equal to 32 (in units of the solvent–solvent interaction strength), and for two fixed values $\eta = 0.1$ and $\eta = 0.05$ of the colloid packing fraction. The colloids interact with the members of solvent species a and with each other via a hard-core repulsion. The dotted orange line is the binodal of the colloid-free a – b solvent. Each aggregation line ends at a critical point of the ternary mixture, which is removed from the binodal of the solvent reservoir (see the main text). The origin of the break in slopes of the aggregation curves is not discussed by Edison, Belli *et al.* (2015). The bending of the aggregation lines near their critical points implies the occurrence of reentrant dissolution upon cooling. From Edison, Belli *et al.*, 2015.

extended to $d = 3$ (Edison, Belli *et al.*, 2015) but no new features of the phase behavior have been found. Although the uncertainties generated by the large differences of length scales prevent a quantitative comparison with the available experimental data, the studies reported by Edison, Belli *et al.* (2015) and Edison, Tasios *et al.* (2015) are valuable because they reveal the possible scenarios for the phase behavior, which can occur in such ternary mixture, highlighting the physical mechanisms behind it.

IV. EXPERIMENTS

A. Experimental studies of critical Casimir interactions

Following the example of the “classical” Casimir effect, the first experimental investigations of CCFs have been carried out for the film geometry. Even for such a simple geometry, the experimental detection of f_C^{\parallel} is particularly challenging

due to the difficulty of realizing, maintaining, and controlling with sufficient accuracy the parallel alignment between the confining surfaces less than a micrometer apart. Moreover, CCFs are rather weak. On the basis of the theoretical results discussed in the previous sections, a rough estimate reveals that the Casimir force f_C^{\parallel} acting on the confining surfaces of a film of transverse area $S = 1 \text{ mm}^2$ and thickness $D = 1 \text{ }\mu\text{m}$ is expected to be about 10^{-10} N for critical points at room temperature. The natural solution for this challenge is to use fluid wetting films. Such films occur in systems which in the bulk exhibit a first-order phase transition such as a gas–liquid phase transition. The wetting films form as a result of the subtle interplay between the substrate potential, the interaction among the fluid molecules, and the fluctuations of the depinning interface. Under the action of the so-called effective interface potential (Dietrich, 1988), the fluid forming a wetting film is confined naturally by the substrate–fluid and the fluid–vapor interfaces, which are perfectly aligned.

In wetting films of classical binary liquid mixtures, the CCFs arise near a critical end point of the binary liquid mixtures, at which the line of the continuous liquid–liquid demixing transitions ends at the liquid–liquid–vapor triple line (Nightingale and Indekeu, 1985; Krech and Dietrich, 1992). The CCFs originate from the restriction of the critical fluctuations of the composition of the binary mixture imposed by the solid substrate and the liquid–vapor interface. The CCF acts on the movable liquid–vapor interface and, together with the omnipresent background dispersion forces and gravity, determines the equilibrium thickness ℓ of the wetting films. The dependence of ℓ on temperature T provides an indirect measurement of the CCF. It is also possible to probe the universal properties of the CCF as given by its scaling function. By varying the undersaturation of the vapor one can tune the film thickness and thus determine the scaling behavior of the CCF as a function of T and ℓ .

Classical binary liquid mixtures near their demixing transition belong to the 3D Ising universality class. Since the two confining surfaces typically exhibit opposite preferences for the two species forming binary liquid mixtures, wetting films of classical binary mixtures are generically characterized by opposing effective surface fields [(+ –) BCs], which results in a repulsive CCF. Following this theoretical suggestion, such an experimental approach has successfully provided the first experimental evidences for the occurrence of CCFs in wetting films of a binary liquid mixture of methylcyclohexane (MeC) ($\text{C}_6\text{H}_{11}\text{-CH}_3$) and perfluoromethylcyclohexane (PF) ($\text{C}_6\text{F}_{11}\text{-CF}_3$) on a SiO_2/Si substrate (Fukuto, Yano, and Pershan, 2005). Around 30°C , this system exhibits complete wetting by the mixed fluid with an enhanced concentration of (MeC) at the substrate and of PF at the fluid–vapor interface. Upon approaching the demixed phase from the mixed one, in the middle of the wetting film a strongly fluctuating (MeC)/PF interface is forming. The variations of the film thickness along several thermodynamic paths near the bulk critical demixing point of the binary mixture have been measured by using x-ray reflectivity. The measure of the actual film thickness ℓ was obtained from the extremum positions of the well-defined interference fringes arising from the substrate/film and film/vapor interfaces.

Rafai *et al.* (2007) measured via ellipsometry the thickness of a wetting film of the binary liquid mixture of methanol and an alkane as formed on a silica substrate. By changing the alkane chain length in the mixture Rafai *et al.* (2007) were able to modify the affinity of the boundaries from being opposite to equal, i.e., to change the effective BCs from $(+ -)$ to $(+ +)$. Rafai *et al.* observed a thinning of the wetting film due to an attractive CCF, which led to its collapse when the attractive CCF overpowers its dispersion counterpart in the effective interface potential. These resulting thin films no longer probe the CCF.

It is worthwhile to stress that, following theoretical proposals (Nightingale and Indekeu, 1985; Krech and Dietrich, 1992), the first convincing evidence for CCFs has been provided by superfluid ^4He films adsorbed on a solid substrate and close to the lambda point (Garcia and Chan, 1999; Ganshin *et al.*, 2006) as well as by ^3He - ^4He mixtures close to the tricritical point (Garcia and Chan, 2002). In wetting films of ^4He , the CCF stems from the confined critical fluctuations associated with the superfluid transition in the fluid film. Similarly as for the classical binary liquid mixtures, the CCF emerges near the critical end point of the fluid; for ^4He this is the point at which the λ line of the second-order phase transitions to the superfluid phase ends at the liquid-vapor coexistence curve. Capacitance measurements of the equilibrium thickness of ^4He wetting films provided quantitative evidence for an attractive CCF (Garcia and Chan, 1999; Ganshin *et al.*, 2006), in agreement with the corresponding theoretical predictions (Krech and Dietrich, 1992) for the bulk XY universality class with *symmetric* Dirichlet-Dirichlet BCs (O,O). They correspond to the vanishing superfluid order parameter both at the surface of the substrate and at the liquid-vapor interface.

The experimental approach based on studying wetting films requires rather detailed knowledge of the material-dependent, nonuniversal properties of both the fluid and the substrate. Indeed, in order to determine the CCF from the observed variation of the film thickness ℓ , it is essential to know the van der Waals interactions among the materials involved. Moreover, since the universal properties of the CCF emerge only in the scaling limit in which the film thickness ℓ and the correlation length ξ are both large on the molecular scale (typically set by the correlation length amplitude ξ_0^+), experiments based on incomplete wetting or being not sufficiently close to the critical point are seriously affected by nonuniversal corrections to scaling so that a quantitative comparison with theoretical predictions is no longer possible.

The first direct measurement of the CCF or, equivalently, of the associated potential has been performed for the geometry of a sphere in front of the planar wall. Within this geometrical setting, the experimental challenge is to detect the onset of the contribution of the CCF to the total force acting on the sphere as the critical point of the surrounding fluid is approached. In order for the effects of the CCF to be detectable, f_C has to be comparable in magnitude with other forces acting on the sphere. This suggests the use of a micrometer-sized colloid, which is suspended in a binary liquid mixture. Within such a system the typical scale of the interaction energy is $k_B T$, i.e., the same scale as the one for the CCP. The necessary

sensitivity for the measurement of the force can be achieved by using TIRM, which is capable of measuring forces with femto-Newton force resolution (Walz, 1997; Prieve, 1999; Hertlein, 2008). With this technique it has been possible (Hertlein *et al.*, 2008; Gambassi *et al.*, 2009; Nellen, Helden, and Bechinger, 2009) to study the onset of CCFs acting on a single colloid near a wall as the temperature T of a water-lutidine solvent is increased toward its lower critical point $T_c \approx 34^\circ\text{C}$ at a fixed lutidine mass fraction equal to its critical value $\omega_{c,L} \approx 0.286$. For a hydrophilic colloid of radius $R = 1.2 \mu\text{m}$ and a hydrophilic wall, corresponding to $(- -)$ BCs, the attractive CCF sets in between $T_c - T = 0.30$ and 0.21 K. The same experiment, but with a hydrophobic colloid of radius $R = 1.8 \mu\text{m}$, changes the BCs into $(- +)$. The repulsive force is already detected for temperatures $T_c - T = 0.9$ K. If, via a suitable chemical surface treatment, the adsorption preference of the silica wall is changed from hydrophilic $(-)$ to hydrophobic $(+)$, attraction is recovered in agreement with theoretical expectations. After subtracting the gravity contribution, the measured potentials could be successfully fitted to the model of the minimal effective potential given by Eq. (23).

In Sec. IV.C we discuss measurements of the CCP for two colloidal particles.

B. Phase transitions and aggregation in bulk

The view that aggregation, as observed in pioneering experiments by Beysens and Estève (1985), is in fact a reversible phase transition in a ternary suspension has been tested via early experimental studies by Guo *et al.* (2008). In these studies, charge-stabilized polystyrene spheres of radius $R = 105$ nm suspended in a mixture of 3-methylpyridine (3MP), water, and heavy water near its lower critical point have been considered. The mass fractions ω of the components of this latter mixture have been chosen such that the mass density of the solvent mixture closely matches that of the colloidal particles in the region of the parameter space where phase transitions have occurred. If the system is density matched, the growth of the nucleated liquid or solid phases is not perturbed by gravity at a very early stage and can be followed until macroscopically large coexisting phases are formed. In order to characterize the phase behavior of the system Guo *et al.* used small angle x-ray scattering. Transition temperatures were also determined by measuring the sample turbidity. Moreover, the samples have been observed directly with a charged coupled device camera. The only information which has been provided about the phase diagram of the 3MP-water-heavy-water mixture at the mass fractions actually used is the coexistence temperature $T_{cx}^{(s)} \approx 65^\circ\text{C}$ at which the chemically, in fact, binary solvent mixture at the studied composition demixes. The schematic phase diagram Fig. 1(a) of Guo *et al.* (2008) suggests that the considered mass fraction ω_{3MP} of 3-methylpyridine investigated in this study (and therein denoted as c_{3MP}) has been smaller than the critical one. Instead of the deviation $t = 1 - T/T_c^{(s)}$ from the critical temperature of the solvent, Guo *et al.* (2008) used the deviation $\Delta T = T - T_{cx}^{(s)}(\omega_{3MP})$ from the phase coexistence for the studied mass fraction ω_{3MP} as the actual control

parameter. Upon increasing the temperature from a value in the one-phase region of the pure solvent toward $T_{cx}^{(s)}(\omega_{3MP})$, the onset of colloid aggregation, at which the system separates into a colloid-rich and a colloid-poor phase as indicated by regions of high and low turbidity and by the appearance of peaks in the structure factor, has been observed at a sharply defined temperature T_a . Depending on the particle volume fraction of the colloids in the suspension (which is the ratio between the volume of all colloids in the suspension and the volume of the system), two or three phases of the colloidal suspension have been found: at low volume fractions this is a fluid phase in equilibrium with a fcc crystal, whereas at larger volume fractions there is a gas phase in equilibrium with a liquid phase and this liquid phase is coexisting with a fcc solid. Interestingly, upon quickly increasing the temperature the measured structure factor indicated the formation of a glassy state as in a molecular system. On the basis of the experimental results reported by Guo *et al.* (2008), it is not possible to uniquely infer the physical origin of the attractive potential which gives rise to the observed reversible aggregation, mainly due to insufficient information about the relevant parameters. Thus it is not surprising that it was concluded that all mechanisms discussed in Sec. II can play a role. Indeed, the bulk correlation length of the solvent at the aggregation temperature $T = T_a$, as estimated from light scattering to be ca. 8 nm, is somewhat short, which suggests that the system has been off the critical region. However, the experiments were performed at an off-critical composition of 3MP such that along the corresponding thermodynamic path the phase is relatively poor in the solvent component preferred by the colloids. If $T_a < T_c^{(s)}$, this composition precludes that colloidal aggregation arises from complete wetting and capillary condensation (Evans, 1990). On the other hand, it is this thermodynamic region where the CCFs are expected to be strongest although their range, governed by bulk correlation length, is smaller than the one at the critical composition. Thus it is rather plausible that CCFs are playing a crucial role in this experiment.

In a subsequent study by Bonn *et al.* (2009), the aggregation of colloidal particles suspended in the same (quasi)binary mixture of 3MP, water, and heavy water has been observed directly by using confocal microscopy. The fluorescent fluorinated latex colloids of radius $R = 200$ nm used in this study exhibit affinity for water. In this experiment the refractive indices between the colloids and the solvent have been closely matched. Two different compositions of 3MP have been studied, one below (mass fraction $\omega_{3MP}^{(1)} = 0.24$) and one above (mass fraction $\omega_{3MP}^{(2)} = 0.37$) the critical composition $\omega_{3MP,c} = 0.31$. [Bonn *et al.* (2009) denoted the critical mass fraction of 3MP as X_c .] The colloid volume fraction has been kept fixed at the rather small value 0.002 and the D_2O/H_2O mass ratio was chosen as 0.25. For the suspension poor in 3MP no aggregation has been observed upon increasing temperature within the homogeneous one-phase region of the solvent until phase separation of the whole mixture has taken place. This is expected to occur for 3MP mass fractions so far off the critical value that the CCFs are negligibly small. Above $\omega_{3MP,c}$, within a rather wide temperature range of $T_{cx}^{(s)} - T_a = 8$ K, reversible aggregation has been observed. For the very small volume fraction of colloids

used, the formation of clusters rather than a colloid phase transition has been observed and the kinetics of this aggregation process has been studied (see Sec. IV.G). Based on these studies, Bonn *et al.* were able to estimate the energy scale of the attraction between the particles to be $3k_B T$. They rightfully argued that the CCFs alone are sufficient to induce aggregation in charged-stabilized colloids. In order to show that this is indeed the case for their experiments, they analyzed their data assuming that the pair potential between the colloidal particles is the sum of two competing exponentials: a repulsive one decaying on the scale of the Debye screening length κ^{-1} [denoted as ℓ_D by Bonn *et al.* (2009)] and an attractive one decaying on the scale of the bulk correlation length. Based on these oversimplified shapes of the CCP, the hypothesis was put forward that aggregation should occur when both decay lengths ξ_t and κ^{-1} become comparable.

This data analysis has been objected and was redone by Gambassi and Dietrich (2010) with the conclusion that, in fact, most of the data reported by Bonn *et al.* (2009) for the onset of aggregation have been located within ranges of values of ξ and κ for which the proposed pair potential does not apply. In other words, the model proposed by Bonn *et al.* (2009) does not predict aggregation to occur at $\xi_t = \kappa^{-1}$ (see Fig. 9). However, the reanalysis presented by Gambassi and Dietrich (2010) does not exclude the possibility that the observed aggregation is solely due to the competing effects of repulsive electrostatic and attractive critical Casimir interactions (Bonn, Wegdam, and Schall, 2010). As emphasized by Bonn, Wegdam, and Schall (2010), a more accurate form of the CCP is needed in order to resolve this issue.

C. Effective colloid-colloid pair potential

Recently, several attempts have been made to determine the colloid-colloid pair CCP experimentally. Dang *et al.* (2013) and Nguyen *et al.* (2013) inferred the effective pair potential between colloidal particles for a dilute (volume fraction 2%) suspension of poly-*n*-isopropyl acrylamid microgel (PNIPAM) particles with a radius of $R = 250$ nm from the pair correlation function $g(r)$. For a sufficiently dilute suspension of solute, the potential of mean force $V_{mf}(r) \sim -k_B T \ln g(r)$ can be identified with the effective pair potential $V(r)$; $g(r)$ has been determined from the 2D images obtained by confocal microscopy. The spatial resolution has been estimated to be ca. $0.03 \mu\text{m}$ in the image plane and ca. $0.05 \mu\text{m}$ in the direction perpendicular to it. The solvent was, as before, a (quasi)binary mixture of 3MP-water-heavy water with various compositions, including the critical one and compositions slightly off the critical one (toward the 3MP poor phase). The measurements have been performed for various temperatures upon approaching the solvent two-phase coexistence curve from the homogeneous mixed phase. The obtained pair potential displayed a very soft repulsion at small separations and developed an increasingly deep minimum as T approaches the coexistence temperature $T_{cx}^{(s)}$ of the solvent. At low temperatures, at which $V(r)$ is purely repulsive, they were able to fit $V(r)/k_B T$ to the screened electrostatic, exponentially decaying potential U_{rep} [see Eq. (2)] with plausible values of the parameters. From this

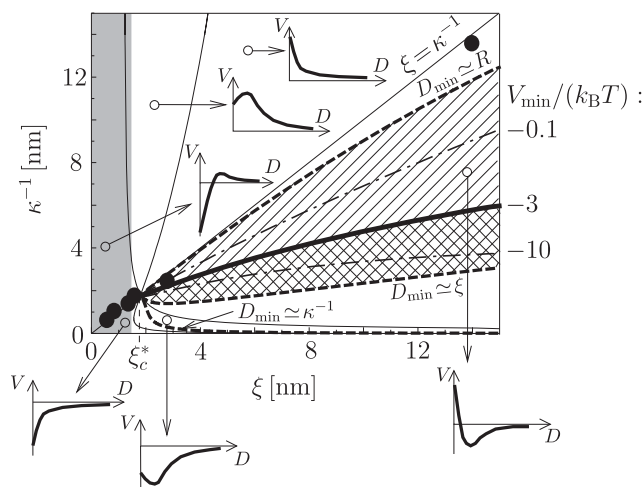


FIG. 9. Shapes of the effective total potential $V(D) = V_{el}(D) + V_C(D)$ of the force acting on two identical colloids of radius R , with both contributions purely exponential functions of D , for various values of the bulk correlation length $\xi = \xi(t, h_b = 0) = \xi_t$ and the Debye screening length κ^{-1} , where D is the surface-to-surface distance of the two colloids. Six different regions of distinct shapes of $V(D)$ are limited by the thin solid lines. These lines meet at $\kappa^{-1} = \xi_t \equiv \xi_c^*$. D_{\min} is the position V_{\min} of the minimum of $V(D)$. Within the hatched area enclosed by the thick dashed lines the condition $R \gg D_{\min} \gtrsim \xi_t, \kappa^{-1}$ is satisfied. The additional requirement that $V_{\min} \lesssim -3k_B T$ is fulfilled in the cross-hatched part of the hatched area. The black dots mark the experimentally determined (Bonn *et al.*, 2009) aggregation line. From Gambassi and Dietrich, 2010.

the CCP has then been determined by the best fit to the exponential form given in Eq. (20), but with the amplitude and the decay length treated as fit parameters, assuming that the total $U(r)$ is the sum of U_C and U_{rep} [as in Eq. (23)]. This assumption is justified for small salt concentrations (Bier *et al.*, 2011; Pousaneh and Ciach, 2011; Pousaneh, Ciach, and Maciolek, 2014) which has been the case for the samples studied there. [There is experimental (Nellen *et al.*, 2011) and theoretical (Bier *et al.*, 2011; Pousaneh and Ciach, 2011; Pousaneh, Ciach, and Maciolek, 2014) evidence that at larger salt concentrations the coupling between the charge density and the OP can significantly alter the standard critical adsorption and CCFs.] Moreover, it was assumed that for the temperatures studied, within a range $\Delta T < -1$ K, the “background” repulsive contribution is *de facto* temperature independent. This data analysis has rendered the length scale for the experimental decay of the CCP, which, however, differs from the bulk correlation length. This discrepancy as well as the softness of the repulsion at small separations has been attributed to the fluffiness of the colloidal particles. It is plausible that PNIPAM soft particles behave similarly to a single polymer chain near the critical point of the binary solvent, i.e., they may shrink [see the Introduction and Brochard and de Gennes (1980) and Venkatesu (2006)], which might explain the softness of the repulsion at small separations. The choice of PNIPAM particles has been motivated by their special properties when dissolved in the solvent described. They swell, which prevents sedimentation,

and in this swollen state their refractive index matches that of the solvent.

In a subsequent paper (Dang *et al.*, 2013), the fitting procedure was improved in the sense that the bulk correlation length ξ_t was no longer an adjustable parameter. Assuming the standard scaling law for ξ_t as a function of temperature, the amplitude $\xi_{t,+}^{(0)}$ has been used as a fit parameter in addition to the amplitude and the decay length of U_{rep} . Using one set of these three fit parameters, Dang *et al.* (2013) fitted all experimental data to the sum of two exponentially decaying functions. The fitted analytic expression for the potential has been further used for performing MC simulations of the colloidal sample. The colloidal gas-liquid coexistence was investigated by using Gibbs ensemble MC (Frenkel and Smit, 2001) whereas colloidal liquid-solid coexistence was determined by using Kofke’s Gibbs-Duhem integration technique (Kofke, 1993). The conclusiveness of these MC simulation results for the actual colloidal phase behavior may be questioned because the fits of the experimental data to the analytic expression for the potential are not completely satisfactory. The strongest deviations have occurred at small separations, where the potential has been finite even for center-to-center separations smaller than the diameter of the particles. Moreover, the pair potentials obtained from the fitting have not followed the data around the minimum of the total potential, especially close to T_c . Also these deviations have been attributed to the softness of the PNIPAM particles and to the fact that the scaling variable Λ describing off-critical compositions has been neglected. It has been tested if all these deviations may significantly affect the observed phase behavior by calculating the reduced second virial coefficient $B_2^* = B_2/B_2^{(HS)}$. Empirically, gas-liquid phase transitions are expected to occur for $B_2^* \lesssim -1.5$ (Noro and Frenkel, 2000; Vliegthart and Lekkerkerker, 2000). Applying this criterion for experimentally determined and fitted potentials has led to an estimate for an upper bound for the deviation $\Delta T = T_{cx} - T_{cx}^{(s)}(c_a) < -0.3$ K of the temperature T_{cx} , at which a colloidal gas-liquid transition takes place from that of the pure solvent phase separation [i.e., $T_{cx}^{(s)}(c_a)$], which is in agreement with both the experiments and the simulations reported by Dang *et al.* (2013). The comparison between computed and measured phase diagrams at fixed composition of a pure solvent in the plane spanned by $\Delta T = T_{cx} - T_{cx}^{(s)}$ and by the colloidal volume fraction [in Dang *et al.* (2013) denoted as ϕ] is shown in Fig. 10 [Fig. 2 of Dang *et al.* (2013)]. For solutions with off-critical compositions of a pure solvent, a reasonable agreement has been found, given the large uncertainties in the experimental determinations of the volume fraction and of ΔT , as well as given the simplified functional form taken for U_C . On the other hand, for solutions with the supposedly critical composition, the agreement is not as good. Deviations occur concerning the shape of the colloidal gas-liquid coexistence curve, which in simulations is shifted toward values of ΔT lower than those for the experimental data. Such a shift suggests that the fitted potentials underestimate the attractions between the colloids. According to Dang *et al.*, this is due to many-body interactions and too small simulation boxes; both

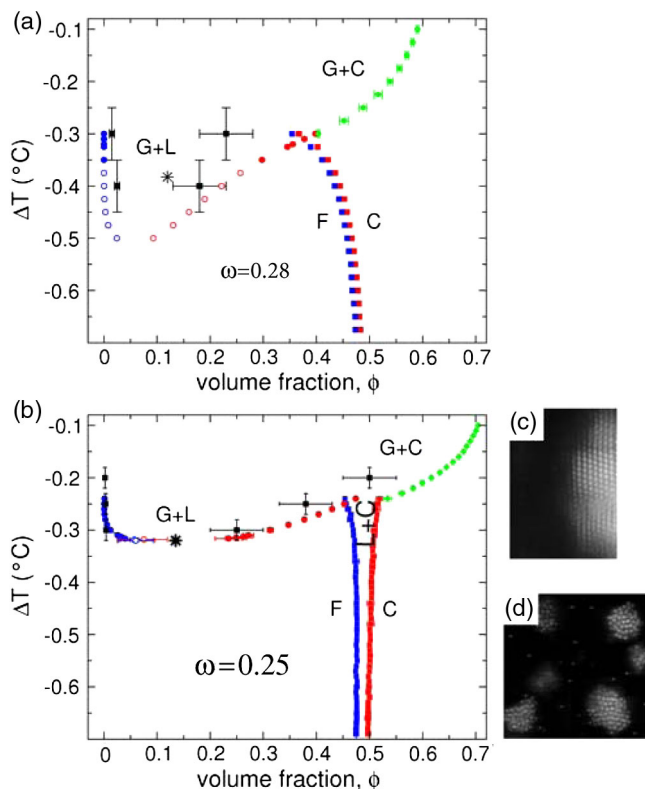


FIG. 10. Phase diagram in terms of $\Delta T = T - T_{cx}^{(s)}$ and volume fraction, in Dang *et al.* (2013) denoted as $\phi = V_s/V_{\text{tot}}$, where V_s is the volume of colloids and V_{tot} is the total volume of the sample. These data have been obtained from MC simulations (colored symbols) for the effective one-component colloidal system governed by a pair potential which is the sum of repulsive and attractive, exponentially decaying functions describing screened electrostatic and critical Casimir interactions. G, L, F, and C denote colloidal gas, liquid, fluid, and crystal phases, respectively. G + L, G + C, and L + C stand for the gas-liquid, gas-crystal, and the liquid-crystal coexistence regions. Black squares with error bars are experimental data for PNIPAM particles suspended (a) in the 3MP-heavy water mixture at the critical 3MP mass fraction $\omega_{3\text{MP}} = 0.28 \simeq \omega_{3\text{MP},c}$ and (b) in the 3MP-water-heavy water mixture at the off-critical 3MP mass fraction $\omega_{3\text{MP}} = 0.25$. Dang *et al.* (2013) interpreted the snapshots of confocal microscopy images for the mixture in (b) as the coexistence of colloidal gas and crystal at (c) $\Delta T = -0.2$ and colloidal gas and liquid at (d) $\Delta T = -0.3$. Stars indicate the experimental position of the colloidal gas-liquid critical point as estimated by using the law of rectilinear diameters. (a) The star appears as being placed at a too small value of $|\Delta T|$. From Dang *et al.*, 2013.

are particularly relevant for systems at the critical composition. Another possibility is that the effective one-component approach is not adequate to describe the considered experimental system. Concerning the colloidal liquid-solid phase coexistence in this system, there are currently no experimental data.

The experimental data for $g(r)$ at a 3MP mass fraction of 0.28, which is close to the critical value, and for the phase segregation have been reanalyzed by Mohry *et al.* (2014). The main improvement over the earlier analyses has been due to a better treatment of the CCP contribution $U(r) = U_{\text{bck}} + U_C$

to the total pair potential, where U_{bck} is a background term. Within this approach, the dependence of U_C on the solvent mass fraction has also been taken into account. The scaling function of U_C as a function of the scaling variable $\Sigma = \text{sgn}(th_b)\xi_t/\xi_h$ [see Eq. (23) and Fig. 1] has been calculated within the Derjaguin approximation by using a local-functional approach. In order to minimize the number of fit parameters, the amplitude $\xi_{t,+}^{(0)}$ has been set to the value extracted from the experimental data presented by Sorensen and Larsen (1985). Because the value of the critical mass fraction $\omega_{3\text{MP},c}$ of the 3MP-heavy water binary liquid mixture is not well established, the reduced OP $\tilde{\phi} = (\omega_{3\text{MP},c} - \omega_{3\text{MP}})/\mathcal{B}$ has been used as a fitting parameter for achieving the weakest variation of the background potential U_{bck} with temperature. [\mathcal{B} is the nonuniversal amplitude of the bulk coexistence curve $\omega_{3\text{MP},cx}(t < 0) = \omega_{3\text{MP},c} \pm \mathcal{B}|t|^\beta$.] A fair agreement with the experimental data has been obtained by allowing the value of $\omega_{3\text{MP},c}$ to differ significantly from the value cited by the authors of the experiment [see Fig. 5 of Mohry *et al.* (2014)]. The best fit has been achieved for $\tilde{\phi} = -0.088$; it has rendered the background potential which varies slightly with temperature and has an attractive part. This might be due to the coupling between critical fluctuations and electrostatic interactions and thus deserves further studies. The colloidal gas-liquid coexistence has been calculated within the effective one-component DFT approach for the off-critical composition of the solvent, which renders the best expression for U_{bck} (i.e., the least temperature-dependent one) extracted from the experimental data of Dang *et al.* (2013). The RPA has been employed for the free energy together with the Percus-Yevick expression for the hard-sphere reference contribution. Unfortunately, gas-liquid coexistence turns out to be rather sensitive to even a slight temperature variation of U_{bck} . Therefore the estimate for a phase diagram has been obtained by taking the mean curve of U_{bck} which correspond to the various temperatures considered. The corresponding results together with the experimental and MC simulation data from Dang *et al.* (2013) are shown in Fig. 11. At high colloidal densities, the RPA is in surprisingly good agreement with the experimental data. On the other hand, at low densities the RPA agrees well with the MC simulations, while for these densities both approaches underestimate the experimental values which, in turn, agree well with the RPA spinodal. While this latter “agreement” might be accidental, it nevertheless raises the question whether the experimental system had actually been fully equilibrated at the time of the measurements. As pointed out by Dang *et al.* (2013) and Nguyen *et al.* (2013), the phase diagrams shown in Fig. 10 are analogous to those of molecular fluids modeled, e.g., by Lennard-Jones or square-well fluids, but with a lower critical point. The peculiarity of the CCP, i.e., the strong temperature dependence of the shape of the potential and of its range, is mirrored by the small temperature range over which colloidal gas-liquid coexistence extends and in the shift of the critical point and of colloidal liquid-solid coexistence to lower volume fractions.

Experience gained from these studies summarized tells that a meaningful comparison of experimental data and theoretical predictions for the CCP requires accurate experimental knowledge of the solvent bulk phase diagram and of the solvent

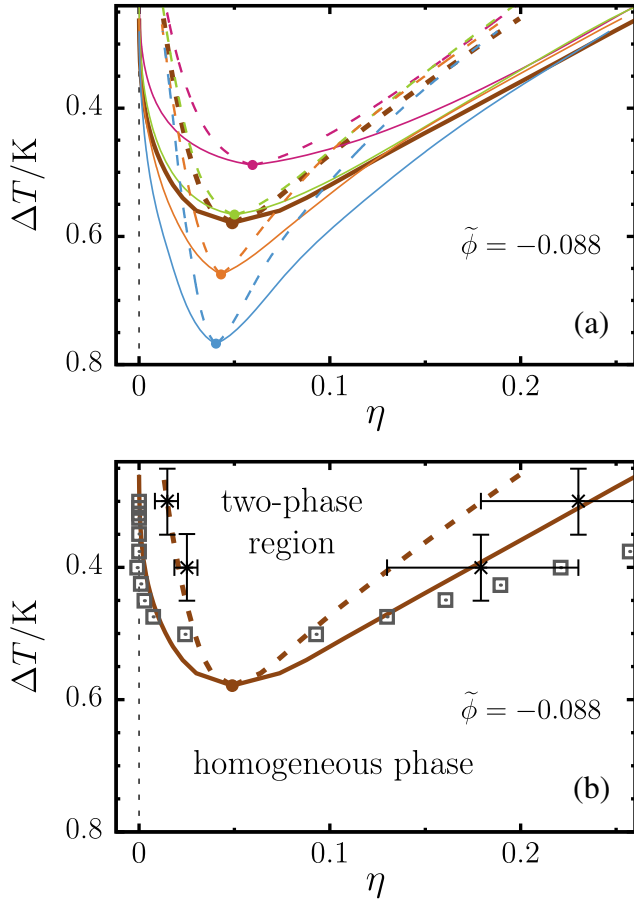


FIG. 11. Segregation phase diagrams obtained from theory (RPA), experiment, and simulations (MC). (a) The phase diagram obtained within the RPA using the four available background potentials U_{bck} extracted from effective potentials inferred from experimental data (Mohry *et al.*, 2014) at $\Delta T/K = 0.6$ (magenta), 0.5 (green), 0.4 (orange), and 0.3 (blue) and using U_{bck} as obtained by averaging these four potentials U_{bck} (thick dark red curve). The solid lines show the colloidal liquid-gas phase boundaries in terms of the packing fraction η of the colloids, whereas the dashed lines correspond to the spinodals, and dots represent critical points. (b) Comparison of the theoretical predictions for the phase boundaries (based on the mean U_{bck}) [thick dark red curve in (a)] with MC simulation data (\square) and experimental data (\times , with error bars) from Dang *et al.* (2013). On the temperature axis $\Delta T = T_c^{(s)} - T$ increases from top to bottom in order to mimic the visual impression of a lower critical point $T_c^{(s)}$ (of the solvent) as observed experimentally. (Note that compared with Fig. 10, ΔT has reversed its sign.) $\tilde{\phi} = (\omega_{3\text{MP},c} - \omega_{3\text{MP}})/\mathcal{B} = -0.088$, where \mathcal{B} is the nonuniversal amplitude of the bulk coexistence curve (see the main text). From Mohry *et al.*, 2014.

bulk correlation length. Such corresponding dedicated measurements have been reported by Stuij *et al.* (2017) for PNIPAM particles suspended in a binary liquid mixture of 3MP and heavy water with the addition of 1 mM KCl salt. The solvents have been prepared with 3MP mass fractions $\omega_{3\text{MP}}$ (and therein denoted as c and given in units of weight percentage $\text{wt}\%$ $3\text{MP} = 100\omega_{3\text{MP}}$) ranging from 23.5% to 33% around the critical value $\omega_{3\text{MP},c}^{(s)} \approx 28.0\%$, and for each of

them the temperature has been varied from the homogeneous, mixed phase toward the solvent two-phase coexistence. In order to achieve intrinsic consistency of the experimental data and to link them to theoretical predictions, the measurements of the pair potentials of the particles in terms of radial distribution functions $g(r)$ have been complemented with dynamic light scattering measurements of the solvent phase diagram and of the bulk correlation length. Below the lower critical temperature $T_c^{(s)}$, the solvent correlation lengths have been inferred from the temperature-dependent correlation functions determining the scattered intensity, which are well described by single-exponential decays with a characteristic time scale τ_d related to the effective diffusion coefficient $D = (q^2\tau_d)^{-1}$, where q is the wave vector of the incident wave (equal to $19 \mu\text{m}^{-1}$ in these specific measurements). This effective diffusion coefficient depends on the linear extent ξ of the correlated regions via a relation analogous to the Stokes-Einstein relation for Brownian particles. However, close to the critical point one has to take into account that $D = D_c + D_{\text{bg}}$ decomposes into a critical and a background part (Sorensen and Larsen, 1985), where (Burstyn and Sengers, 1982; Burstyn *et al.*, 1983; Sorensen and Larsen, 1985)

$$D_c = \frac{\mathcal{R}k_B T}{6\pi\eta\xi} K(q\xi)[1 + b^2(q\xi)^2]^{z/2}$$

and

$$D_{\text{bg}} = \frac{k_B T}{16\eta_{\text{bg}}\xi} \frac{1 + (q\xi)^2}{q_c\xi}.$$

Here $\mathcal{R} \approx 1.05$ is a universal dynamic amplitude ratio (Burstyn and Sengers, 1982; Burstyn *et al.*, 1983; Das, Sengers, and Fisher, 2007), $K(x) = (3/4x^2)[1 + x^2 + (x^3 - x^{-1}) \arctan x]$ is the Kawasaki function (Kawasaki, 1972), $b = 0.55$ (Burstyn and Sengers, 1982; Burstyn *et al.*, 1983) is a correction to the scaling amplitude, and η_{bg} is the background viscosity. The latter has been obtained as a function of T and $\omega_{3\text{MP}}$ by extrapolating the available viscosity data (Oleinikova, Bulavin, and Pipich, 1999) to the critical region. This detailed analysis has allowed one to determine the correlation length for various compositions and to extract the amplitude $\xi_{r,+}^{(0)} = 0.44 \text{ nm}$. The phase separation temperatures have been defined as those which correspond to the minimum of the diffusion constant for various values of $\omega_{3\text{MP}}$. They are fitted to the relation $\omega_{3\text{MP}} - \omega_{3\text{MP},c} = \mathcal{B}|t|^\beta$ with the fixed critical exponent $\beta = 0.3265$ leading to the estimate $\mathcal{B} = 0.6$ for the OP amplitude. The diameter $2R = 2.12 \mu\text{m}$ of the particles has been deduced by using confocal microscopy whereas their surface charge density $\Upsilon \approx -0.17e \text{ nm}^{-2}$ has been obtained from electrophoresis. The experimental radial distribution function $g(r)$, determined by particle tracking, reveals a very soft repulsion, according to which the measured effective potential fulfills $U(r < 2R) > 0$ and is very large but not infinite as one would expect for hard-core repulsion. As mentioned in the present section, in the previous studies (Nguyen *et al.*, 2013) this softness has been attributed to the fluffiness of the colloidal particles. A plausible alternative explanation for this softness consists of the

inaccuracy associated with determining a three-dimensional $g(r)$ from two-dimensional images and, in addition, a certain polydispersity. [Stuij *et al.* \(2017\)](#) compared this inaccuracy of the experimental radial distribution function with the projected theoretical function

$$g_{\text{proj}}\left(r' = \sqrt{x^2 + y^2}\right) = \int_{-\infty}^{\infty} dz \int_{-\infty}^{\infty} dy \int_{-\infty}^{\infty} dx f_{\{0,\sigma_z\}}(z) f_{\{y',\sigma\}}(y) f_{\{x',\sigma\}}(x) \times g\left(\sqrt{x^2 + y^2 + z^2}\right),$$

where $f_{\{x',\sigma\}}(x)$, $f_{\{y',\sigma\}}(y)$, and $f_{\{0,\sigma_z\}}(z)$ are the probability distributions, which account for the uncertainty in the two horizontal directions and the vertical direction, respectively, with the in-plane spreads $\sigma = \sigma_x = \sigma_y$ being equal. [Stuij *et al.* \(2017\)](#) took these distributions to be the normal ones. Building upon the consistent description of the bulk properties of the binary solvent, the comparison between the measured pair potentials and the theoretical model, given by Eq. (23) within the Derjaguin approximation for the CCP, would not have required any fitting parameter if the surface of the colloids had exhibited strong preferential adsorption. However, the PNIMP particles are only weakly hydrophilic. In such a case the CCP depends also on the surface field h_s via the scaling variable $\hat{h}_s = h_s |t|^{-\Delta_1}$, where Δ_1 is the surface counterpart of the bulk gap exponent ([Diehl, 1986](#)) (see Secs. II.B and II.B.4). For the film geometry, within mean field theory the dependence on \hat{h}_s at the critical concentration ($\Sigma = 0$) can be reduced to a remapping $\tilde{\vartheta}_{\parallel}^{(d)}(\mathcal{Y}, \Sigma; \hat{h}_s) = s^d \vartheta_{\parallel}^{(d)}(s^{-1}\mathcal{Y}, \Sigma)$ with a rescaling parameter s , which depends on \hat{h}_s ([Mohry, Maciolek, and Dietrich, 2010](#)). [Stuij *et al.* \(2017\)](#) found that within the experimentally accessible range of the CCP scaling function, which usually consists of only its exponential tail, one may mimic such a rescaling by using an effective temperature offset t_{off} which shifts the reduced temperature according to $t' = (T_c - T + \Delta T_{\text{off}})/T_c = t + t_{\text{off}}$. Assuming that such a rescaling is valid also beyond mean field theory, [Stuij *et al.* \(2017\)](#) were able to fit all pair correlation functions for a variety of temperatures and even of off-critical compositions, by taking the single parameter t_{off} to vary smoothly with composition. Based on these fits the predictions for the pair potential are also given (see Fig. 12). Remarkably, any distorting influence on $g(r)$, which can be described by probability distribution functions which are symmetric about their argument, leaves the second virial coefficient unchanged. This holds because B_2 is determined by the integrated pair potential [see Eq. (25)]. Taking advantage of this property, [Stuij *et al.* \(2017\)](#) compared virial coefficients computed from the raw data of $g(r)$ directly with theoretical predictions, without any need to account for experimental inaccuracies and particle polydispersity. The experimental and theoretical values of B_2^* show very good agreement in the entire temperature-composition plane (see Fig. 13). The comparison based directly on the raw data provides clear evidence that in the investigated solvent composition range it is indeed the critical Casimir interaction which underlies the colloidal attraction. Hence, this direct comparison

suggests that not only at the critical composition, but also at these off-critical compositions, the attraction is described in terms of the CCF rather than by wetting effects. Yet, at even larger off-critical compositions, wetting effects are expected to eventually take over and dominate the attraction as observed by [Hertlein *et al.* \(2008\)](#).

Using the same experimental imaging and particle tracking techniques, [Newton *et al.* \(2017\)](#) extracted the effective interaction potentials for nonspherical dumbbell particles from observed radial and angular distributions. The colloidal patchy dumbbell particles have been suspended in heavy water and 3MP with a mass fraction $\omega_{3\text{MP}} = 0.25$ (therein denoted as $c_{3\text{MP}}$). At this subcritical composition, the hydrophobic spherical ends prefer 3MP, while the neck joining these two spherical ends (called a “shell”) prefers water. While the one-to-one mapping between radial distribution function and the effective, angularly averaged pair potential still holds for the anisotropic particles, the simple procedure of inferring the effective potential from the radial distribution function is not valid anymore. In order to find an optimal effective potential [Newton *et al.* \(2017\)](#) assumed that dumbbells are the rigid construction of two isotropic spheres each of which interacts via an isotropic pair potential. They used several distribution functions which facilitate the comparison of simulations, theory, and experiment—this way determining that set of potential parameters which renders the best match. Because the corresponding experimental system has not been density matched, the particles sedimented, which was taken into account by including the gravitational potential and a surface field in order to describe the interaction with the bottom wall. Concerning the CCP, [Newton *et al.* \(2017\)](#) adopted an oversimplified expression such as the one given by Eq. (19), in line with [Bonn *et al.* \(2009\)](#), [Dang *et al.* \(2013\)](#), and [Nguyen *et al.* \(2013\)](#). As discussed, such a form is valid only in the limit $D/\xi \rightarrow \infty$ and at the critical composition. Neither condition is met in the experiment under consideration. Moreover, the amplitude of the bulk correlation length of the solvent and the surface charge, which determines the strength and the decay length of the electrostatic repulsion, respectively, have not been measured. As a consequence, the numerous adjustable parameters have been used to fit the theoretically proposed effective potentials to the measured ones. Following [Stuij *et al.* \(2017\)](#), [Newton *et al.* \(2017\)](#) used the projected theoretical distribution functions in order to mimic the experimental uncertainties. Nevertheless, the extent of agreement between the measured and the theoretically proposed effective potentials depends on temperature and is not satisfactory. The results for the dumbbell effective pair potentials, based on so many crude approximations and numerous fit parameters, are not conclusive and cannot be predictive. In particular, the quantitative modeling carried out by [Newton *et al.* \(2017\)](#) is not able to provide an explanation for the observed two ranges of temperatures featuring distinct aggregation behaviors (see Sec. IV.D).

On theoretical grounds CCFs are expected to exhibit many-body interactions ([Hobrecht and Hucht, 2015](#); [Mattos, Harnau, and Dietrich, 2015](#); [Vasilyev, Dietrich, and Kondrat, 2018](#)). Direct *experimental* evidence for the non-additivity of CCFs was reported by [Paladugu *et al.* \(2016\)](#) for three colloidal microspheres immersed in a mixture of water and 2,6-lutidine at the critical lutidine mass fraction

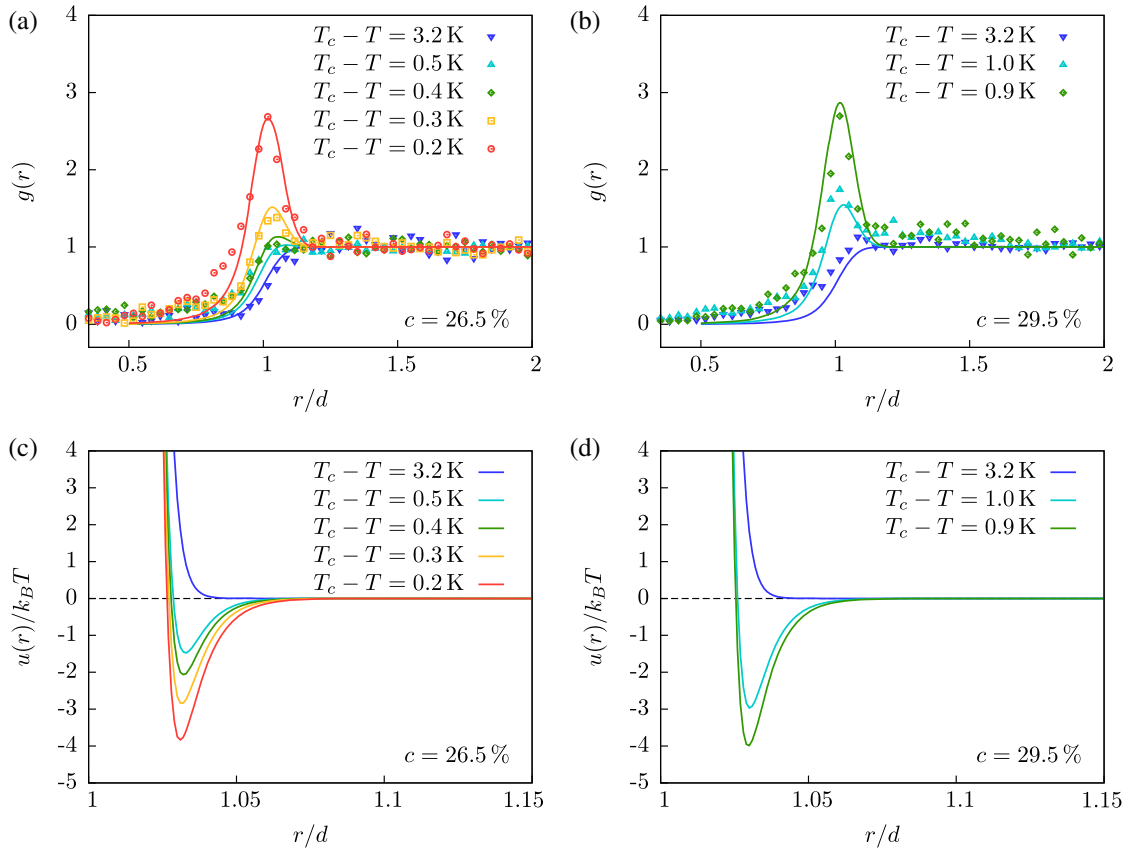


FIG. 12. (a), (b) Radial distribution function $g(r)$ of the PNIPAM particles suspended in the 3MP-heavy water liquid mixture for the off-critical mass fractions ω_{3MP} (in the figures denoted as c and given in units of weight percentage wt% 3MP = $100\omega_{3MP}$), $c = 26.5\%$ (with $\Delta T_{\text{off}} = 0.7$ K) and $c = 29.5\%$ (with $\Delta T_{\text{off}} = 0.18$ K), where the effective temperature offset ΔT_{off} defined via $(T_c - T + \Delta T_{\text{off}})/T_c \equiv t + t_{\text{off}}$ is a fit parameter. The experimental data (symbols), obtained by [Stuij et al. \(2017\)](#) by using confocal microscopy, are compared with the theoretical predictions (solid lines) based on the model given by Eq. (25) with the Derjaguin approximation for the CCP. (c), (d) Theoretically predicted pair potentials $u(r)$ for the same compositions. From [Stuij et al., 2017](#).

$\omega_{c,L} = 0.286$ [denoted as c_L^c by [Paladugu et al. \(2016\)](#)]. These particles have been held by holographic optical tweezers, which are realized by shaping a laser beam using a spatial light modulator. In the bulk of the critical mixture the particles are fixed in space with nanometric accuracy at the corners of an almost equilateral triangle. For this setup digital video microscopy has been used in order to measure the probability distribution $P_2(D_{12})$ of the in-plane surface-to-surface distance D_{12} between the particles 1 and 2 and the probability distribution $P_3(D_{12})$ of the in-plane distance between particles 1 and 2 in the presence of particle 3. The effective pair potentials have been inferred from the relation $U_\alpha(D_{12}) \equiv -k_B T \ln P_\alpha(D_{12})$, $\alpha = 2, 3$. In order to allow for both attractive and repulsive CCFs the surfaces of hydrophilic silica colloids of diameter $2R = 2.06 \pm 0.05 \mu\text{m}$ have been treated with octyltriethoxysilane to make them hydrophobic. Upon approaching the critical point of the solvent, the two-body CCF has been measured for each of the three pairs of particles in the absence of the remaining colloid, which has been temporarily placed into an auxiliary trap. Assuming additivity of CCFs, these measurements would predict the forces acting on a pair of particles in the presence of a third one. Then the prediction based on additivity has been compared with the actually measured

three-body potential. The observed significant discrepancies have been interpreted as manifestations of the actual non-additivity of CCFs. The experiment has been performed for three hydrophilic particles [(- - -) BCs] and repeated for one hydrophobic (3) and two hydrophilic (1, 2) particles (- - +). The results for the measured and predicted potential $U_3(D_{12})$ for symmetric (- - -) BCs are shown in Fig. 14. The experimental results for the effective potentials for each pair of particles compare well with the theoretical ones based on the effective model given by Eq. (23), complemented by the harmonic potentials exerted by the optical traps.

D. Applications of critical Casimir forces for self-assembly and aggregation of colloids

The possibility of controlled aggregation by exploiting CCFs has been used, near the lower critical point of the suspension, for the self-assembly of cadmium telluride quantum dots in water-3MP liquid mixtures with NaCl salt ([Marino et al., 2016](#)). By measuring the intensity of scattered light as a function of time and by following the time evolution of the intensity correlation function, it was found that 1 K below the phase separation temperature of the suspension the hydrophilic quantum dots with a size of ca. 2.6 nm form aggregates

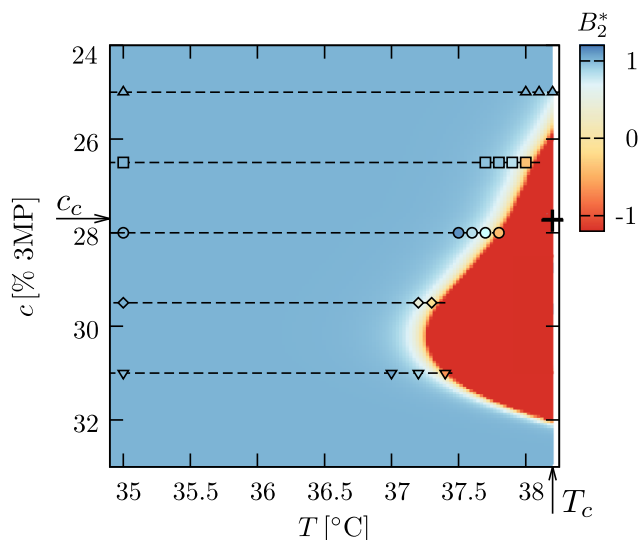


FIG. 13. Reduced second virial coefficient $B_2^* = B_2/B_2^{(HS)}$ as a function of T and c for the same system as in Fig. 12. The color of the shading provides the theoretically predicted values of $B_2^*(T, c)$, while the colored symbols provide the experimental value of $B_2^*(T, c)$ as obtained by numerically integrating the measured radial distribution function $g(r)$ [Eq. (25)]. The weak color contrast between the colors of the symbol and the corresponding underlying shading indicates agreement between the experimental and theoretical data. The values $B_2^* \approx 1$ depicted in blue indicate a significant repulsion, while the values $B_2^* \approx -1$ depicted in red indicate strong attraction. Yellow marks the crossover. The critical temperature $T_c^{(s)}$ (denoted as T_c) and the critical mass fraction c_c are indicated by arrows and the critical point is indicated by $+$. Via the color, B_2^* is shown in the entire (T, c) plane. The black dashed lines correspond to those five concentrations for which there are experimental data; each dashed line corresponds to a certain symbol type. From *Stuij et al., 2017*.

with an average radius of ca. 700 nm. As expected, for a composition with the 3MP volume fraction being larger than its critical value, i.e., corresponding to the phase poor in the component preferred by the quantum dots, aggregation takes place on shorter time scales and within a larger temperature interval than for a mixture with a 3MP volume fraction being smaller than the critical one.

Critical Casimir interactions can be utilized for aggregation of colloids being induced by a substrate such that the colloids follow the chemical pattern designed on the surface of a substrate which characterizes the boundary conditions. This is because CCFs respond sensitively to the chemical properties of the confining surfaces. As discussed in Sec. II, depending on whether the surfaces of the colloid and the substrate have the same or opposite preferences for the species of the solvent (symmetric or asymmetric BCs), attractive or repulsive CCFs arise. *Soyka et al. (2008)* and *Tröndle et al. (2009)* suspended charged polystyrene spheres with $R = 1.2 \mu\text{m}$ in a water-2,6-lutidine mixture at its critical composition, i.e., a lutidine mass fraction of $\omega_{L,c} \cong 0.286$. The suspension has been exposed to a chemically patterned substrate with well-defined, spatially varying adsorption preferences. This was achieved by first coating the glass surface with a monolayer of hexamethyldisilazane which rendered the glass surface hydrophobic with a

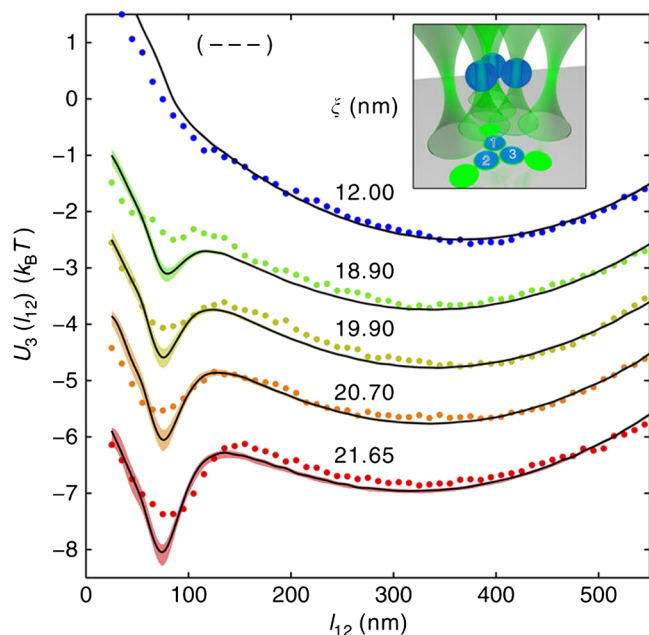


FIG. 14. Many-body CCFs with symmetric boundary conditions. The symbols represent the measured effective potential $U_3(D_{12})$ between particles 1 and 2 (labeled in black in the inset) in the presence of particle 3 (labeled in white in the inset) as a function of the in-plane surface-to-surface distance D_{12} [denoted by *Paladugu et al. (2016)* as l_{12}] upon increasing (from top to bottom) the correlation length ξ . All particles are hydrophilic (---), resulting in attractive CCFs. The solid lines represent the corresponding theoretical predictions obtained by assuming additivity of the measured pair potentials between particles 1–2, 1–3, and 2–3, with the associated uncertainty indicated by the shading. The observed discrepancy increases as ξ increases, providing quantitative evidence of the nonadditive nature of the CCFs. The symbols and lines are vertically separated by $1k_B T$ for clarity. Inset: The trap and colloid configuration during the measurement. From *Paladugu et al., 2016*.

preferential adsorption of lutidine, corresponding to a (+) BC. Spatial patterning of the BCs has been obtained by using a focused ion beam (FIB) of positively charged gallium ions which created well-defined hydrophilic (–) areas with a lateral resolution on the order of several tens of nanometers extending over an area of approximately $400 \times 400 \mu\text{m}^2$. Close to the lower critical demixing point $T_c \approx 307 \text{ K}$ of water-2,6-lutidine mixture (*Beysens and Estève, 1985*), normal and lateral CCFs lead to a strongly temperature-dependent attraction between the hydrophilic (–) polystyrene particles and the hydrophilic squares (forming a 2D square lattice of locally symmetric boundary conditions) and to a repulsion from the hydrophobic regions (+) (locally asymmetric boundary conditions). This gives rise to the formation of highly ordered colloidal self-assemblies, the structure of which is controlled by the underlying chemical pattern (see Fig. 15). At higher particle concentrations, additional CCFs between neighboring particles arise and eventually lead to the formation of three-dimensional, faceted colloidal islands on the substrate. In order to quantify lateral CCFs, substrates with a periodic one-dimensional chemical pattern have been created forming hydrophilic (–) and hydrophobic (+) stripes with widths of 24.6 and 5.2 μm , respectively. For these

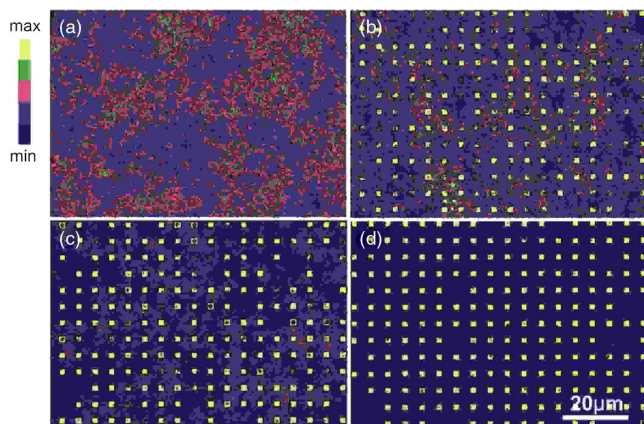


FIG. 15. Mean particle density distribution (represented by different colors ranging from black to yellow for minimal to maximal density, respectively) of a dilute colloidal suspension of spherical particles with $R = 2.4 \mu\text{m}$ dissolved in a critical water-2,6-lutidine mixture in the presence of a chemically patterned substrate. Particle positions were determined by digital video microscopy with a spatial resolution of ca. 50 nm. (a) $T_c^{(s)} - T = 0.72$, (b) 0.25, (c) 0.23, and (d) 0.14 K. From *Soyka et al., 2008*.

one-dimensional surface patterns the particle distribution was measured by digital video microscopy and from the two-dimensional projection of this distribution the effective one-dimensional CCP was determined by resorting to the Boltzmann factor. *Tröndle et al. (2009)* repeated the experiment for substrates with the chemical pattern created by microcontact printing, which provided sharper, chemical steplike, one-dimensional interfaces between alternating regions of antagonistic adsorption preferences than the FIB technique does. The reason for the disadvantage of FIB is that the ion beam charges the substrate surface and thus deflects the incoming beam which gives rise to fuzzy chemical steps. It turns out that the agreement between theory and the experimental data is so sensitive (Fig. 16) that the CCP can be used to probe the geometry of the chemical structures, which at present cannot be achieved by other experimental techniques. Accordingly, CCFs can be used as novel surface sensitive probes.

Reversible aggregation of spherical Janus particles has been studied experimentally for microsized silica particles half covered by a layer of gold and suspended in the water-2,6-lutidine mixture at the critical concentration (*Iwashita and Kimura, 2013*). The gold caps of the particles have been modified chemically by sulfonic groups, which have bestowed a large charge density on their surfaces, leading to an adsorption property which differs from that of the bare silica surfaces. Because of this anisotropy, the particles assembled to clusters with a very specific structure, followed by a hierarchical growth of the clusters. These structures depend on the “valence” of the Janus particle, i.e., the maximum possible number of bonded nearest neighbors. In two spatial dimensions, which applies to the dispersion of the sedimented particles considered in the experiment, the valence is equal to six. Direct visual observation has revealed that particles, randomly dispersed at low temperatures, have started to form micellar structures upon increasing T toward the lower critical point of the water-2,6-lutidine mixture. Most of the clusters

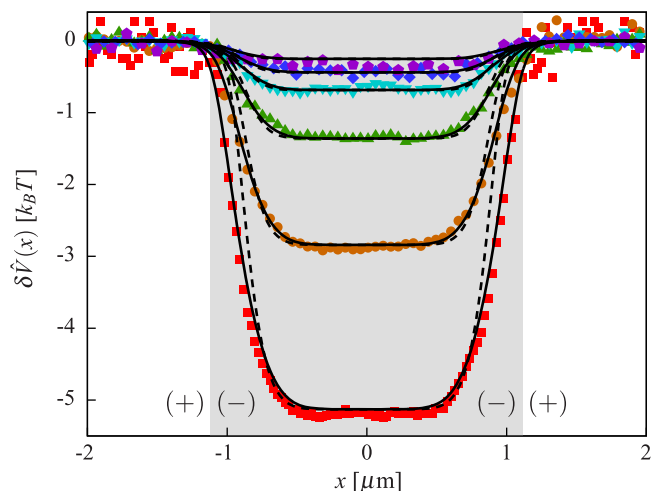


FIG. 16. Total effective potential $\delta\hat{V}(x) = \hat{V}(x) - \hat{V}(x = P/2)$ of the forces acting on hydrophilic polystyrene spheres of radius $R = 1.2 \mu\text{m}$ above a chemically striped pattern of periodicity P with alternating $(-)$ and $(+)$ boundary conditions and immersed in a water-2,6-lutidine mixture at its critical concentration as a function of its lateral position x for various temperatures $T_c^{(s)} - \Delta T$ below the experimental value $T_c^{(s)}$ of the lower critical temperature of the solvent. The potential is given by $\hat{V}(x) = -k_B T \ln[\hat{\rho}(x)]$, where $\hat{\rho}(x)$ is the effective number density of the colloids at x , obtained by projecting the actual number density onto the x axis. The width of $(-)$ and $(+)$ stripes is $2.25 \mu\text{m}$. Symbols indicate experimental data, whereas the lines are the corresponding theoretical predictions for sharp (dashed lines) and fuzzy (solid lines) chemical steps. From top to bottom the measured temperature deviations ΔT are 0.175 (0.165), 0.16 (0.152), 0.145 (0.143), 0.13, 0.115, and 0.10 K. If indicated, the values in parentheses are corrected values of temperature (but compatible within the experimental inaccuracy) which have been used for evaluating the theoretical predictions. From *Tröndle et al., 2009*.

have been trimers and tetramers, with gold-coated hemispheres inside the micelle and silica hemispheres always facing outward. No “inverted” micelles have been observed, which indicates that the effective attraction between golden patches of colloids has been much stronger than the attraction between the silica parts of the particles. At higher temperatures small clusters, mostly tetramers, have assembled into chainlike structures, finally forming a percolating network. The reversibility of the aggregation, the value of the onset temperature, and the apparent increase of the strength of attraction upon approaching $T_c^{(s)}$ have supported the expectation that this aggregation is due to CCFs. The structures of the clusters observed in the experiments are similar to those obtained within MC simulations of hard disks with a pairwise square-well potential acting between the semicircular patches of the particles. However, the strength of attraction could not be determined from the experimental data. The analysis of the cluster structures corresponding to the lowest internal energy and of the hierarchical clustering suggested the possibility that the self-assembly of Janus particles is governed by the valence structure of the clusters and not by that of a single particle.

Recent progress in synthesizing colloidal building blocks allowed Nguyen, Newton, Kraft *et al.* (2017) and Nguyen, Newton, Veen *et al.* (2017) to fabricate particles with complex shapes and surface patch properties which act as analogs of molecular valence. Multivalent particles such as dimers, trimers, and tetramers have been produced by swelling and polymerizing clusters of poly(methylmethacrylate) spheres with a methylmethacrylate/methacrylic acid shell, resulting in geometrically well-defined patches. The specific solvent affinity of the particle patches has been achieved by grafting a polyhydroxy stearic acid copolymer onto the surface patch, which renders it hydrophobic. The central part of the patchy particles is made hydrophilic by using the ionic initiator potassium persulfate. The particles have been suspended in the homogeneous phase of a binary solvent of heavy water and 3MP at temperatures below the lower critical temperature $T_c = 38.55$ °C, which has been determined by light scattering and microscopy from solvent phase separation at the critical composition. The solvents were prepared with 3MP mass fractions $\omega_{3MP} = 0.25$ and 0.31 (therein denoted as c_{3MP}), i.e., slightly below and above the critical composition $\omega_{3MP,c} = 0.28$, respectively. The hydrophobic patches have a strong affinity for the nonaqueous component 3MP of the binary solvent, while the hydrophilic central part has an affinity for water. It has been observed that, in solvents poor in the component preferred by the particle patches, the patches approach each other at temperatures close to $T_c^{(s)}$, and that dimer particles assemble into directed, chainlike structures. The bending stiffness of the chains has been directly measured by monitoring thermally activated bending fluctuations. In contrast, in 3MP-rich solvents, the particles approach each other sideways resulting in distinct parallel structures. For trimers, the patch-to-patch binding in 3MP-poor solvents leads to staggered chains, while the side-by-side binding in 3MP-rich solvents leads to bent filaments associated with the dense alternating stacking of trimers. In all cases, the assembly is fully reversible as confirmed by the breakup of aggregates upon lowering the temperature several degrees below $T_c^{(s)}$. Interestingly, in the case in which the chain structure is formed by dimers, upon further approaching $T_c^{(s)}$, Nguyen, Newton, Veen *et al.* (2017) observed that the chain spontaneously

collapses into a compact state, the dimer particles approach each other sideways, and eventually form a close-packed arrangement. It has been argued that in this close-packed state a particle has more bonding neighbors, and hence a more negative bond energy. Nguyen, Newton, Veen *et al.* (2017) regarded this as being similar to the collapse transition of a polymer, which occurs if the solvent conditions go from good to poor. For polymers, too, the reduction of the conformational entropy of the chain is offset by the stronger interparticle interaction energy. Using MC simulations with the effective pair potential determined by Newton *et al.* (2017) (see the preceding Sec. IV.C), Nguyen, Newton, Veen *et al.* (2017) argued that the colloidal chain collapse results from the enlarged interaction range due to the increase of the solvent correlation length upon approaching the solvent critical point. Nguyen, Newton, Kraft *et al.* (2017) experimentally investigated the effect of patch width on the topology of colloidal aggregates.

E. Colloidal mixtures

The way the unique properties of CCFs can be harnessed to manipulate colloidal suspensions was demonstrated by experiments on colloidal mixtures (Zvyagolskaya, Archer, and Bechinger, 2011). This experimental system has been composed of a binary mixture of microsized silica particles with slightly different diameters which were suspended in the water-2,6-lutidine mixture. For this small size difference of the colloids the inherent depletion interaction cannot induce demixing. However, the CCFs can accomplish this, if the two types of particles carry opposite adsorption preferences. The *a*-type particles were functionalized with silane rendering them hydrophobic, i.e., (+) BC, whereas the *b*-type particles had a strong adsorption preference for water, i.e., (−) BC. For such BCs the CCFs among the *a*-type and *b*-type particles are attractive, whereas between *a* particles and *b* particles they are repulsive. At the same temperature and the same distance, the repulsive CCF is stronger than the attractive CCF. In the system under consideration, the van der Waals forces have been eliminated by index matching so that besides the CCFs the only remaining forces have been the screened electrostatic interactions. In the suspension, this mixture of colloids

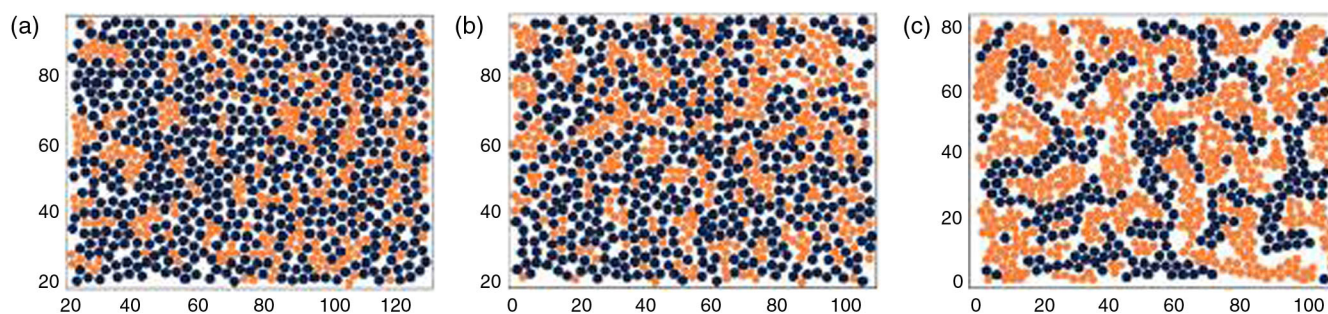


FIG. 17. The two-dimensional configurations of binary colloidal systems (black and orange disks) for three different compositions, expressed in terms of the concentration $x_a = \rho_a / (\rho_a + \rho_b)$, where ρ_a and ρ_b are (areal) number densities of the particles of type *a* and *b*, respectively. (a) $x_a = 0.28$, (b) $x_a = 0.32$, and (c) $x_a = 0.54$ with $a = \text{orange}$, exhibiting distinct structures formed after 1 h at a temperature deviation $\Delta T = T_c^{(s)} - T = 0.01$ K from the lower critical point of the solvent. The horizontal scales range from 20 to 120 in (a) and from 0 to 100 in (b) and (c), whereas the vertical scales range from 20 to 80 in (a) and (b) and from 0 to 80 in (c); the authors have not provided the units. From Zvyagolskaya, Archer, and Bechinger, 2011.

sedimented at the bottom of the cell forming a dense monolayer. One species has been labeled with a fluorescent dye and traced by using video microscopy. As expected, upon approaching the lower critical point of the binary solvent at its critical composition, large structural changes in the colloidal mixture have been observed, signaling the demixing process. It was found that the morphology of this process depends strongly on the mixing ratio $x_{a,b} = \rho_{a,b}/(\rho_a + \rho_b)$ of a and b particles, where $\rho_{a,b}$ are the number density of a and b particles (see Fig. 17). For $x_a = 0.54$ and at low temperatures an initially random distribution of particles transforms into a bicontinuous network, which is coarsening further upon increasing the temperature. For $x_a = 0.28$, no bicontinuous structure has been observed; demixing has proceeded via the growth of small clusters of the minority phase (here rich in a particles).

In the theoretical part of this study (Zvyagolskaya, Archer, and Bechinger, 2011), the effective approach has been employed in order to construct an approximation for the Helmholtz free energy of the colloid mixture. It has been assumed that the effective pair potential $U_{i,j}$, $i, j = a, b$ can be split into a hard-disk part and a tail, which for identical particles is attractive and for the distinct ones repulsive. For the hard-disk part of the free energy the scaled particle approximation has been used, whereas the attractive or repulsive tail has been treated within the mean field van der Waals approximation. The predictions of this simple theory for the locations of the colloid demixing transitions and their critical point agree fairly well with the experimental data.

F. Effects of depletants on colloidal phase separations

Buzzaccaro *et al.* (2010) and Piazza *et al.* (2011) studied experimentally the colloidal phase separation in suspensions with a depletion agent, which occurred near the critical point of the depletant enriched solvent. They used the so-called Hyflon™ MFA latex particles (a copolymer of tetrafluoroethylene and perfluoromethylvinylether) of average size $R \sim 90$ nm suspended in water with the nonionic surfactant $C_{12}E_8$. Salt (NaCl) has been added in order to screen electrostatic interactions between the colloids, caused by their surfaces carrying a negative charge. In addition, this surfactant has also provided steric stabilization of the suspension due to its spontaneous adsorption on the colloid surfaces. What makes this system interesting is that at concentrations above the critical micellar concentration, $C_{12}E_8$ in water forms globular micelles with a radius $\sigma = 3.5$ nm. These micelles act as a depletant for the MFA particles. Moreover, the surfactant-water mixture exhibits a liquid-liquid phase transition terminating at a lower critical point ($T_c^{(s)}, c_s^{(c)}$) with a very small value of the critical concentration $c_s^{(c)}$ of the surfactant (1.8% mass fraction $c_s = m_s/m_{\text{tot}}$, where m_s is the mass of the surfactant and m_{tot} is the total mass of the sample). (We use superscript s as an acronym for the solvent and subscript s for the surfactant.) Above this critical point two liquid phases exist, one rich and the other poor in micelles. They determined, as a function of temperature, the minimum concentration $c_s^{(m)}$ of surfactants required to induce colloidal

gas-liquid phase separation. The onset of this phase separation has been assumed to manifest itself via the sudden increase of turbidity followed by fast sedimentation of the colloidal particles. The results of these measurements (see Fig. 18) show a drastic decrease of $c_s^{(m)}$ upon increasing temperature toward the consolute point ($T_c^{(s)}, c_s^{(c)}$) of the surfactant-water mixture, such that $c_s^{(m)}$ approaches $c_s^{(c)}$ as $T \rightarrow T_c^{(s)}$. Far below the surfactant-water miscibility gap, the colloidal phase separation has been obtained due to the action of depletion forces, provided that a sufficient amount of surfactant has been added. The range of the depletion interaction is set by the ratio ≈ 0.03 between the micelle and the particle size and is very short, but the strength depends on the concentration of the micelles. In Fig. 18, the solid dots ($T_s^{(m)}, c_s^{(m)}$) show the minimum amount $c_s^{(m)}$ of surfactant required to induce colloidal phase separation at the temperature $T_s^{(m)}$. These points are expected to correspond to the thermodynamic states of the surfactant-water solvent for which the strength of the effective attractive potential between the colloidal particles is roughly constant. They have interpreted the reduction in $c_s^{(m)}$ observed at higher temperatures as an increase of depletant “efficiency.” Although the colloidal gas-liquid coexistence line crosses continuously from a depletion force to a CCF governed region, one should keep in mind that depletion and CCF originate from very different physical mechanisms (see Sec. II.B).

Inspired by these experiments, Gnan *et al.* (2012) performed a numerical study of the phase separation of hard spheres dispersed in an implicit solvent (i.e., there are no direct interactions, beyond the hard-core ones, between the solvent molecules and these spheres) in the presence of interacting depletant particles. The particles have been taken to interact via the corresponding effective potential V_{eff} as determined by MC simulations for SW and 3P models of depletants [see Eq. (8) as well as Secs. II and IV.F]. The phase separation of the colloids as a function of the depletant concentration for various depletant-colloid size ratios has been determined within grand canonical MC simulations. The numerically determined loci of the onset of colloidal gas-liquid phase separation has been displayed within the phase diagram of the depletant which exhibits an upper critical point. This revealed that for almost all parameters studied in the MC simulations, the colloidal phase separation induced by CCFs is preempted by the one driven by standard depletion forces. The important message of this study is that only by weakening the attractive depletion interactions, either by lowering the critical depletant concentration $c_s^{(c)}$ or by introducing a repulsive interaction between the colloids, is it possible to exploit CCFs for the fine-tuning of the self-assembly of colloids in solvents with interacting depletant agents.

G. Aggregation kinetics and structures of aggregates

Aggregation of colloids in a near-critical binary solvent was studied experimentally on the ground and under microgravity conditions (Bonn *et al.*, 2009; Veen *et al.*, 2012; Shelke *et al.*, 2013; Potenza *et al.*, 2014). The advantage of the critical Casimir effect of providing the ability to tune the effective

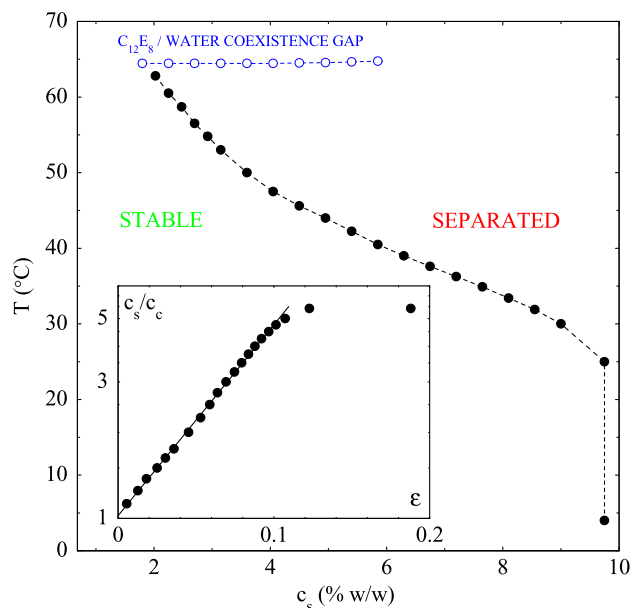


FIG. 18. Experimental phase diagram of aqueous suspensions of MFA latex particles in the presence of a nonionic surfactant of mass fraction $c_s = m_s/m_{\text{tot}}$ (in units of mass percentage, sometimes called weight percentage, wt % w/w = $100 \times c_s$), where m_s is the mass of all surfactant particles and m_{tot} is the total mass of the sample. For state points of the surfactant-water mixtures to the left of the line of dots (denoted as “stable”) the dissolved colloidal particles with a volume fraction $V_c/V_{\text{tot}} = 0.03$ form a homogeneous colloidal phase whereas for state points to the right of the line of dots (denoted as “separated”) the colloids phase separate into a colloidal gas and a colloidal liquid. (V_c is the volume taken by colloidal particles and V_{tot} is the total volume of the sample.) At a given temperature, the solid black dots represent the minimum amount $c_s^{(m)}$ of surfactant required to induce colloidal gas-liquid phase separation at a given temperature. The rather shallow coexistence curve of the surfactant-water mixture with a lower critical point (located around 1.8% of c_s , not marked in the plot) is shown by open blue dots. The data correspond to 250 mM added NaCl salt. The inset shows (in our present notation) $c_s^{(m)}$ in units of its critical value $c_s^{(c)}$ (i.e., c_s at the critical point) as a function of reduced temperature $t = (T_c^{(s)} - T)/T_c^{(s)}$ [note that, as in Piazza *et al.* (2011), in this figure $c_s^{(m)}/c_s^{(c)}$ and t are denoted by c_s/c_c and ε , respectively]. From Piazza *et al.*, 2011.

interactions between the colloids by varying the temperature has been used in order to study systematically the internal structure of the aggregates as a function of their interparticle attraction. Direct visual observations via confocal microscopy of a dilute suspension of latex particles of radius R in a $\text{D}_2\text{O}/\text{H}_2\text{O} - 3\text{MP}$ mixture have revealed the formation of fractal clusters of colloidal particles near the critical point of the solvent (Bonn *et al.*, 2009). The analysis of the time-dependent intensity $I(q, t)$ revealed that $I(q, t)$ exhibits a maximum at $q = q^*(t)$, which corresponds to the inverse of the mean cluster size. It has been found that in the course of time q^* decreases as $q^*(t) \propto t^{-1}$ and that this linear growth of the size of the clusters with time t is self-similar. The latter property has been inferred from the data collapse of $I(q, t)$

plotted as a function of the rescaled wave vector $q' = q/q_0 = (t/t_0)qR$ with $t_0 = 33 \text{ min}$.² The fractal dimensions d_f determined from 2D projection images have indicated that this system exhibits diffusion-limited cluster aggregation rather than diffusion-limited particle aggregation, for which d_f is larger (Dutcher and Maragoni, 2004). The fractal dimension reflects the internal structure of an aggregate and relates its radius R_g of gyration to the number of particles N according to $R_g \propto N^{1/d_f}$; $d_f \lesssim 3$ corresponds to a close-packed structure. R_g measures the mean size of the fractal aggregate. It is defined in terms of the mass density $\rho(r)$ of the particles at a distance r from the center of mass of the aggregate as $R_g^2 = \int_0^\infty r^4 \rho(r) dr / \int_0^\infty r^2 \rho(r) dr$ or, alternatively, based on the pair correlation function $g(r)$ of colloidal particles $R_g^2 = (1/2) \int_0^\infty r^4 g(r) dr / \int_0^\infty r^2 g(r) dr$ (Van Saarloos, 1987). For fractal structures consisting of spheres with spherically symmetric mass density distribution $\rho(r)$, one has $R_g = R_c$, where R_c is the largest radius beyond which the aggregate has zero mass. The images from confocal microscopy showed that the width of the branches of the clusters is a few particle sizes and that the particles escape from the aggregate at a finite rate. The latter observation provides an estimate of the energy scale of the attraction between the particles by comparing the observed escape frequency with the corresponding attempt frequency, which is the inverse of the Brownian time, i.e., the time in which a particle diffuses a distance equal to its radius. By assuming that this whole process is thermally activated, this renders $\approx 3k_B T$ as an estimate for the energy scale of attraction. A more detailed investigation of the structure of the clusters and its evolution was impeded by sedimentation.

In order to avoid this complication, using near field light scattering (NFS), new measurements for the same type of particles have been performed under microgravity conditions on board the International Space Station and, simultaneously, on the ground (Veen *et al.*, 2012; Potenza *et al.*, 2014). [For these experiments, the composition of the solvent and the volume fraction of the colloidal particles have been taken to be different from those in Bonn *et al.* (2009). Moreover, different amounts of salt (NaCl) have been added. Thus the results of both studies cannot be compared directly.] The normalized variance of the light scattering intensity $I(q, t)$, defined as $\langle I^2(q, t) \rangle / \langle I(q, t) \rangle^2 - 1$, with the angular brackets $\langle \dots \rangle$ denoting the time average, has been used as an indicator of the onset and the time scale of the aggregation process. The time dependence of the normalized variance results from variations of the number density of the scatters. Accordingly, the start of aggregation has been marked by the time t_a at which this quantity starts to increase from zero. From the slope in the log-log plot of $I(q, t)$ at large momentum transfer q , which has been temporally constant during the growth process (which is characteristic of scattering off fractal structures), a fractal dimension has been inferred. It has been found that, upon varying the temperature toward $T_c^{(s)}$, d_f has decreased from a value, which is close to the theoretical one of 2.5 for

²In the original paper (Bonn *et al.*, 2009) q' is given as $q' = (t_0/t)qR$, which we consider as a typo.

diffusion-limited aggregation, to about 1.8. This indicates that more open structures of clusters are formed if, as expected, the strength of the attraction increases. This has been interpreted to the effect that for an attractive interaction potential with a well depth of ca. $1k_B T$ the restructuring of the aggregates into more compact objects can proceed, whereas for deeper attraction wells restructuring gradually stops and the resulting structure is more open. Such more open structures have been observed in the presence of gravity with $d_f \simeq 1.6$ – 1.8 for all temperatures studied. In both cases, i.e., in the presence and absence of gravity, only a slight variation with the salt concentration has been found. The observation made already by [Bonn et al. \(2009\)](#) that, independent of temperature and thus of the strength of the attraction the aggregates grow similarly, has been confirmed and analyzed in more detail. Specifically, the scattered intensity of the growing aggregates as obtained at different times has been reduced to a scaling function $I(q, t) \approx (q_{\text{red}})^{-d_f} F(q/q_{\text{red}}(t))$, where the time-dependent characteristic momentum transfer $q_{\text{red}}(t)$ has been determined from the best fit in the sense of $I(q, t)(q_{\text{red}})^{d_f}$ yielding data collapse to a function F of a single variable $q/q_{\text{red}}(t)$. Based on this apparent scaling behavior, an analogy has been drawn between the observed aggregation process and spinodal decomposition processes. For the latter, a similar scaling holds with d_f replaced by the spatial dimension d ([Carpinetti and Giglio, 1992](#)). As for spinodal decomposition, $I(q)$ exhibits a maximum at $q \simeq q_{\text{red}}$ corresponding to the inverse of the characteristic length in the system. Over the course of time the momentum q_{red} shifts to smaller values indicating the growth of this characteristic length. The decrease of $I(q)$ for small values of q reflects the fact that a region around the cluster is depleted of colloids ([Carpinetti and Giglio, 1992](#)). The growth rate of the characteristic length scale $q_{\text{red}}^{-1} \propto R_g \propto N^{1/d_f}$ of the aggregates has been found to be a power law with exponent $1/d_f$, regardless of the salt concentration. This is characteristic of diffusion-limited models of aggregation ([Witten and Sander, 1983](#); [Meakin, 1984](#)). Under gravity, the growth rate has been observed to be significantly faster and nonmonotonic (see Fig. 19). At early stages it has followed the purely diffusive behavior. After that, aggregation has been influenced strongly by convection of the solvent and by sedimentation. The aggregation among clusters has been found to set in rather fast, resulting in an exponential growth rate, which is characteristic of reaction limited aggregation with a strong dependence on temperature and thus on the strength of the attraction. At still later times, a sudden drop in q_{red}^{-1} has been observed, which corresponds to the sedimentation of the largest clusters.

Whereas in [Veen et al. \(2012\)](#) the static properties of the aggregates, i.e., their structure factor $S(q)$, have been measured as aggregation proceeds, in the subsequent NFS study of this system ([Potenza et al., 2014](#)) the dynamical counterpart of $S(q)$, the intermediate scattering function $\mathfrak{S}(q, t)$ has been measured under microgravity conditions. The aim has been to determine the ratio $\beta \equiv R_h/R_g$ of the hydrodynamic radius R_h of the aggregate and its gyration radius R_g . This ratio provides information about the density distribution within an aggregate as function of its fractal dimension, which in turn depends on the strength of the particle attraction. The hydrodynamic

radius R_h of the aggregate is defined through the translational diffusion coefficient $D = k_B T / 6\pi\eta R_h$, where η is viscosity of the solvent. For a densely packed spherical aggregate of radius R_c and with $d_f = 3$ one expects R_h to be very close to R_c . The intermediate scattering function $\mathfrak{S}(q, t)$ is the spatial (three-dimensional) Fourier transform of the van Hove distribution function $G(r, t)$, which is the dynamical counterpart of the radial distribution function $g(r)$ ([Hansen and McDonald, 1986](#)). The NFS technique enables one to measure $\mathfrak{S}(q, t)$ instantaneously, on the time scale of the much slower aggregation and diffusion processes. This provides the concurrent measurement of R_h from the dynamic and R_g from the static structure factor, simultaneously for all accessible wave vectors. R_g follows from the Fisher-Burford expression ([Fisher and Burford, 1967](#)) $S(q; R_g) = [1 + (2/3d_f)q^2 R_g^2]^{-d_f/2}$, which is valid for monodisperse fractal aggregates. R_h has been determined via the effective diffusion constant D_{eff} obtained from the measured decay time t_d of $\mathfrak{S}(q, t) \propto e^{-t/t_d}$ via $t_d = 1/D_{\text{eff}} q^2$ followed by relating D_{eff} to D by using $S(q)$ ([Lin et al., 1990](#)). The analysis of the data has shown that upon approaching the critical point of demixing (i.e., for stronger attraction) the ratio β has varied between 0.76 for $d_f = 1.8$ and 0.98 for $d_f = 2.5$ at the onset of aggregation (i.e., for weaker attraction). [Potenza et al. \(2014\)](#) assumed that the fractals are spherically symmetric. Accordingly, they defined the radial density distribution of the fractal objects as $\rho(r) = r^{d_f-3} f_{\text{cut}}(r)$, where r is the distance from the center of mass of the cluster and f_{cut} is a cutoff function which accounts for the finite size of the aggregates. [The exponent follows from the fact that $\rho(r) = \mathcal{N}(r)/V(r) \sim r^{d_f-3}$, where $\mathcal{N}(r) \sim r^{d_f}$ is the number of particles within a sphere of radius r from the center of the cluster and $V(r) \propto r^3$ is the volume of such sphere.] The expected behavior of the ratio for various forms of a cutoff function has been then compared with the experimental data. It was observed (see Fig. 20) that the data for the ratio β have been closest to those values which correspond to the assumption of fully compact objects with a Heaviside step function for f_{cut} , independent of the strength of the attraction and of the fractal dimension.

The way to avoid sedimentation for experiments performed on the ground ([Shelke et al., 2013](#)) has been to use PNIPAM, which swell in solution. This swelling adjusts their buoyancy, preventing particle sedimentation. This also has allowed one to directly observe individual particles (after labeling them with a fluorescent dye) even deep in the bulk of the suspension. Using confocal microscopy, the compactness of aggregates of PNIPAM particles, suspended at small volume fractions in the $D_2O/H_2O - 3MP$ mixture, has been studied by determining the number of particles $\mathcal{N}(r)$ within a sphere of radius r from the center of the cluster for quenches with various temperature deviations ΔT from and below the lower critical point $T_c^{(s)}$ of the demixing transition of the solvent. These data have confirmed the fractal character of the structures, i.e., the relation $\mathcal{N}(r) \sim r^{d_f}$, with d_f decreasing continuously upon increasing temperature toward $T_c^{(s)}$ from $d_f \approx 3$ to ≈ 2.1 . This indicates the formation of more compact structures for weaker attraction [see Fig. 21(h)], in agreement

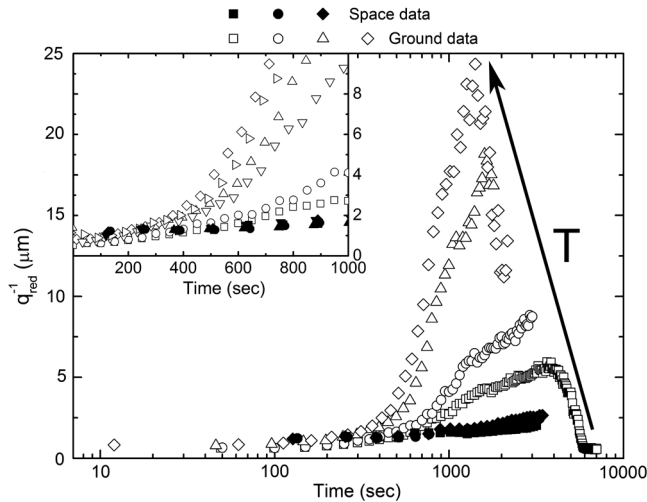


FIG. 19. The evolution of the characteristic size scale of the aggregating colloidal suspension studied by Veen *et al.* (2012) (see Fig. 3 therein) as given by the quantity $q_{\text{red}}^{-1}(t)$, which renders a reduced description of the light scattering intensity $I(q, t)$ of the growing aggregates in terms of a scaling function $F(q/q_{\text{red}}(t))$ of a single variable (see the main text). Results from both microgravity (solid symbols) and ground experiments (open symbols) are shown. (The sample contains 1.5 mmol/liter NaCl.) The curves correspond to various temperatures T ramped up beyond the aggregation temperature T_{agg} , up to $T_{\text{agg}} + 0.4$ [from bottom to top as indicated by the arrow; the caption to Fig. 3 of Veen *et al.* (2012) does not provide the temperature values corresponding to the various symbols]. The temperature T_{agg} at which the aggregation starts is identified (somewhat loosely) as the onset of the rapid increase of the normalized variance of $I(q)$ (see the main text). The sudden drop of q_{red}^{-1} at late times is due to the massive sedimentation of the aggregates so that the suspension becomes poor in large aggregates and rich in small ones which shifts down q_{red}^{-1} . The inset provides an enlarged view of the data concerning the onset of the aggregation process, at which the characteristic length scale q_{red}^{-1} starts to increase. From Veen *et al.*, 2012.

with the behavior observed for the latex particles under microgravity (see the previous paragraph). MC simulations of diffusion-limited particle aggregation in $d = 2$ and 3 have been used in order to relate d_f to the attractive effective interaction potential of the particles. Experimentally, the pair potential has been determined from the radial distribution function of the colloids in a way similar to that described by Nguyen *et al.* (2013). The depth $V_0 < 0$ of the attractive well of this pair potential has been related to the quantity $\alpha \propto \exp(V_0/k_B T)$ used in the simulations for the probability with which the particles can detach from the growing cluster. The experimental variations of $d - d_f$ as a function of V_0 and α in simulations exhibit a common curve after suitable rescaling. They interpreted this result as a manifestation of a certain type of universality which occurs although the corresponding simulations have been carried out for different spatial dimensions ($d = 2$ and 3) and although the mechanisms of aggregation differ, i.e., diffusion-limited cluster aggregation in the actual experiments, in which clusters aggregate to form a fractal, and diffusion-limited particle aggregation in

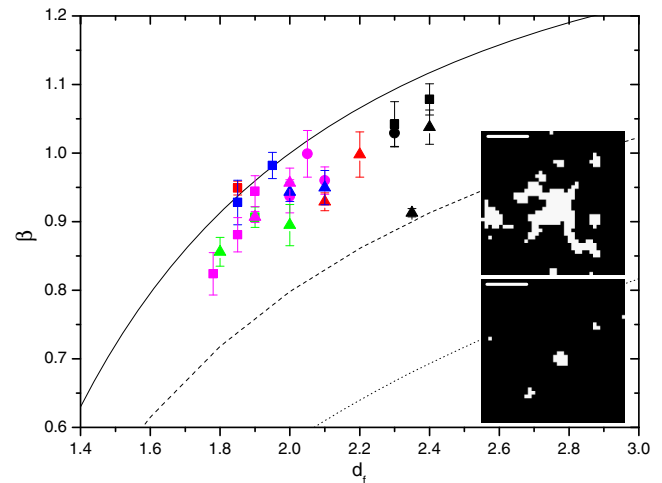


FIG. 20. Ratio $\beta = R_h/R_g$ of the hydrodynamic to the gyration radius of aggregates as a function of their fractal dimension d_f for various temperature deviations ΔT above the aggregation temperature T_{agg} characterized by the colors of the symbols: $\Delta T = 0$ (black), 0.1 K (red), 0.2 K (blue), 0.3 K (green), and 0.4 K (violet). T_{agg} is determined as in Fig. 19, i.e., from the behavior of the normalized variance of the scattered intensity $I(q)$. The types of symbols indicate the salt concentrations of 0.31 mmol/liter (squares), 1.5 mmol/liter (circles), and 2.7 mmol/liter (triangles), corresponding to the Debye screening length κ^{-1} [denoted as λ_D in Potenza *et al.* (2014)] of 14, 6.4, and 4.8 nm, respectively. Concerning the values of β , from top to bottom the lines indicate the dependence on d_f as expected for steplike, Gaussian, and exponentially decaying cut functions of the density distribution of the aggregates, respectively (see the main text). The insets show holographic reconstructions of the real-space shape of the aggregates (white regions) grown at $T = T_{\text{agg}} + 0.4$ K (closest to $T_c^{(s)}$ and hence strongest attraction between the colloids, top) and $T = T_{\text{agg}}$ (farthest from $T_c^{(s)}$ and hence weakest attraction between the colloids, bottom). The length of the scale bar is 25 μm . From Potenza *et al.*, 2014.

simulations, in which a fractal grows by aggregation of single particles. It is worth noting that reversible diffusion-limited cluster aggregation has been extensively studied in the past, both theoretically and experimentally. For example, the theoretical model developed by Kolb (1986) has been extended in order to incorporate rearrangements of the particles and clusters, based on energetic considerations rather than on effects due to random bonding (Shih, Aksay, and Kikuchi, 1987). Fernandez-Nieves *et al.* (2001) experimentally studied and analyzed the reversible aggregation of soft particles, such as PNIPAM, based on the aforementioned theoretical models.

V. PERSPECTIVES

We have presented a detailed account of the theoretical and experimental investigations concerning the collective behavior of colloidal particles suspended in a binary liquid mixture close to its demixing point. These studies also cover the reversible aggregation of particles into small clusters, which takes place in dilute suspensions, as well as the occurrence of

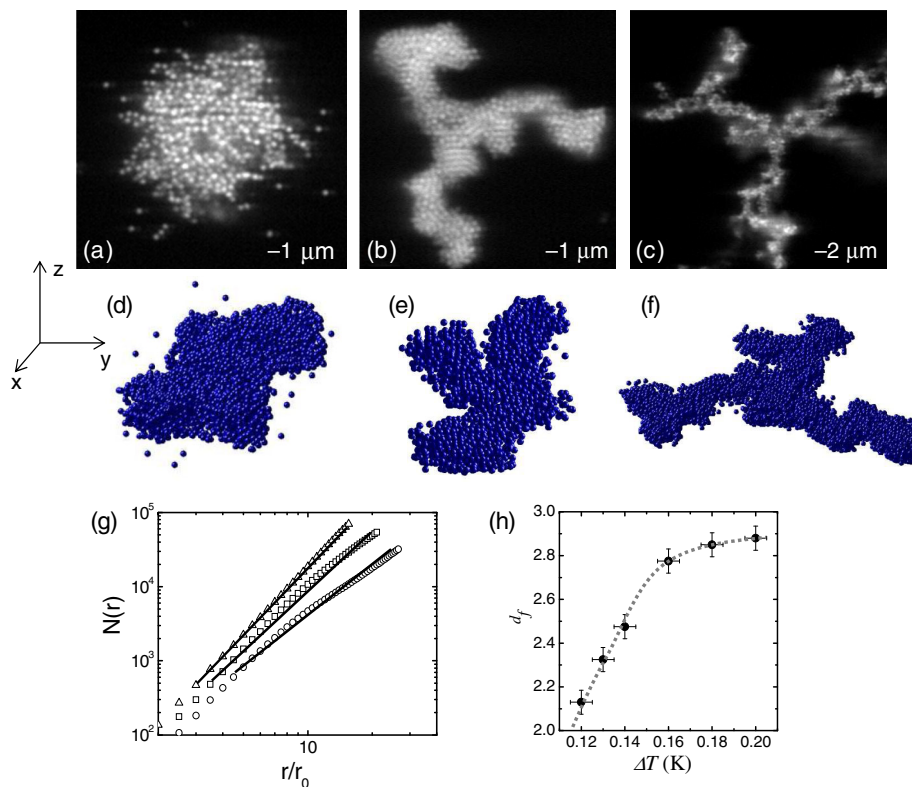


FIG. 21. Tuning the morphology of colloidal aggregates by CCFs. Confocal microscopy images and the three-dimensional reconstructions of the aggregates formed upon temperature quenches to (a), (d) $\Delta T = T_c^{(s)} - T = 0.2$ K, (b), (e) 0.14 K, and (c), (f) 0.12 K below the lower critical phase separation temperature $T_c^{(s)}$ of the binary solvent. (g) Scaling of the number of particles $\mathcal{N}(r)$ within a sphere of radius r from the center of the cluster at $\Delta T = 0.2$ K (triangles), $\Delta T = 0.14$ K (squares), and $\Delta T = 0.12$ K (circles); r_0 is the radius of the particles. (h) Fractal dimension as a function of ΔT determined from $\mathcal{N}(r) \sim r^{d_f} f_{\text{cut}}(r)$ and thus from the slopes in (g). The dashed line is a guide to the eye. Upon increasing ΔT a continuous increase of the fractal dimension to the space-filling limit $d_f = 3$ is observed (see the main text). From [Shelke et al., 2013](#).

phase transitions in suspensions which are more dense in colloids. Based on the actual knowledge of the CCP it is possible to identify that region in the thermodynamic space of the suspensions where these phenomena are due to CCFs. In addition, the effective pair potential approach can correctly predict the specific structures into which homogeneous, Janus, and other patchy particles self-assemble under the action of CCFs. An accurate determination of the corresponding phase diagrams requires one to incorporate the apparent partitioning of colloids into that phase of the phase-separated binary solvent, which is preferred by the colloids. This effect is not captured by the effective pair potential approach. Therefore, the appropriate description of colloidal suspensions with a binary solvent is the one of a ternary mixture. The challenge is that a microscopic theoretical treatment of a ternary mixture consisting of microsized colloids and a binary molecular liquid is currently not feasible. Even MC simulations of a simplified lattice model mimicking such a suspension constitute a serious computation challenge. Thus, currently in a certain sense one is thrown back to the effective one-component approach. Accordingly, combined experimental and theoretical efforts, which help to assess the validity of this approach, are highly welcome.

The bibliography of this review testifies that critical Casimir interactions in colloidal systems are an active research field

which generates an abundance of interesting challenges for various disciplines. Some future avenues of research can easily be identified. For example, a detailed knowledge of the pair potentials is essential for the effective one-component approach. However, it remains as a challenge to accurately determine the CCP and its scaling function within the range of the relevant parameters and boundary conditions. This applies to chemically homogeneous or Janus particles of spherical or anisotropic shapes such as cylinders, ellipsoids, cubes, or even more complex shapes such as dumbbells or L -like ones. Quantitative reliability demands to carry out calculations beyond mean field theory and the Derjaguin approximation. This requires the development of new theoretical approaches and simulation algorithms.

Janus particles have already been used in experiments on aggregation in near-critical binary solvents ([Iwashita and Kimura, 2013](#)). Colloids with chemically homogeneous or inhomogeneous surfaces, forming patchy particles ([Nguyen et al., 2016](#); [Garcia, Gnan, and Zaccarelli, 2017](#)), with various shapes as well as their mixtures are attractive building blocks for generating a large variety of self-assembled structures by using CCFs. This lends itself to be explored further by experiments and computer simulations. In addition, suitably designed surfaces might provide temperature-controlled confining potentials which might find applications for

self-assembly processes. Further analyses of the interplay between CCFs and other forces, such as electrostatic, retarded, and nonretarded van der Waals ones, are needed to further understand the observed aggregation phenomena. More elaborate as well as combined experimental and theoretical investigations are required in order to determine material-dependent quantities, such as Hamaker coefficients, colloid surface charges, Debye screening lengths, and solvent correlation lengths, which enter into the effective pair potential. With this, the number of fit parameters in the theoretical models will be reduced. For an optimal tuning of colloidal self-assembly it is important to explore the crossover from colloidal aggregation driven by CCFs to the one due to wetting or bridging. This crossover is still not fully understood and calls for further theoretical and simulation studies. New opportunities for colloidal assembly can be created by using mixtures of active and passive colloidal particles immersed in a near-critical binary liquid mixture. The mobility of one component of a colloidal mixture might accelerate self-assembly processes and help to improve the perfection of the emerging structures.

Concerning the thermodynamic properties of colloidal suspensions with near-critical solvents, a multicomponent theory beyond the effective approach and beyond mean field theory is needed. One of the challenges along this line is to construct a suitable theory, which accounts for all relevant degrees of freedom of the solvent and the solute particles and which masters the size differences of the various species.

A rewarding line of research would be to study aggregation of colloids in lipid membranes, close to the corresponding lipid phase segregation, or in a liquid analog of such quasi-two-dimensional systems.

It is very likely that the unique features of CCFs will find useful applications, which can even be patented. An actual recent example thereof is concerned with a size-selective nanoparticle purification or separation method based on CCFs (Guo, Stan, and Liu, 2018). These perspectives are already now so wide that the further development of this research field appears to be very promising and rewarding.

ACKNOWLEDGMENTS

A. M. was partially supported by the Polish National Science Center (Harmonia Grant No. 2015/18/M/ST3/00403).

REFERENCES

- Abraham, D. B., and A. Maciolek, 2010, *Phys. Rev. Lett.* **105**, 055701.
- Abraham, D. B., and A. Maciolek, 2013, *Europhys. Lett.* **101**, 20006.
- Alexander, S., P. M. Chaikin, P. Grant, G. J. Morales, and P. P., 1984, *J. Chem. Phys.* **80**, 5776.
- Andersen, H. C., J. D. Weeks, and D. Chandler, 1971, *Phys. Rev. A* **4**, 1597.
- Andon, R. J. L., and J. D. Cox, 1952, *J. Chem. Soc. (Resumed)*, 4601.
- Anzini, P., and A. Parola, 2016, *Phys. Rev. E* **94**, 052113.
- Archer, A. J., R. Evans, R. Roth, and M. Oettel, 2005, *J. Chem. Phys.* **122**, 084513.
- Asakura, S., and F. Oosawa, 1954, *J. Chem. Phys.* **22**, 1255.
- Barber, M. N., 1983, *Phase Transitions and Critical Phenomena* (Academic, New York), Vol. 8.
- Barrat, J. L., and J.-P. Hansen, 2003, *Basic concepts for simple and complex liquids* (Cambridge University Press, Cambridge).
- Bauer, C., T. Bieker, and S. Dietrich, 2000, *Phys. Rev. E* **62**, 5324.
- Baxter, R. J., 1968, *J. Chem. Phys.* **49**, 2770.
- Belloni, L., 1998, *Colloids Surf. A* **140**, 227.
- Benet, J., F. Paillusson, and H. Kusumaatmaja, 2017, *Phys. Chem. Chem. Phys.* **19**, 24188.
- Bennett, C. H., 1976, *J. Comput. Phys.* **22**, 245.
- Beysens, D., and D. Estève, 1985, *Phys. Rev. Lett.* **54**, 2123.
- Beysens, D., and T. Narayanan, 1999, *J. Stat. Phys.* **95**, 997.
- Beysens, D., J.-M. Petit, T. Narayanan, A. Kumar, and M. L. Broide, 1994, *Ber. Bunsenges. Phys. Chem.* **98**, 382.
- Bieker, T., and S. Dietrich, 1998a, *Physica A (Amsterdam)* **259**, 466.
- Bieker, T., and S. Dietrich, 1998b, *Physica A (Amsterdam)* **252**, 85.
- Bier, M., A. Gambassi, M. Oettel, and S. Dietrich, 2011, *Europhys. Lett.* **95**, 60001.
- Bimonte, G., T. Emig, and M. Kardar, 2013, *Europhys. Lett.* **104**, 21001.
- Bonn, D., J. Otwinowski, S. Sacanna, H. Guo, G. Wegdam, and P. Schall, 2009, *Phys. Rev. Lett.* **103**, 156101.
- Bonn, D., G. Wegdam, and P. Schall, 2010, *Phys. Rev. Lett.* **105**, 059602.
- Borjan, Z., and P. J. Upton, 1998, *Phys. Rev. Lett.* **81**, 4911.
- Borjan, Z., and P. J. Upton, 2008, *Phys. Rev. Lett.* **101**, 125702.
- Brankov, J. G., D. M. Dantchev, and N. S. Tonchev, 2000, *The Theory of Critical Phenomena in Finite-Size Systems—Scaling and Quantum Effects*, Series in modern condensed matter physics, Vol. 9 (World Scientific, Singapore).
- Brochard, F., and P. G. de Gennes, 1980, *Ferroelectrics* **30**, 33.
- Broide, M. L., Y. Garrabos, and D. Beysens, 1993, *Phys. Rev. E* **47**, 3768.
- Burkhardt, T. W., and E. Eisenriegler, 1995, *Phys. Rev. Lett.* **74**, 3189.
- Burstyn, H. C., and J. V. Sengers, 1982, *Phys. Rev. A* **25**, 448.
- Burstyn, H. C., J. V. Sengers, J. K. Bhattacharjee, and R. A. Ferrell, 1983, *Phys. Rev. A* **28**, 1567.
- Buzzaccaro, S., J. Colombo, A. Parola, and R. Piazza, 2010, *Phys. Rev. Lett.* **105**, 198301.
- Caccamo, C., 1996, *Phys. Rep.* **274**, 1.
- Cardy, J. L., 1987, *Phase Transitions and Critical Phenomena* (Academic, New York), Vol. 11.
- Carpinetti, M., and M. Giglio, 1992, *Phys. Rev. Lett.* **68**, 3327.
- Casimir, H. G. B., 1948, *Proc. R. Acad. Sci. Amsterdam* **51**, 793 [<http://inspirehep.net/record/24990/>].
- Cattuto, C., R. Britto, U. M. B. Marconi, F. Nori, and R. Soto, 2006, *Phys. Rev. Lett.* **96**, 178001.
- Cox, J. D., 1952, *J. Chem. Soc., (Resumed)*, 4606.
- Curtin, W. A., and N. W. Ashcroft, 1985, *Phys. Rev. A* **32**, 2909.
- Dang, M. T., A. V. Verde, V. D. Nguyen, P. G. Bolhuis, and P. Schall, 2013, *J. Chem. Phys.* **139**, 094903.
- Dantchev, D., F. Schlesener, and S. Dietrich, 2007, *Phys. Rev. E* **76**, 011121.
- Das, S. K., J. V. Sengers, and M. E. Fisher, 2007, *J. Chem. Phys.* **127**, 144506.
- de Gennes, P. G., 1981, *C. R. Acad. Sci. Paris Ser. IV* **202**, 701.
- Derjaguin, B., 1934, *Kolloid Z.* **69**, 155.
- Diehl, H. W., 1986, *Phase Transitions and Critical Phenomena*, edited by C. Domb and J. L. Lebowitz (Academic Press, London), Vol. 10.
- Dietrich, S., 1988, *Phase Transitions and Critical Phenomena*, edited by C. Domb and J. L. Lebowitz (Academic Press, London), Vol. 12.

- Dijkstra, M., R. van Roij, and R. Evans, 1998, *Phys. Rev. Lett.* **81**, 2268.
- Dijkstra, M., R. van Roij, and R. Evans, 1999, *Phys. Rev. E* **59**, 5744.
- Dutcher, J. R., and A. G. Maragoni, 2004, *Soft Materials: Structure and Dynamics* (Marcel Dekker, New York).
- Dzyaloshinskii, I. E., E. M. Lifshitz, and L. P. Pitaevskii, 1961, *Adv. Phys.* **10**, 165.
- Edison, J. R., S. Belli, R. Evans, R. Van Roij, and M. Dijkstra, 2015, *Mol. Phys.* **113**, 2546.
- Edison, J. R., N. Tasios, S. Belli, R. Evans, R. van Roij, and M. Dijkstra, 2015, *Phys. Rev. Lett.* **114**, 038301.
- Eisenriegler, E., 2004, *J. Chem. Phys.* **121**, 3299.
- Eisenriegler, E., and U. Ritschel, 1995, *Phys. Rev. B* **51**, 13717.
- Errington, J. R., 2003, *Phys. Rev. E* **67**, 012102.
- Esser, A., V. Dohm, and X. S. Chen, 1995, *Physica A (Amsterdam)* **222**, 355.
- Evans, R., 1979, *Adv. Phys.* **28**, 143.
- Evans, R., 1990, *J. Phys. Condens. Matter* **2**, 8989.
- Evans, R., R. J. F. Leote de Carvalho, J. R. Henderson, and D. C. Hoyle, 1994, *J. Chem. Phys.* **100**, 591.
- Evans, R., and J. Stecki, 1994, *Phys. Rev. B* **49**, 8842.
- Fernandez-Nieves, A., A. Fernandez-Barbero, B. Vincent, and F. J. De las Nieves, 2001, *Langmuir* **17**, 1841.
- Fisher, M. E., and H. Au-Yang, 1980, *Physica A (Amsterdam)* **101**, 255.
- Fisher, M. E., and R. J. Burford, 1967, *Phys. Rev.* **156**, 583.
- Fisher, M. E., and P. G. de Gennes, 1978, *C. R. Acad. Sci. Paris Ser. B* **287**, 207.
- Fisher, M. E., and P. J. Upton, 1990, *Phys. Rev. Lett.* **65**, 2402.
- Fisk, S., and B. Widom, 1969, *J. Chem. Phys.* **50**, 3219.
- Flöter, G., and S. Dietrich, 1995, *Z. Phys. B* **97**, 213.
- Foffi, G., and F. Sciortino, 2007, *J. Phys. Chem. B* **111**, 9702.
- Frenkel, D., and B. Smit, 2001, *Understanding Molecular Simulations: From Algorithms to Applications* (Academic, San Diego).
- Frydel, D., S. Dietrich, and M. Oettel, 2007, *Phys. Rev. Lett.* **99**, 118302.
- Fuchs, N., 1934, *Z. Phys. Chem.* **171**, 199.
- Fukuto, M., Y. F. Yano, and P. S. Pershan, 2005, *Phys. Rev. Lett.* **94**, 135702.
- Gallagher, P. D., L. M. Kurnaz, and J. V. Maher, 1992, *Phys. Rev. A* **46**, 7750.
- Gallagher, P. D., and J. V. Maher, 1992, *Phys. Rev. A* **46**, 2012.
- Gambassi, A., 2009, *J. Phys. Conf. Ser.* **161**, 012037.
- Gambassi, A., and S. Dietrich, 2010, *Phys. Rev. Lett.* **105**, 059601.
- Gambassi, A., A. Maciolek, C. Hertlein, U. Nellen, L. Helden, C. Bechinger, and S. Dietrich, 2009, *Phys. Rev. E* **80**, 061143.
- Ganshin, A., S. Scheidemantel, R. Garcia, and M. H. W. Chan, 2006, *Phys. Rev. Lett.* **97**, 075301.
- Garcia, N. A., N. Gnan, and E. Zaccarelli, 2017, *Soft Matter* **13**, 6051.
- Garcia, R., and M. H. W. Chan, 1999, *Phys. Rev. Lett.* **83**, 1187.
- Garcia, R., and M. H. W. Chan, 2002, *Phys. Rev. Lett.* **88**, 086101.
- Gazzillo, D., 2011, *J. Chem. Phys.* **134**, 124504.
- Gilroy, J. B., T. Gädt, G. R. Whittell, L. Chabanne, J. M. Mitchels, R. M. Richardson, M. A. Winnik, and I. Manners, 2010, *Nat. Chem.* **2**, 566.
- Gnan, N., E. Zaccarelli, and F. Sciortino, 2012, *J. Chem. Phys.* **137**, 084903.
- Gnan, N., E. Zaccarelli, and F. Sciortino, 2014, *Nat. Commun.* **5**, 3267.
- Gnan, N., E. Zaccarelli, P. Tartaglia, and F. Sciortino, 2012, *Soft Matter* **8**, 1991.
- Götzelmann, B., R. Evans, and S. Dietrich, 1998, *Phys. Rev. E* **57**, 6785.
- Gray, E., J. Karslake, B. B. Machta, J. P. Sethna, and S. L. Veatch, 2013, *Biophys. J.* **105**, 2751.
- Grüll, H., and D. Woermann, 1997, *Ber. Bunsenges. Phys. Chem.* **101**, 814.
- Guo, H., T. Narayanan, M. Sztuchi, P. Schall, and G. H. Wegdam, 2008, *Phys. Rev. Lett.* **100**, 188303.
- Guo, H., G. Stan, and Y. Liu, 2018, *Soft Matter* **14**, 1311.
- Gurfein, V., D. Beysens, and F. Perrot, 1989, *Phys. Rev. A* **40**, 2543.
- Hamaker, H., 1937, *Physica (Utrecht)* **4**, 1058.
- Hanke, A., and S. Dietrich, 1999, *Phys. Rev. E* **59**, 5081.
- Hanke, A., F. Schlesener, E. Eisenriegler, and S. Dietrich, 1998, *Phys. Rev. Lett.* **81**, 1885.
- Hansen, J. P., 1993, *J. Phys. Condens. Matter* **5**, B117.
- Hansen, J. P., and H. Löwen, 2000, *Annu. Rev. Phys. Chem.* **51**, 209.
- Hansen, J. P., and I. R. McDonald, 1986, *Theory of Simple Liquids* (Academic, London).
- Hasenbusch, M., 2010, *Phys. Rev. B* **82**, 104425.
- Hasenbusch, M., 2011, *Phys. Rev. B* **83**, 134425.
- Hasenbusch, M., 2012, *Phys. Rev. B* **85**, 174421.
- Hasenbusch, M., 2013, *Phys. Rev. E* **87**, 022130.
- Hasenbusch, M., 2015, *Phys. Rev. E* **91**, 022110.
- Heinrich, M. C., I. Levental, P. A. Gelman, H. Janmey, and T. Baumgart, 2008, *J. Phys. Chem. B* **112**, 8063.
- Henderson, J. R., 1986, *Mol. Phys.* **59**, 89.
- Heringa, J. R., and H. W. J. Blöte, 1998, *Phys. Rev. E* **57**, 4976.
- Hertlein, C., 2008, *Messung kritischer Casimir-Kräfte mit TIRM*, Ph.D. thesis (University of Stuttgart).
- Hertlein, C., L. Helden, A. Gambassi, S. Dietrich, and C. Bechinger, 2008, *Nature (London)* **451**, 172.
- Hobrecht, H., and A. Hucht, 2014, *Europhys. Lett.* **106**, 56005.
- Hobrecht, H., and A. Hucht, 2015, *Phys. Rev. E* **92**, 042315.
- Honerkamp-Smith, A. R., P. Cicuta, M. D. Collins, S. L. Veatch, M. den Nijs, M. Schick, and S. L. Keller, 2008, *Biophys. J.* **95**, 236.
- Hong, L., A. Cacciuto, E. Luijten, and S. Granick, 2006, *Nano Lett.* **6**, 2510.
- Israelachvili, J. N., 1998, *Intermolecular and Surface Forces* (Academic, London).
- Iwashita, Y., and Y. Kimura, 2013, *Soft Matter* **9**, 10694.
- Iwashita, Y., and Y. Kimura, 2014, *Soft Matter* **10**, 7170.
- Jayalakshmi, Y., and E. W. Kaler, 1997, *Phys. Rev. Lett.* **78**, 1379.
- Jiang, K., J. Wang, Q. Li, L. Liu, C. Liu, and S. Fan, 2011, *Adv. Mater.* **23**, 1154.
- Kardar, M., and R. Golestanian, 1999, *Rev. Mod. Phys.* **71**, 1233.
- Kawasaki, K., 1972, *Phase Transitions and Critical Phenomena*, edited by C. Domb and J. L. Lebowitz (Academic Press, London), Vol. 2.
- Kern, N., and D. Frenkel, 2003, *J. Chem. Phys.* **118**, 9882.
- Kimchi, O., and B. B. Machta, 2015, *Biophys. J.* **108**, 437.
- Kirkpatrick, T. R., J. M. Ortiz de Zárate, and J. V. Sengers, 2015, *Phys. Rev. Lett.* **115**, 035901.
- Klimchitskaya, G. L., U. Mohideen, and V. M. Mostepanenko, 2009, *Rev. Mod. Phys.* **81**, 1827.
- Kline, S. R., and E. W. Kaler, 1994, *Langmuir* **10**, 412.
- Koehler, R. D., and E. W. Kaler, 1997, *Langmuir* **13**, 2463.
- Kofke, D. A., 1993, *J. Chem. Phys.* **98**, 4149.
- Kolb, M., 1986, *J. Phys. A* **19**, L263.
- Kondrat, S., L. Harnau, and S. Dietrich, 2009, *J. Chem. Phys.* **131**, 204902.
- Krech, M., 1994, *The Casimir effect in critical systems* (World Scientific, Singapore).
- Krech, M., 1997, *Phys. Rev. E* **56**, 1642.

- Krech, M., and S. Dietrich, 1992, *Phys. Rev. A* **46**, 1886.
- Kurnaz, M. L., and J. V. Maher, 1995, *Phys. Rev. E* **51**, 5916.
- Kurnaz, M. L., and J. V. Maher, 1997, *Phys. Rev. E* **55**, 572.
- Labbé-Laurent, M., and S. Dietrich, 2016, *Soft Matter* **12**, 6621.
- Labbé-Laurent, M., A. Law, and S. Dietrich, 2017, *J. Chem. Phys.* **147**, 104701.
- Labbé-Laurent, M., M. Tröndle, L. Harnau, and S. Dietrich, 2014, *Soft Matter* **10**, 2270.
- Landau, D. P., and K. Binder, 2009, *A Guide to Monte Carlo Simulations in Statistical Physics* (Cambridge University Press, Cambridge, England).
- Largo, J., and N. B. Wilding, 2006, *Phys. Rev. E* **73**, 036115.
- Law, B. M., 2001, *Prog. Surf. Sci.* **66**, 159.
- Leidl, R., and H. Wagner, 1993, *J. Chem. Phys.* **98**, 4142.
- Levin, Y., 2002, *Rep. Prog. Phys.* **65**, 1577.
- Li, W., Y. Liu, G. Brett, and J. D. Gunton, 2012, *Soft Matter* **8**, 6027.
- Lifshitz, E. M., 1955, *Zh. Eksp. Teor. Fiz.* **29**, 94 [*Sov. Phys. JETP* **2**, 73 (1956)].
- Likos, C. N., 2001, *Phys. Rep.* **348**, 267.
- Lin, M. Y., H. M. Lindsay, D. A. Weitz, R. C. Ball, R. Klein, and P. Meakin, 1990, *Phys. Rev. A* **41**, 2005.
- Lingwood, D., and K. Simons, 2010, *Science* **327**, 46.
- Liu, Y., W. Li, T. Perez, J. D. Gunton, and G. Brett, 2012, *Langmuir* **28**, 3.
- Löwen, H., 1995, *Phys. Rev. Lett.* **74**, 1028.
- Machta, B. B., S. Papanikolaou, J. P. Sethna, and S. L. Veatch, 2011, *Biophys. J.* **100**, 1668.
- Machta, B. B., J. P. Sethna, and S. L. Veatch, 2012, *Phys. Rev. Lett.* **109**, 138101.
- Marino, E., T. E. Kodger, J. B. ten Hove, A. H. Velders, and P. Schall, 2016, *Sol. Energy Mater. Sol. Cells* **158**, 154.
- Mattos, T. G., L. Harnau, and S. Dietrich, 2013, *J. Chem. Phys.* **138**, 074704.
- Mattos, T. G., L. Harnau, and S. Dietrich, 2015, *Phys. Rev. E* **91**, 042304.
- Meakin, P., 1984, *J. Colloid Interface Sci.* **102**, 491.
- Mohry, T. F., S. Kondrat, A. Maciołek, and S. Dietrich, 2014, *Soft Matter* **10**, 5510.
- Mohry, T. F., A. Maciołek, and S. Dietrich, 2012a, *J. Chem. Phys.* **136**, 224902.
- Mohry, T. F., A. Maciołek, and S. Dietrich, 2012b, *J. Chem. Phys.* **136**, 224903.
- Mohry, T. F., A. Maciołek, and S. Dietrich, 2010, *Phys. Rev. E* **81**, 061117.
- Mon, K. K., 1989, *Phys. Rev. B* **39**, 467.
- Mon, K. K., and K. Binder, 1990, *Phys. Rev. B* **42**, 675.
- Mukamel, D., and M. Blume, 1974, *Phys. Rev. A* **10**, 610.
- Namba, K., and G. Stubbs, 1986, *Science* **231**, 1401.
- Narayanan, T., A. Kumar, E. S. R. Gopal, D. Beysens, P. Guenoun, and G. Zalczer, 1993, *Phys. Rev. E* **48**, 1989.
- Narayanan, T., J. M. Petit, M. E. Broide, and D. Beysens, 1995, *Phys. Rev. E* **51**, 4580.
- Nellen, U., J. Dietrich, L. Helden, S. Chodankar, K. Nygard, J. Friso van der Veen, and C. Bechinger, 2011, *Soft Matter* **7**, 5360.
- Nellen, U., L. Helden, and C. Bechinger, 2009, *Europhys. Lett.* **88**, 26001.
- Netz, R. R., 1996, *Phys. Rev. Lett.* **76**, 3646.
- Newton, A. C., T. A. Nguyen, S. J. Veen, D. J. Kraft, P. Schall, and P. G. Bolhuis, 2017, *Soft Matter* **13**, 4903.
- Nguyen, T. A., A. Newton, D. J. Kraft, P. G. Bolhuis, and P. Schall, 2017, *Materials* **10**, 1265.
- Nguyen, T. A., A. Newton, S. J. Veen, D. J. Kraft, P. G. Bolhuis, and P. Schall, 2017, *Adv. Mater.* **29**, 1700819.
- Nguyen, V. D., M. T. Dang, T. A. Nguyen, and P. Schall, 2016, *J. Phys. Condens. Matter* **28**, 043001.
- Nguyen, V. D., S. Faber, Z. Hu, G. H. Wegdam, and P. Schall, 2013, *Nat. Commun.* **4**, 1584.
- Ni, R., M. A. C. Stuart, and P. G. Bolhuis, 2015, *Phys. Rev. Lett.* **114**, 018302.
- Nightingale, M. P., and J. O. Indekeu, 1985, *Phys. Rev. Lett.* **54**, 1824.
- Noro, M. G., and D. Frenkel, 2000, *J. Chem. Phys.* **113**, 2941.
- Okamoto, R., and A. Onuki, 2011, *Phys. Rev. E* **84**, 051401.
- Okamoto, R., and A. Onuki, 2012, *J. Chem. Phys.* **136**, 114704.
- Okamoto, R., and A. Onuki, 2013, *Phys. Rev. E* **88**, 022309.
- Oleinikova, A., L. Bulavin, and V. Pipich, 1999, *Int. J. Thermophys.* **20**, 889.
- Orea, P., and Y. Duda, 2008, *J. Chem. Phys.* **128**, 134508.
- Paladugu, S., A. Callegari, Y. Tuna, L. Barth, S. Dietrich, A. Gambassi, and G. Volpe, 2016, *Nat. Commun.* **7**, 11403.
- Parisen Toldin, F., M. Tröndle, and S. Dietrich, 2013, *Phys. Rev. E* **88**, 052110.
- Parola, A., and L. Reatto, 1995, *Adv. Phys.* **44**, 211.
- Parsegian, V. A., 2006, *Van der Waals forces* (Cambridge University Press, New York).
- Pelissetto, A., and E. Vicari, 2002, *Phys. Rep.* **368**, 549.
- Pérez-Juste, J., I. Pastoriza-Santos, L. M. Liz-Marzán, and P. Mulvaney, 2005, *Coord. Chem. Rev.* **249**, 1870.
- Piazza, R., S. Buzzaccaro, A. Parola, and J. Colombo, 2011, *J. Phys. Condens. Matter* **23**, 194114.
- Potenza, M. A. C., A. Manca, S. J. Veen, B. Weber, S. Mazzoni, P. Schall, and G. H. Wegdam, 2014, *Europhys. Lett.* **106**, 68005.
- Pousaneh, F., and A. Ciach, 2011, *J. Phys. Condens. Matter* **23**, 412101.
- Pousaneh, F., A. Ciach, and A. Maciołek, 2014, *Soft Matter* **10**, 470.
- Prafulla, B. V., T. Narayanan, and A. Kumar, 1992, *Phys. Rev. A* **46**, 7456.
- Prasad, N., J. Perumal, C.-H. Choi, C.-S. Lee, and D.-P. Kim, 2009, *Adv. Funct. Mater.* **19**, 1656.
- Prieve, D. C., 1999, *Adv. Colloid Interface Sci.* **82**, 93.
- Privman, V., 1990, *Finite Size Scaling and Numerical Simulation of Statistical Systems*, edited by V. Privman (World Scientific, Singapore).
- Puosi, F., D. L. Cardozo, S. Ciliberto, and P. C. W. Holdsworth, 2016, *Phys. Rev. E* **94**, 040102.
- Rabani, E., D. R. Reichman, P. L. Geissler, and L. E. Brus, 2003, *Nature (London)* **426**, 271.
- Rafaï, S., D. Bonn, and J. Meunier, 2007, *Physica A (Amsterdam)* **386**, 31.
- Rathke, B., H. Gröll, and D. Woermann, 1997, *J. Colloid Interface Sci.* **192**, 334.
- Ray, D., C. Reichhardt, and C. O. Olson Reichhardt, 2014, *Phys. Rev. E* **90**, 013019.
- Rice, O. K., 1976, *J. Chem. Phys.* **64**, 4362.
- Roth, R., R. Evans, and S. Dietrich, 2000, *Phys. Rev. E* **62**, 5360.
- Russel, W. B., D. A. Saville, and W. R. Schowalter, 1989, *Colloidal Dispersions* (Cambridge University Press, Cambridge).
- Santos, A., M. López de Haro, and S. Bravo Yuste, 1995, *J. Chem. Phys.* **103**, 4622.
- Schlesener, F., A. Hanke, and S. Dietrich, 2003, *J. Stat. Phys.* **110**, 981.
- Schmidt, M., 2011, *J. Phys. Condens. Matter* **23**, 415101.
- Schmidt, M., and A. R. Denton, 2002, *Phys. Rev. E* **65**, 021508.
- Sciortino, F., A. Giacometti, and G. Pastore, 2009, *Phys. Rev. Lett.* **103**, 237801.

- Shelke, P. B., V. D. Nguyen, A. V. Limaye, and P. Schall, 2013, *Adv. Mater.* **25**, 1499.
- Shih, W. Y., I. A. Aksay, and R. Kikuchi, 1987, *Phys. Rev. A* **36**, 5015.
- Sivardière, J., and J. Lajzerowicz, 1975, *Phys. Rev. A* **11**, 2090.
- Sluckin, T. J., 1990, *Phys. Rev. A* **41**, 960.
- Sorensen, C. M., and G. A. Larsen, 1985, *J. Chem. Phys.* **83**, 1835.
- Soyka, F., O. Zvyagolskaya, C. Hertlein, L. Helden, and C. Bechinger, 2008, *Phys. Rev. Lett.* **101**, 208301.
- Stuij, S. G., M. Labbe-Laurent, T. E. Kodger, A. Maciołek, and P. Schall, 2017, *Soft Matter* **13**, 5233.
- Swendsen, R. H., and J.-S. Wang, 1987, *Phys. Rev. Lett.* **58**, 86.
- Tarazona, P., 1985, *Phys. Rev. A* **31**, 2672.
- Tasios, N., and M. Dijkstra, 2017, *J. Chem. Phys.* **146**, 134903.
- Tasios, N., J. R. Edison, R. van Roij, R. Evans, and M. Dijkstra, 2016, *J. Chem. Phys.* **145**, 084902.
- Toldin, F. P., and S. Dietrich, 2010, *J. Stat. Mech.* **11**, P11003.
- Tröndle, M., S. Kondrat, A. Gambassi, L. Harnau, and S. Dietrich, 2009, *Europhys. Lett.* **88**, 40004.
- Tröndle, M., S. Kondrat, A. Gambassi, L. Harnau, and S. Dietrich, 2010, *J. Chem. Phys.* **133**, 074702.
- Valchev, G., and D. Dantchev, 2017, *Phys. Rev. E* **96**, 022107.
- Van Saarloos, W., 1987, *Physica A (Amsterdam)* **147**, 280.
- Vasilyev, O., A. Gambassi, A. Maciołek, and S. Dietrich, 2007, *Europhys. Lett.* **80**, 60009.
- Vasilyev, O., A. Gambassi, A. Maciołek, and S. Dietrich, 2009, *Phys. Rev. E* **79**, 041142.
- Vasilyev, O., A. Maciołek, and S. Dietrich, 2011, *Phys. Rev. E* **84**, 041605.
- Vasilyev, O. A., 2014, *Phys. Rev. E* **90**, 012138.
- Vasilyev, O. A., and S. Dietrich, 2013, *Europhys. Lett.* **104**, 60002.
- Vasilyev, O. A., S. Dietrich, and S. Kondrat, 2018, *Soft Matter* **14**, 586.
- Veatch, S. L., and S. L. Keller, 2005, *Biochim. Biophys. Acta* **1746**, 172.
- Veen, S. J., O. Antoniuk, B. Weber, M. A. C. Potenza, S. Mazzoni, P. Schall, and G. H. Wegdam, 2012, *Phys. Rev. Lett.* **109**, 248302.
- Venkatesu, P., 2006, *J. Phys. Chem. B* **110**, 17339.
- Verwey, E. J. W., and J. T. G. Overbeek, 1948, *Theory of the Stability of Lyophobic Colloids* (Elsevier, Amsterdam).
- Vilgis, T., A. Sans, and G. Jannink, 1993, *J. Phys. II (France)* **3**, 1779.
- Viry, L., C. Mercader, P. Miaudet, C. Zakri, A. Derre, A. Kuhn, M. Maugey, and P. Poulin, 2010, *J. Mater. Chem.* **20**, 3487.
- Vliegthart, G. A., and H. N. W. Lekkerkerker, 2000, *J. Chem. Phys.* **112**, 5364.
- Vrij, A., 1976, *Pure Appl. Chem.* **48**, 471.
- Vrij, A., E. A. Nieuwenhuis, H. M. Fijnout, and W. G. M. Agtero, 1978, *Faraday Discuss. Chem. Soc.* **65**, 101.
- Walther, A., M. Drechsler, S. Rosenfeldt, L. Harnau, M. Ballauff, V. Abetz, and A. H. Müller, 2009, *J. Am. Chem. Soc.* **131**, 4720.
- Walz, J. Y., 1997, *Curr. Opin. Colloid Interface Sci.* **2**, 600.
- Witten, T. A., and L. M. Sander, 1983, *Phys. Rev. B* **27**, 5686.
- Wolff, U., 1989, *Phys. Rev. Lett.* **62**, 361.
- Yabunaka, S., and A. Onuki, 2017, *Phys. Rev. E* **96**, 032127.
- Yi, G.-R., D. J. Pine, and S. Sacanna, 2013, *J. Phys. Condens. Matter* **25**, 193101.
- Young, D. A., and B. J. Alder, 1979, *J. Chem. Phys.* **70**, 473.
- Zhao, Y., and J. Fang, 2006, *Langmuir* **22**, 1891.
- Zvyagolskaya, O., A. J. Archer, and C. Bechinger, 2011, *Europhys. Lett.* **96**, 28005.